TEX264-mediated selective autophagy in the repair of cytotoxic trapped PARP1

Gwendoline Hoslett

St Hugh's College

Supervisor: Professor Kristijan Ramadan

A thesis submitted to the University of Oxford for the degree of Doctor of Philosophy

Trinity term 2024

Department of Oncology

MRC Weatherall Institute of Molecular Medicine

University of Oxford

Contents

Acknowledgements

Firstly, I would like to thank Professor Kristijan Ramadan for his support and expertise throughout my DPhil. His support has been invaluable for not only helping to direct the project but ensuring my development as an independent and thoughtful scientist. All members of the Ramadan laboratory, past and present, have also been instrumental in providing feedback, technical guidance and, most importantly, creating a welcoming and inspiring environment that has made my DPhil experience an enjoyable one. Dr Shudong Li and Dr Pauline Lascaux deserve specific thanks for taking so much time during the busiest times of their DPhil studies to help guide my project. I would also like to thank Dr James Bancroft and Dr Edward Drydale for assisting with microscopy experiments.

I am very appreciative of practical and emotional support provided by family and friends over the last four years. I would especially like to thank Nanny Moira and Grandad Howard who encouraged me to pursue a DPhil, and my parents and brother for their constant support and encouragement. Finally, I would like to thank Jacob, for his endless care and patience during this process, from cheering me up through periods of failed experiments and uncertainty, to celebrating successes and publications.

Declaration

I declare that the work presented in this thesis is wholly my own, except when clearly stated otherwise. This work has not been submitted for any other degree.

Abstract

Targeting genomic instability in cancer therapy has been achieved by exploiting the synthetic lethal interaction between PARP inhibitors (PARPi) and homologous recombination (HR). PARPi induce cytotoxicity in HR-deficient cancers by causing PARP1 to become tightly bound to chromatin, a phenomenon known as PARP1 trapping, resulting in irreparable replication-associated DNA damage. Despite their initial promise, resistance commonly arises in PARPi-treated cancers, highlighting a need for improved understanding of cellular PARPi response and tolerance mechanisms. Previous work demonstrated that p97 extracts trapped PARP1 from chromatin, allowing tolerance to PARPi treatment, but regulation of its function and downstream processing remain unclear. Using immunofluorescence and cell viability assays, I identified a novel role of the p97 co-factor and selective autophagy receptor TEX264 in regulation of trapped PARP1. Further biochemical and cell biological studies uncovered a mechanism of selective nucleophagy of trapped PARP1, mediated by TEX264 and p97 and regulated by ubiquitination and SUMOylation, which promotes shuttling of trapped PARP1 to the lysosome. Impairing this process resulted in increased genomic instability, replication stress and sensitivity to PARPi. This was found to be highly dependent on PARP1 trapping, with only trapped PARP1 processed this way. Strikingly, inhibition of TEX264-orchestrated nucleophagy re-sensitised PARPi resistant cells, implying a potential relevance of this pathway for improving therapy. Overall, I demonstrate a novel mechanism of trapped PARP1 clearance by selective nucleophagy mediated by dual functions of the p97 co-factor and selective autophagy receptor TEX264, which regulates tolerance of sensitive and resistant cells to PARPi.

List of Figures and Tables

List of abbreviations

AMPK: AMP-activated protein kinase

ARH3: ADP-ribosyl hydrolase 3

ATG: autophagy-related gene

ATP: Adenosine triphosphate

BER: base excision repair

CQ: chloroquine

DDR: DNA damage response

DMEM: Dulbecco's Modified Eagle Medium

DNA: deoxyribonucleic acid

DPC: DNA-protein crosslink

DSB: double-strand break

DUB: deubiquitinase

ER: endoplasmic reticulum

ERAD: endoplasmic reticulum-associated degradation

FBS: fetal bovine serum

GFP: Green Fluorescent Protein

GyrI: gyrase inhibitor

HCQ: hydroxychloroquine

HER2: human epidermal growth factor receptor 2

HPF1: Histone PARylation factor 1

HR: homologous recombination

IC50: half-maximal inhibitory concentration

LIR: LC3-interacting region

LysoIP: Immunoprecipitation of intact lysosomes

MAD: mitochondrial-associated degradation

MMS: methyl methanesulfonate

MS: mass spectrometry

mTORC1: mechanistic target of rapamycin complex 1

NAD+: nicotinamide adenine dinucleotide

NER: nucleotide excision repair

NHEJ: non-homologous end-joining

OS: overall survival

PARG: poly(ADP-ribose) glycohydrolase

PARP1: poly(ADP-ribose) polymerase 1

PARPi: poly(ADP-ribose) polymerase inhibitor

PBS: phosphate buffered saline

PDE6: phosphodiesterase VI

PE: phosphatidylethanolamine

PEI: Polyethylenimine

PFS: progression free survival

PI3K: phosphatidylinositol 3-kinase

PI3P: phosphatidylinositol-3-phosphate

PLA: proximity ligation assay

PML: promyelocytic leukaemia protein

PSM: peptide-spectrum matches

PTM: post-translational modification

RNA: ribonucleic acid

RNAi: RNA interference

ROS: reactive oxygen species

SAR: selective autophagy receptor

shRNA: short hairpin RNA

SIM: SUMO-interacting motif

SSB: single-strand break

ssDNA: single stranded DNA

STUbL: SUMO-targeted ubiquitin ligase

TBS: tris buffered saline

TNBC: triple negative breast cancer

TOP1: topoisomerase I

TOP1cc: topoisomerase I cleavage complex

TOP2: topoisomerase II

TOP2cc: topoisomerase II cleavage complex

UBX: ubiquitin regulatory X

UPS: ubiquitin-proteasome system

VBM: VCP-binding motif

VIM: VCP-interacting motif

WT: wild-type

1. Introduction

1.1 Targeting genomic instability in cancer therapy

1.1.1 Genomic instability in cancer

Genome instability underlies all hallmarks of cancer and is an essential component in all stages of cancer emergence, progression and response to treatment (Hanahan & Weinberg, 2011). Cancer driving mutations, caused through chromosomal rearrangements or deletions, amplification or point mutations of individual genes, determine a cell's ability to resist cell death, evade growth suppressors and sustain proliferative signalling, resulting in tumorigenesis and hyperproliferation. As cancer progresses, mutations promote metastasis and angiogenesis, as well as telomeric alterations that allow immortality. A greater mutational burden also results in greater diversity within the tumour cell population, increasing the chance of resistance to therapy or tumour recurrence. Therefore, cells possess a complex and conserved DNA damage response (DDR) pathway to maintain genomic stability and mediate cellular response to genotoxic stress (Groelly, Fawkes, Dagg, Blackford, & Tarsounas, 2023). Heritable genetic disorders that predispose to cancer often stem from a single mutation in specific groups of DDR genes, such as Fanconi anaemia, caused by deficient interstrand crosslink repair, ataxia telangiectasia, characterised by defective double-strand break (DSB) repair (Taylor et al., 2019), and Ruijs-Aalfs syndrome, where DNA-protein crosslink (DPC) repair is impaired (Lopez-Mosqueda et al., 2016; J. Stingele et al., 2016; Vaz et al., 2016).

Despite the significance of increased genomic instability in cancer progression, it also presents a therapeutic window whereby cancer cells are over-reliant on the

DDR. Exogenous genotoxic agents, such as radiotherapy, alkylating agents, and topoisomerase inhibitors cause an accumulation of unrepaired DNA damage and increased replication stress in cancer cells that can no longer be tolerated, leading to cell death (Groelly et al., 2023). However, inducing genomic instability as a means of therapy often causes off-target effects due to its indiscriminate nature.

1.1.2 PARPi and synthetic lethality

An alternative therapeutic strategy is targeting genomic instability exclusively in cancer cells through synthetic lethality. Mutations in DDR factors, often by a combination of germline mutations and those that arise during tumorigenesis, can eliminate certain repair pathways, leaving tumour cells reliant on alternative pathways that are non-essential in normal tissue. Only tumour cells are sensitive to inactivation of this alternate pathway, meaning cytotoxic levels of DNA damage and replication stress can be induced exclusively in tumour cells. The first example of this therapeutic strategy entering the clinic is with the treatment of homologous recombination (HR)-deficient cancers using poly(ADP-ribose) polymerase inhibitors (PARPi) (Bryant et al., 2005; Deeks, 2015; Farmer et al., 2005).

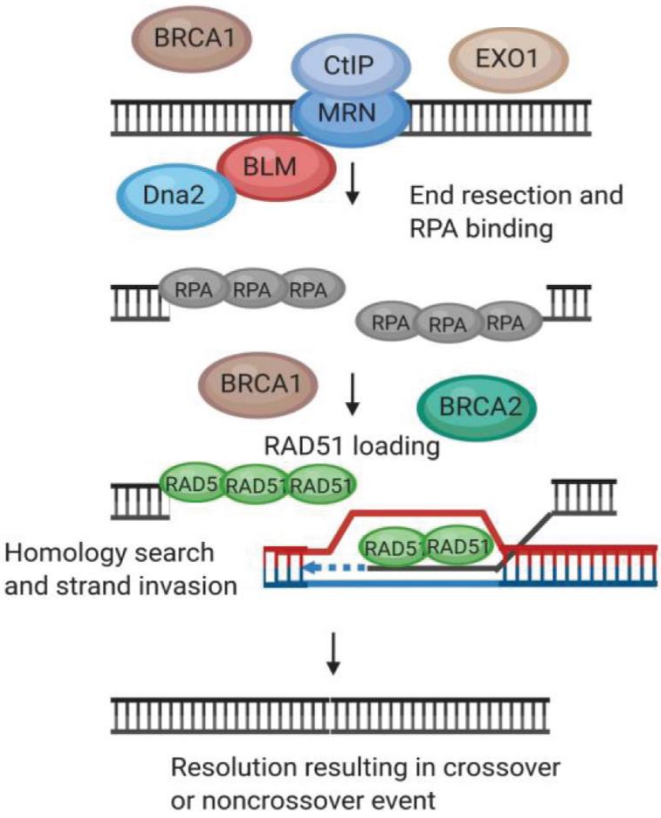

Figure 1: Homologous recombination pathway. BRCA1 promotes loading of nucleases, driving end resection and RPA loading. BRCA1 and BRCA2 promote RAD51 loading, allowing homology searching and strand invasion for DNA synthesis and repair. Adapted from Ketley and Gullerova (2020).

HR is an error-free pathway of DSB repair, shown in Figure 1, which utilises extensive homology between broken DNA and a template DNA strand. It requires nucleolytic processing of DSB ends to reveal long 3' ssDNA overhangs. These are bound by RAD51 to form a nucleoprotein filament that carries out homology searching. Once the invading filament has located a region of homology, a polymerase extends the broken DNA until the break is filled in (Scully, Panday, Elango, & Willis, 2019). BRCA2 drives RAD51 loading onto the resected ssDNA strand (Thorslund et al., 2010; H. Yang, Li, Fan, Holloman, & Pavletich, 2005), whilst BRCA1 has multiple roles including promoting DNA end resection (Cruz-García, López-Saavedra, & Huertas, 2014; Escribano-Díaz et al., 2013; Schlegel, Jodelka, & Nunez, 2006), recruitment of RAD51 and strand exchange (W. Zhao et al., 2017). Whilst HR maintains DNA fidelity, its reliance on homologous sequences means it

must be constrained only to the S and G2 phases of the cell cycle, where chromosomes are replicated. Non-homologous end-joining (NHEJ) is the major pathway to act outside of this, with pathway choice essential for maintaining genome stability (Scully et al., 2019). In two seminal papers, a variety of *BRCA1*$^{-/-}$ and *BRCA2*$^{-/-}$ cell lines were found to show acute sensitivity to a number of different PARPi, with some as much as 1000-fold more sensitive than their wild-type counterparts. They further showed that BRCA-defective xenograft models in mice responded positively to PARPi treatment (Bryant et al., 2005; Farmer et al., 2005). Inheritance of *BRCA1/2* mutations increases a patient's risk of developing cancer considerably, exemplified by an 80% lifetime risk of developing breast cancer (Domchek & Weber, 2006). The unique vulnerability these tumour cells display when challenged with PARPi demonstrates a promising therapeutic strategy for patients.

1.1.3 PARPi in the clinic

Since the discovery that PARPi are synthetic lethal in BRCA1/2-defective cells, four PARPi have been approved as part of standard-of-care approaches for HR-defective breast, ovarian, prostate and pancreatic cancers (Wicks, Krastev, Pettitt, Tutt, & Lord, 2022), with two others approved in China (A. Lee, 2021; Markham, 2021). Olaparib was the first PARPi to be approved in 2014, initially for maintenance treatment of *BRCA*-mutated high-grade, serous epithelial ovarian, fallopian tube or primary peritoneal cancer showing complete or partial response to platinum-based therapies. It significantly improved progression free survival (PFS) in the SOLO2 study, which showed an increase of 13.6 months and an increase in overall survival (OS) from 33.2% to 42.1% (Poveda et al., 2020; Pujade-Lauraine et al., 2017). Olaparib was also shown to be well-tolerated in these patients, with side effects

mainly being mild cases of nausea, fatigue, vomiting and anaemia, with few incidence of severe adverse events (Deeks, 2015; Ledermann et al., 2012; Poveda et al., 2020). Olaparib has since been approved for the treatment of deleterious *BRCA*-mutated human epidermal growth factor receptor 2 (HER2)-negative breast cancer and advanced metastatic breast cancer (Cortesi, Rugo, & Jackisch, 2021), maintenance treatment of BRCA-mutated platinum-sensitive metastatic pancreatic cancer and HR-defective castration-resistant prostate cancer (AstraZeneca Pharmaceuticals LP, 2022). In the OlympiAD trial comparing Olaparib to standard therapy in HER2-negative metastatic breast cancer with a *BRCA* mutation, the response rate was 59.9% with Olaparib treatment compared to 28.9% with standard therapy. In addition, tolerability seemed to improve, with 36.6% of Olaparib-treated patients experiencing severe adverse effects compared to 50.5% in the standard therapy group (Robson et al., 2017). This demonstrates how a synthetic lethal therapeutic approach improves patient outcomes not only through targeting tumour cells, but also by sparing healthy cells which maintain *BRCA1/2* expression and a functioning HR pathway.

Talazoparib (Hoy, 2018), rucaparib (Syed, 2017), niraparib (Scott, 2017), pamiparib (Markham, 2021) and fuzuloparib (A. Lee, 2021) are also approved for clinical use, with the latter two only approved in China. Talazoparib is the most potent of all these PARPi, shown by a 3-fold lower PARP1 50% inhibitory concentration than Olaparib and Rucaparib. This translates to a 50-2000-fold increase in cytotoxicity of BRCA1/2-deficient cancer cells compared to Olaparib or rucaparib treatment (Shen et al., 2013). Talazoparib was first approved for treatment of HER2-negative, locally advanced or metastatic breast cancer with a deleterious or suspected deleterious *BRCA1* or *BRCA2* mutation due to promising results from the EMBRACA (J. K.

Litton et al., 2020; Jennifer K. Litton et al., 2018) and ABRAZO (Turner et al., 2019) trials. It has since been approved for treatment of metastatic castration-resistant prostate cancer with a HR gene mutation, used in combination with enzalutamide, an androgen receptor inhibitor, as a result of the TALAPRO-2 trial showing improved PFS (N. Agarwal et al., 2023).

Despite a considerably improved PFS in the EMBRACA trial, which compared response in patients treated with either standard chemotherapy or talazoparib (Jennifer K. Litton et al., 2018), OS did not significantly improve (J. K. Litton et al., 2020), as was seen in the OlympiaD trial, also in HER2-negative, *BRCA*-mutant breast cancer but treated with Olaparib (Robson et al., 2017). Detrimental OS data from SOLO-3 and ARIEL-4 trials even resulted in Olaparib, Rucaparib and Niraparib being withdrawn as a monotherapy for treatment of advanced ovarian cancers that had previously been treated with 2 or more chemotherapy regimens (J. Y. Lee et al., 2023; Tew, Lacchetti, Kohn, & Panel, 2022), despite earlier PFS data favouring PARPi treatment over standard chemotherapy (Kristeleit et al., 2022; Penson et al., 2020). Whilst some studies have shown improved OS, such as the SOLO2 trial assessing use of Olaparib in maintenance therapy of relapsed ovarian cancer (Poveda et al., 2020), most patients receive subsequent treatments, indicating resistance has arisen (J. K. Litton et al., 2020; Robson et al., 2017). A considerable proportion of patients also show *de novo* resistance which is estimated to account for 40% of ovarian cancer patients with a germline *BRCA* mutation showing no response to either Olaparib (Audeh et al., 2010; Fong et al., 2010; H. Li et al., 2020) or Rucaparib (Kristeleit et al., 2017; Wicks et al., 2022). This highlights resistance as a major challenge facing clinical use of PARPi and an intense area of research focus.

1.2 PARPi mechanism of action and resistance

1.2.1 PARP1 function

PARP1 is the main target of PARPi, although all clinical PARPi also bind PARP2, another of the 17-member PARP superfamily, to varying degrees (Jones, Wilcoxen, Rowley, & Toniatti, 2015; Menear et al., 2008; Shen et al., 2013; Syed, 2017; H. Wang et al., 2020). Whilst PARP1 has pleiotropic roles in programmed cell death (Virág, Robaszkiewicz, Rodriguez-Vargas, & Oliver, 2013), ribosome biogenesis (D. S. Kim et al., 2019) and biomolecular condensate formation (Leung, 2020), its most prominent role is in maintaining genomic stability by acting as a DNA damage sensor and during DNA replication (Kanev, Atemin, Stoynov, & Aleksandrov, 2024; Ray Chaudhuri & Nussenzweig, 2017). PARP1 is recruited to DNA damage sites within seconds (Haince, McDonald, Rodrigue, Dery, et al., 2008), where it modifies itself and a wide range of target proteins by catalysing the polymerisation of ADP-ribose units which are targeted primarily to acceptor serine residues during DNA repair (Palazzo et al., 2018). Ser-ADPr modification by PARP1 relies upon histone PARylation factor 1 (HPF1) which, as its name would suggest, primarily targets PARylation towards serine residues in histones (Bonfiglio et al., 2017; Gibbs-Seymour, Fontana, Rack, & Ahel, 2016; Palazzo et al., 2018). However, recent evidence suggesting HPF1 is dispensable for the most well characterised role of PARP1 in single strand break (SSB) repair (Hrychova et al., 2024) implies other acceptor residues must be involved, with glutamate and aspartate known to be modified by PAR chains in the absence of HPF1 (Palazzo et al., 2018). These PAR chains induced by PARP1 at damage lesions drive repair through a network of proteins containing PAR-binding domains. In SSB repair, XRCC1 is recruited to PARylated PARP1 at the lesion, where it acts as a scaffold to recruit downstream

factors such as LIG3 and DNA polymerase β (K. W. Caldecott, Aoufouchi, Johnson, & Shall, 1996; Hanzlikova, Gittens, Krejcikova, Zeng, & Caldecott, 2017; Polo et al., 2019). Whilst PARP1 is essential for SSB repair, in the case of DSBs it plays a more regulatory role through its interactions with several repair factors (Ray Chaudhuri & Nussenzweig, 2017). Via a PAR-binding domain in MRE11, PARP1 enhances MRE11 and NBS1 recruitment to regulate end resection (Haince, McDonald, Rodrigue, Déry, et al., 2008) whilst it also limits MRE11 activity to prevent excessive end resection, as seen in its role at stalled replication forks. The multifaceted roles of PARP1 in DNA repair, replication and chromatin remodelling are shown in figure 2.

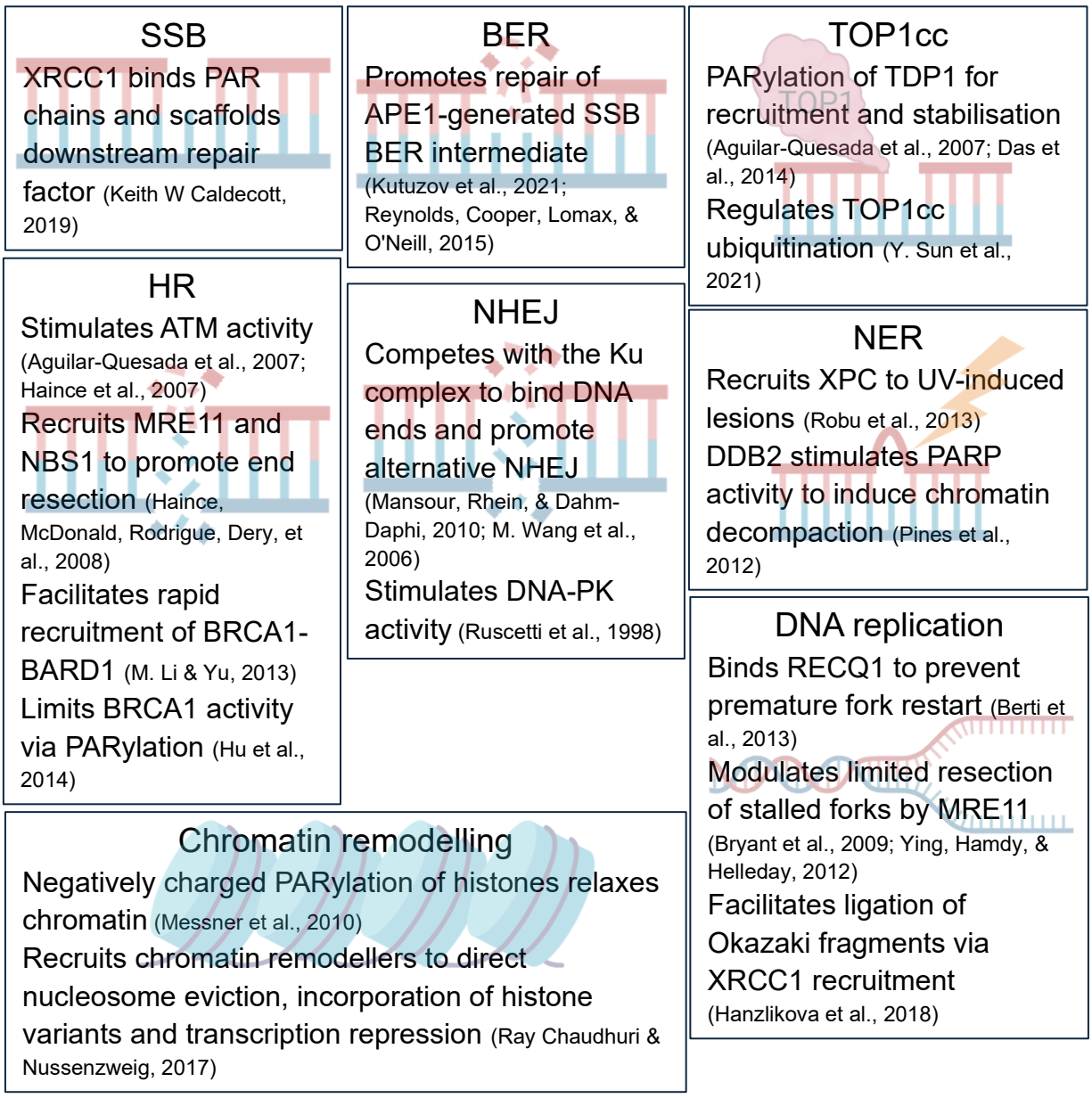

Figure 2: Roles of PARP1 in a variety of DNA repair pathways, chromatin dynamics and DNA replication.

Outside of DNA repair, PARP1 interacts with and stimulates the activity of multiple factors at the replication fork, including MRE11 and RECQ1 to regulate replication fork reversal and prevent premature fork restart during genotoxic stress and replication of hard to replicate regions (Berti et al., 2013; Ray Chaudhuri & Nussenzweig, 2017; Ying et al., 2012). This may explain why inhibition of PARP1 results in accelerated fork speed due to premature fork restart (Maya-Mendoza et

al., 2018). PARP1 also mediates ligation of Okazaki fragments, with this the major cause of PARylation activity in unperturbed cells (Hanzlikova et al., 2018; Vaitsiankova et al., 2022). 90% of PARylation activity during DNA damage repair is mediated by PARP1, whilst the remainder is PARP2-mediated (J.-C. Amé et al., 1999), indicating why its inhibition is so toxic to cells.

1.2.2 PARPi mechanism of action

PARP1 consists of 3 functional domains, the N-terminal DNA-binding domain, containing three zinc finger domains and a nuclear localisation signature, the C-terminal catalytic domain with an active site conserved across the entire PARP superfamily (J. C. Amé, Spenlehauer, & De Murcia, 2004), and a central auto-modification domain containing a BRCT domain with residues for accepting PAR. These domains form a flexible 'beads on a string' inactive conformation which collapses into a compact conformation upon binding to a DNA break due to a network of interactions between domains. This results in a 1000-fold increase in activity (Langelier, Ruhl, Planck, Kraus, & Pascal, 2010) by removal of the autoinhibitory helical domain from the active site (Fig 3) (Chappidi et al., 2024; Dawicki-McKenna et al., 2015; Langelier, Planck, Roy, & Pascal, 2012). Through this allostery, PARP1 activity is controlled to allow robust and rapid activation specifically upon binding to DNA breaks (Lilyestrom, van der Woerd, Clark, & Luger, 2010) and a growing list of other DNA structures (Laspata, Muoio, & Fouquerel, 2024).

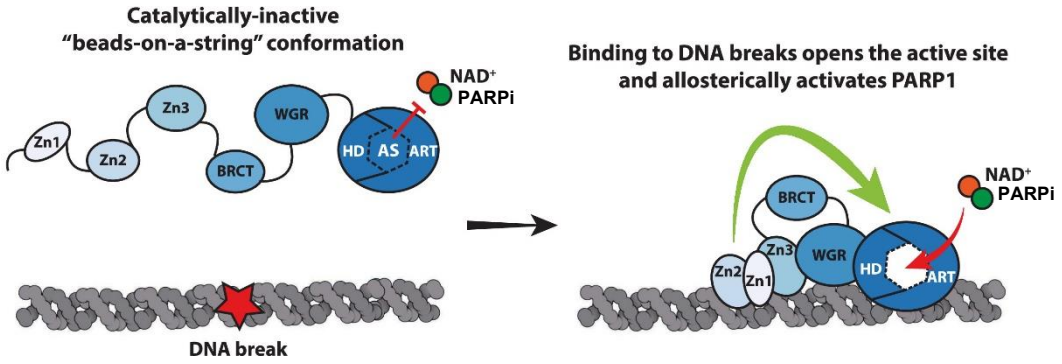

Figure 3: PARP1 structure. PARP1 domains in a loose, beads-on-a-string conformation change into a compact conformation due to interdomain contacts as a result of zinc finger domains binding to DNA. This opens the catalytic site for binding by NAD+ or a PARPi. Adapted from Kanev et al (2024).

NAD+ binds to the catalytic site of PARP1, serving as an ADP-ribose donor for catalysing PAR chains. Competitive inhibition of NAD+ is the basis for all clinically available PARPi and virtually all PARPi produced since the first PARPi, which was based on nicotinamide and shown to impair cell survival in response to DNA-methylating agents (Durkacz, Omidiji, Gray, & Shall, 1980; Purnell & Whish, 1980). Catalytic inhibition was first considered the basis of synthetic lethality in HR-defective cells, whereby PARP1 inactivity causes an accumulation of unrepaired SSBs which collapse into unrepairable DSBs during replication (Bryant et al., 2005; Farmer et al., 2005) (Fig 4B). However, in a seminal paper, Murai *et al* demonstrated that PARP1 loss is not equivalent to chemical inhibition of PARP1, and even results in resistance of cells to PARPi, highlighting that an alternative mechanism must be at play. They discovered that PARPi cause PARP1 to become tightly bound to chromatin, a phenomenon now referred to as PARP trapping, and that the cytotoxicity caused by different PARPi closely correlates to their trapping potency but not their catalytic inhibition potency (Murai et al., 2012). Talazoparib is the most potent of the clinically available PARPi, showing ~100-fold increased cytotoxicity compared to Olaparib and rucaparib as well as a 100-fold increased trapping potency (Murai et al., 2014; Shen et al., 2013). The ability of PARPi to trap PARP1

is, in part, explained by their inhibitory capacity, with the auto-PARylation of PARP1 known to drive its release from DNA (Kanev et al., 2024; Murai et al., 2012). More recent work to explore the differential trapping, and therefore cytotoxic potency, of various PARPi highlighted their ability to alter the allostery of PARP1 by destabilising the helical domain, causing increased retention at DNA breaks (Xue et al., 2022; Zandarashvili et al., 2020), as well as the differential dissociation rates of various PARPi from PARP1 (Gopal, Fernandez, Delano, Weissleder, & Dubach, 2024; Z. Shao et al., 2020), as key to understanding the function of PARPi.

PARPi-induced PARP1 trapping is thought to cause synthetic lethality in HR-defective cells by causing a bulky DPC-like structure that blocks the replisome. This causes fork stalling and eventual collapse into DSBs which go unrepaired in HR-defective cells (Fig 4A) (Dibitetto, Widmer, & Rottenberg, 2024; Helleday, 2011; Wicks et al., 2022). Whilst the formation of a DSB underlying synthetic lethality is consistent with the earlier model of SSB accumulation (Fig 4B), the trapping model is consistent with mutations in PARP1 that alleviate trapping causing resistance to PARPi (S. J. Pettitt et al., 2018) and loss of machinery that removes trapped PARP1 increasing sensitivity (Krastev et al., 2022). In recent months, an alternative model of PARPi-induced DSB formation has been proposed, whereby PARPi impairs a newly discovered role of PARP1 in preventing transcription-replication conflicts (Fig 4C), suggesting that enzymatic inhibition of PARP1 is sufficient for synthetic lethality (Petropoulos et al., 2024). It has also recently been proposed that PARPi sensitivity in BRCA1/2-defective cells relates to a HR-independent role of BRCA1/2 in replication gap suppression, with PARPi inducing the accumulation of post-replicative gaps from unligated Okazaki fragments that drive cell death through RPA exhaustion (Fig 4D) (Cong et al., 2021; Paes Dias et al., 2021). However, both of

these mechanisms remain controversial and lack the amount of evidence that supports PARPi-induced PARP trapping as underlying synthetic lethality in HR-defective cancers.

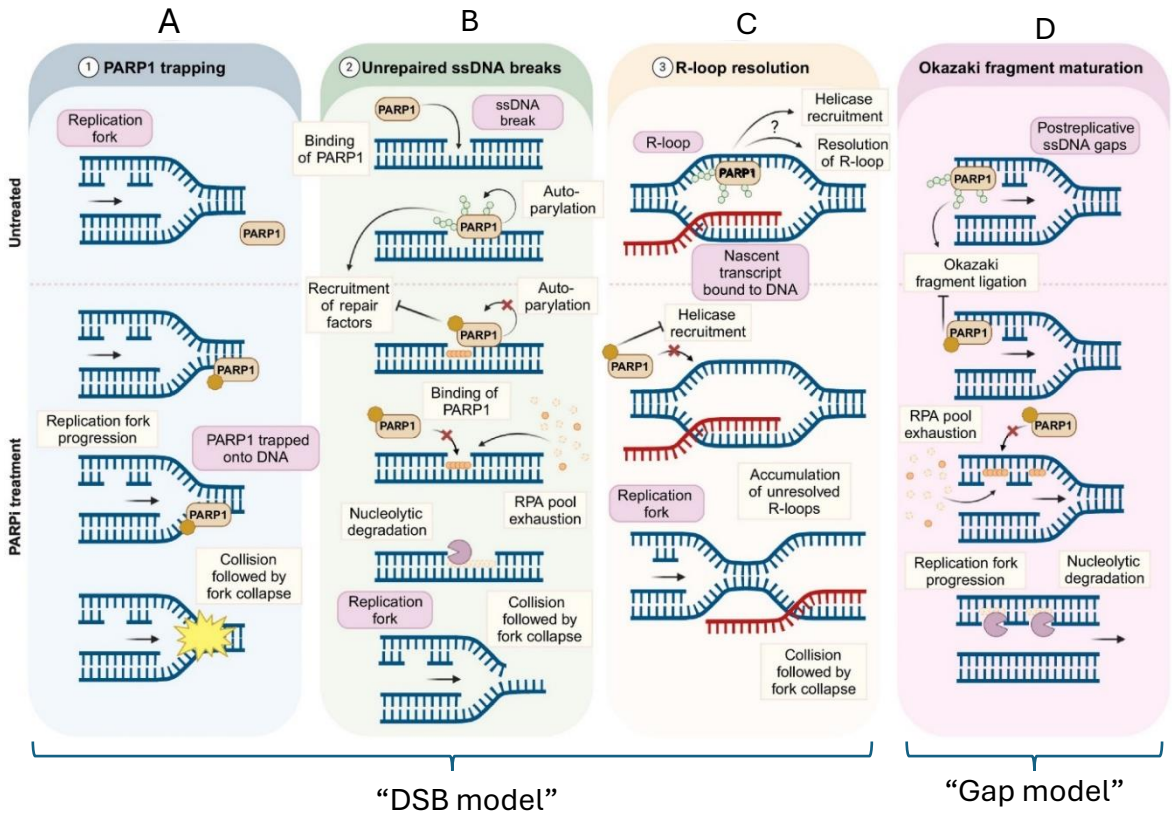

Figure 4: Proposed models of PARPi cytotoxicity. Models are broadly divided into "DSB model" or "gap model" based on the cytotoxic lesion. Adapted from Dibitetto, Widmer and Rottenberg (2024).

1.2.3 The PARPi resistance problem

As previously mentioned, and despite the initial promise of PARPi, resistance poses a major clinical challenge. Extensive research is required to overcome this, so far uncovering several resistance mechanisms (Fig 5); some observed in the clinic and others demonstrated in pre-clinical studies.

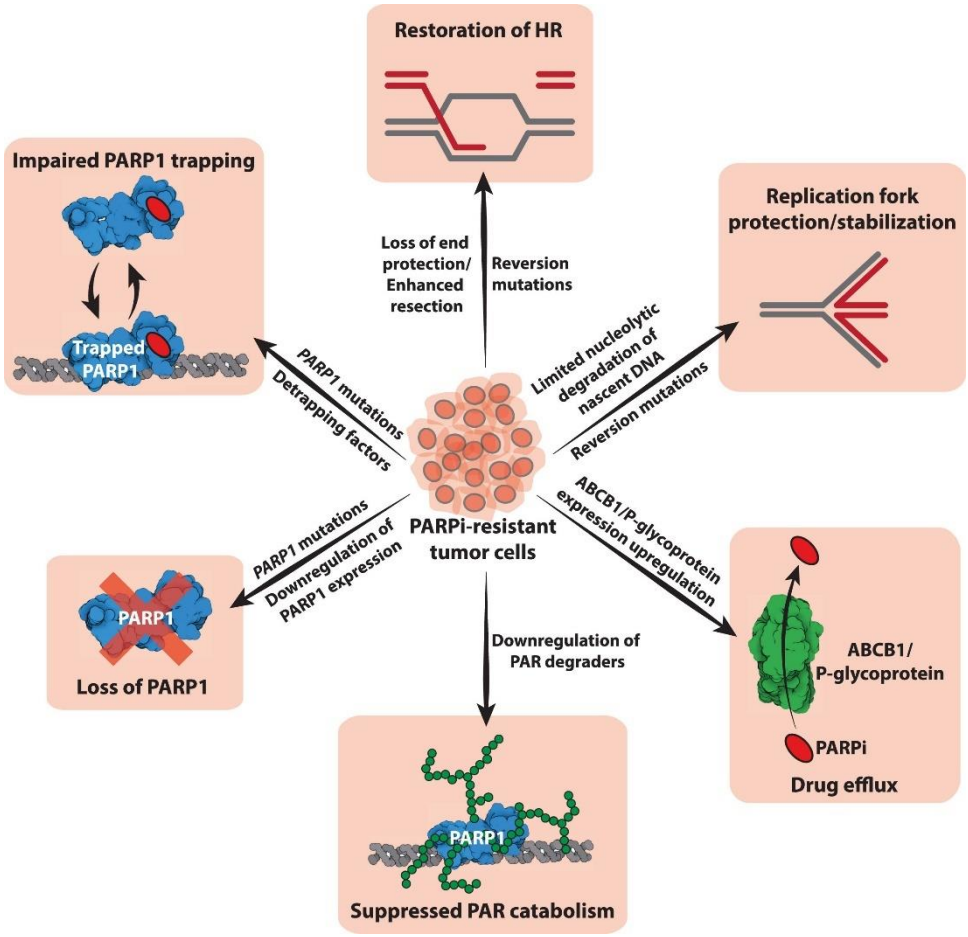

Figure 5: Mechanisms of PARPi resistance. Text around arrows indicates how resistance is acquired. Taken from Kanev et al (2024).

By far the most validated mechanism in the clinic is restoration of *BRCA1/2* expression to restore HR (Dibitetto et al., 2024). This was first observed pre-clinically in PARPi-resistant clones generated by extended PARPi treatment of BRCA2-defective cell lines, identifying secondary reversion mutations in *BRCA2* that restored its function (Edwards et al., 2008; Sakai et al., 2008). In the clinic, reversion mutations are most commonly deletions of less than 100 base pairs that restore the open reading frame, or corrections to the original deleterious mutation (Harvey-Jones et al., 2024; Tobalina, Armenia, Irving, O'Connor, & Forment, 2021). Other mutations have been observed whereby *BRCA1* expression is restored in patient-derived xenografts through gene re-arrangements that placed *BRCA1* under the control of a heterologous promoter, restoring its expression (ter Brugge et al.,

2016). Importantly, under both of these circumstances, mutation sites are often characterised by flanking sequences of microhomology, indicating they have arisen through alternative, deleterious DSB repair pathways like NHEJ and microhomology-mediated end joining (MMEJ) that are essential in HR-defective cells (Edwards et al., 2008; Harvey-Jones et al., 2024; S. J. Pettitt et al., 2020; ter Brugge et al., 2016; Tobalina et al., 2021). This implies resistance occurs due to selective pressure under treatment. Outside of genetic inactivation of *BRCA1/2*, epigenetic inactivation of *BRCA1* has been observed in up to 15% of triple negative breast cancer (TNBC) and serous ovarian carcinomas (ter Brugge et al., 2016). In these instances, methylation of the *BRCA1* promoter drives reduced *BRCA1* expression, making these tumours sensitive to PARPi (Olga Kondrashova et al., 2018). Changes to methylation status has been implicated in driving resistance in several TNBC patients (ter Brugge et al., 2016) and predicts response of ovarian carcinoma patient-derived xenografts and patients to rucaparib treatment (Olga Kondrashova et al., 2018). Genetic reversion mutations and epigenetic changes also cause resistance in patients whose HR-deficiency stems not from loss of *BRCA1/2* but from changes in other HR genes, namely *RAD51C* (Hurley et al., 2021; Nesic et al., 2021), *RAD51D* (O. Kondrashova et al., 2017) and *PALB2* (Goodall et al., 2017). Overall, restored *BRCA* status is a frequently observed phenomenon in cancer patients who progress after PARPi treatment. The variation in the levels of this, from 15% in ovarian cancer (K. K. Lin et al., 2019) to 60% in metastatic breast cancer (Harvey-Jones et al., 2024), demonstrates how different PARPi and treatment regimens create a range of selective pressures that affect the development of resistance (Dibitetto et al., 2024). What is clear from these numbers, however, is that other lesser explored resistance mechanisms must be at play in the

remainder of patients who retain dysfunctional *BRCA1/2* gene copies but whose cancers progress regardless.

In cells where BRCA1 is dysfunctional, HR can be restored through other means. This was first suggested due to the phenomenon that *BRCA1*-knockout mice have shortened lifespan and high levels of tumorigenesis whilst this is rescued by knockout of *TP53BP1*. Loss of 53BP1 in BRCA1-defective cells restores HR and alleviates sensitivity to PARPi (Bouwman et al., 2010; Bunting et al., 2010), due to the antagonising roles 53BP1 and BRCA1 at the early stage of DSB repair. BRCA1 promotes nucleolytic processing of DNA ends to drive HR, whilst 53BP1 protects DNA ends to promote NHEJ (Bunting et al., 2010; Escribano-Díaz et al., 2013; Noordermeer et al., 2018). Therefore, loss of 53BP1 in BRCA1-defective cells allows DNA end resection so HR can proceed. During the search for other NHEJ factors, other proteins have been identified whose loss restores end resection to drive resistance to PARPi, namely components of the Shieldin complex (Dev et al., 2018; Drané et al., 2017; Gupta et al., 2018; Noordermeer et al., 2018; G. Xu et al., 2015), and 53BP1-interactor RIF1 (Chapman et al., 2013; Mirman et al., 2018). Recently, a study sequencing circulating tumour DNA from 47 breast cancer patients who developed PARPi resistance identified 4 patients with loss of function mutations in *TP53BP1*, *RIF1* or both, as well as a patient outside of this cohort who had reduced expression of *SHLD2* (component of Shieldin complex). Crucially, these changes were only evident in samples taken post-treatment (Harvey-Jones et al., 2024), indicating they arose during treatment and may be driving resistance in these patients. It is important to note that this mechanism is restricted to *BRCA1*-mutated tumours which are defective in HR, in part, due to the loss of end resection, whilst

BRCA2-defective tumours are unaffected (Bouwman et al., 2010; Dev et al., 2018; G. Xu et al., 2015) as loss of BRCA2 affects HR at a later stage.

Beyond their role in HR, BRCA1 and BRCA2 are important for maintaining the stability of stalled replication forks (Ray Chaudhuri et al., 2016; K. Schlacher et al., 2011; Katharina Schlacher, Wu, & Jasin, 2012), with this likely contributing to PARPi-induced lethality in BRCA1/2-defective cells. As a result, restoration of fork stability is implicated in PARPi resistance. One example is the loss of PTIP, a protein that recruits MRE11 to stalled forks, driving their degradation. PTIP loss restores fork stability in BRCA-deficient cells (Ray Chaudhuri et al., 2016) and has been observed in circulating tumour DNA from two *BRCA2*-mutated breast cancer patients who developed resistance to PARPi (Harvey-Jones et al., 2024). Loss of various other proteins has also been implicated to drive chemoresistance, including resistance to Olaparib, by restoring fork stability, such as fork remodeller SMARCAL1 (Taglialatela et al., 2017) and nucleosome remodeller CHD4 (Guillemette et al., 2015).

As with many drugs, PARPi resistance can arise through expression of efflux pumps that prevent the accumulation of PARPi in the cell. Early on in the development of Olaparib, upregulation of the P-glycoprotein efflux pump ABCB1 was found to cause resistance in a TNBC mouse model (Rottenberg et al., 2008), and has since been validated in models for several other cancer types (Jaspers et al., 2013; Vaidyanathan et al., 2016). ABCB1 overexpression has been observed in patients due to transcriptional fusions (Patch et al., 2015), with their frequency strongly associated with the number of lines of therapy received (Christie et al., 2019), indicating that this is a clinically relevant mechanism of acquired resistance. Interestingly, PARPi-resistance caused by ABCB1 overexpression in tumour models

can be reversed either by treatment with a P-glycoprotein inhibitor (Rottenberg et al., 2008; Vaidyanathan et al., 2016) or deletion of the *Abcb1* gene encoding the candidate pump (Jaspers et al., 2013), suggesting a means of overcoming resistance by combination therapy. It is also worth noting that, whilst some PARPi such as Olaparib and Rucaparib are substrates for ABCB1, PARPi like veliparib or AZD2461 have much lower affinities (Jaspers et al., 2013; Vaidyanathan et al., 2016), so could generate an improved response. This highlights the importance of better understanding resistance mechanisms for improving therapy.

The observation that loss of PARP1 caused resistance to PARPi was key to uncovering trapping as a cause of synthetic lethality in BRCA1/2-defective cells (Murai et al., 2012), and has been further validated in a genetic screen where PARP1 was found to mediate Olaparib toxicity (Stephen J. Pettitt et al., 2013). Thus, mechanisms to reduce trapping have been implicated in PARPi resistance. Mutations to residues at the DNA-binding interface of PARP1, as well as in its WGR domain that co-ordinates allosteric changes upon DNA-binding, prevent PARP1 binding to DNA or inhibit retention, respectively. In fact, a PARP1 mutation was identified in an ovarian cancer patient tumour that showed *de novo* resistance to PARP1 (S. J. Pettitt et al., 2018), with it located in the WGR domain at the site for interaction with the helical domain. This was shown to impact allosteric changes, inhibiting trapping (S. J. Pettitt et al., 2018; Zandarashvili et al., 2020).

Outside of allostery, retention of PARP1 on DNA is mediated by its level of autoPARylation, which drives its dissociation due to electrostatic repulsion between negatively charged PAR and positively charged DNA. PAR-degrading enzymes, such as PAR glycohydrolase (PARG) and ADP-ribosyl hydrolase 3 (ARH3), are key in the DDR to regulate PARylation levels and prevent premature dissociation of

PARP1 (Kanev et al., 2024; Pascal & Ellenberger, 2015). However, loss of PARG causes resistance to PARPi, both *in vitro* and in BRCA-defective mammary tumours in mice. PARG loss caused increased PAR levels under PARPi-treated conditions, which in the long term caused reduced PARP1 binding to DNA so prevented accumulation of trapped PARP1 (Gogola et al., 2018). Similarly, loss of ARH3, which removes mono(ADP-ribose), causes resistance to Olaparib in several BRCA1/2-defective cell lines (Prokhorova, Agnew, et al., 2021; Prokhorova, Zobel, et al., 2021). In accordance with this, mutation of three key serine residues that serve as sites for autoPARylation causes increased Olaparib sensitivity (Prokhorova, Zobel, et al., 2021). Beyond autoPARylation, trapped PARP1 can be cleared from chromatin by the p97 system which is well-described for clearance of DPCs. Inhibition of this pathway sensitises cells and patient-derived organoids to talazoparib (Krastev et al., 2022). This demonstrates the importance of PARP1 trapping for PARPi sensitivity.

A better understanding of resistance mechanisms is essential for overcoming the challenge it poses in the clinic. This can be broken down into 3 areas. Firstly, identifying better biomarkers to predict patient response to therapy and reduce the burden of *de novo* resistance. Current biomarkers focus on the presence of a deleterious mutation in a *BRCA/HR* gene, prior sensitivity to platinum-based therapy or the presence of a genomic signature of HR-deficiency (Wicks et al., 2022). However, these genomic signatures persist in tumours which have acquired resistance (Harvey-Jones et al., 2024) and a considerable proportion of patients with a germline *BRCA* mutations fail to respond to PARPi, evidenced by 40% of *BRCA*-mutated ovarian cancer patients showing no response either Olaparib (Audeh et al., 2010; Fong et al., 2010; H. Li et al., 2020) or Rucaparib (Kristeleit et

al., 2022). Alternative strategies could include the detection of reversion mutations in circulating tumour DNA (Harvey-Jones et al., 2024) or conversion of research-based assays to the clinical setting, such as detection of RAD51 foci, a robust indicator of HR function (Castroviejo-Bermejo et al., 2018; Cruz et al., 2018; Harvey-Jones et al., 2024), or PARP1 trapping levels. A second major challenge is finding treatments that reduce the likelihood of resistance arising. One example of this is the development of PARPi AZD2461 which has a much lower affinity for ABCB1 (Jaspers et al., 2013), so would not be subject to resistance caused by efflux. Finally, a third challenge is development of targeted therapeutic regimens that could overcome resistance. A better understanding of resistance mechanisms at play could allow for tailored approaches. However, recent work using circulating tumour DNA and tumour biopsies showed multiple resistance mechanisms arise in the same patients, either together or in different lesions (Harvey-Jones et al., 2024), demonstrating the challenge a more personalised approach can pose. What is clear is that improving our understanding of resistance stems from better knowledge of trapped PARP1 biology and regulation.

1.3 The p97 system

1.3.1 p97 structure and function

Recently, trapped PARP1 was shown to be cleared from chromatin by the p97 system. Inhibition of this pathway caused increased levels of trapped PARP1 on DNA, resulting in increased sensitivity to talazoparib in cell lines as well as mouse- and patient-derived organoids (Krastev et al., 2022). p97, an AAA+-type ATPase originally identified as CDC48 in yeast (Moir, Stewart, Osmond, & Botstein, 1982) and also termed VCP in metazoans, is a homohexameric protein, where each

protein unit consists of an N-terminal domain and two ATPase domains, D1 and D2. These assemble to form a barrel like structure with a central pore, where the D1 and D2 domains of each unit form two rings stacked on top of one another (Fig 6A).

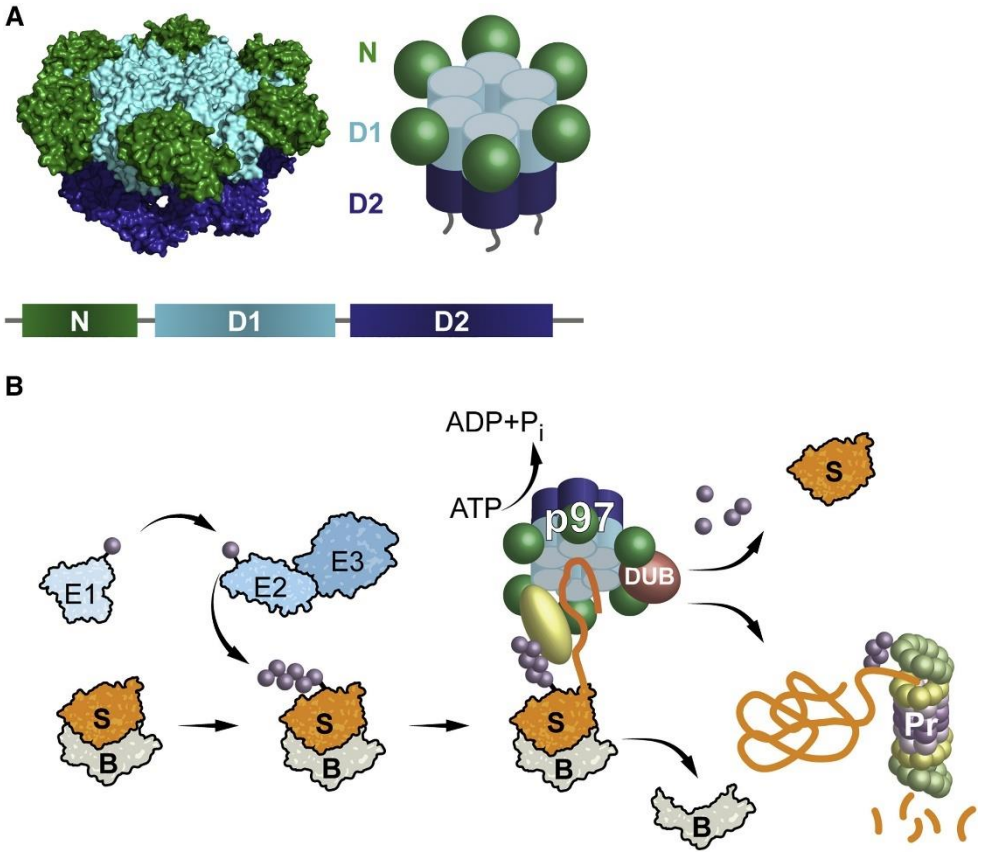

Figure 6: p97 structure and function. (**A**) p97 is a homohexameric barrel-shaped protein. (**B**) A common pathway of p97-mediated substrate degradation. A substrate (S) can be segregated from a binding partner, labelled B, through ubiquitination (purple) to recruit p97 via its co-factor (yellow), driving substrate unfolding and often degradation by the proteasome (Pr). Taken from van den Boom and Meyer (2018) with permission.

p97 acts as an unfoldase, whereby substrates enter through the pore and ATPase activity causes conformational rotational changes, pulling the substrate through facilitating its unfolding (Fig 6B) (Banerjee et al., 2016; Davies, Brunger, & Weis, 2008; van den Boom & Meyer, 2018). Substrates are commonly modified by ubiquitin or SUMO chains which are conjugated on by cascades of an E1-activating enzyme, an E2-conjugating enzyme and an E3 ligase. The exact mechanism by which p97 unfolds its substrates is complex and still a matter for exploration, but *in*

vitro and cryo-EM studies have developed a model of how Cdc48, in conjunction with the co-factor complex UFD1-NPL4, unfolds ubiquitinated substrates (Bodnar & Rapoport, 2017; Ji et al., 2022; Twomey et al., 2019). Interaction of the polyubiquitin chain with NPL4 on the N-terminal domain of p97 induces unfolding of a ubiquitin moiety which initiates unfolding and translocation of the attached substrate through the pore of p97 (Fig 6B). This is dependent upon ATPase activity of the D2 domain, with its pore loops acting to translocate the polypeptide (Ji et al., 2022; Twomey et al., 2019). After unfolding, a deubiquitinase enzyme (DUB) removes the remaining ubiquitin chain, releasing the unfolded polypeptide (Bodnar & Rapoport, 2017). This activity of p97 is essential for segregating its substrates from larger protein assemblies, membranes and chromatin, either to serve a regulatory purpose or to prepare larger protein substrates for degradation by the proteasome (Fig 6B) or through autophagy (van den Boom & Meyer, 2018).

Due to the vastly pleiotropic roles of p97 and its sheer number of substrates, as discussed below, a growing list of 40 co-factors bridge p97 to its substrates, ensuring tight regulation of its activity (Buchberger, Schindelin, & Hanzelmann, 2015). They differ in their function, with most co-factors possessing ubiquitin, SUMO or substrate-binding domains to bridge substrates (Buchberger et al., 2015; Mirsanaye et al., 2024), some having functions to alter length or topology of ubiquitin or SUMO marks (Koegl et al., 1999; Kuhlbrodt et al., 2011) and others able to regulate the activity of p97 itself (Trusch et al., 2015; Zhang et al., 2015). Co-factors can also bring an additional layer of regulation by interacting with other co-factors (Blueggel et al., 2023; Kloppsteck, Ewens, Förster, Zhang, & Freemont, 2012). All co-factors rely on a series of p97 binding domains that interact with p97, usually through its N-terminal domain, such as ubiquitin regulatory X (UBX) domain, UBX-

like domain, VCP-interacting motif (VIM), VCP-binding motif (VBM) or SHP box, but occasionally via p97 C-terminal domain with PUB and PUL domains (Buchberger et al., 2015). However, the discovery of previously unidentified co-factors yields new p97-binding domains, such as the α-helical motif of Vcf1 (Mirsanaye et al., 2024), highlighting that the study of p97 co-factors and their function in its regulation remains an area of active research.

Best described for its activity on ubiquitinated substrates, p97 has far-reaching roles throughout the cell, including endoplasmic reticulum (ER)-associated degradation (ERAD), apoptosis, cell cycle regulation, Golgi assembly, mitochondrial-associated degradation (MAD), ribosomal quality control, lipid droplet biogenesis, endosomal trafficking, gene activation, autophagy and in segregation of aggregates (Kilgas & Ramadan, 2023). Broadly, these functions can be separated into two major purposes – segregation, extraction or pre-processing of misfolded or damaged proteins or organelles to prepare them for degradation, often by the ubiquitin-proteasome system (UPS); or regulation through segregation and extraction of protein complexes. The former encompasses the most well-established role of p97 which is ERAD, where misfolded, unassembled or mislocalised proteins in the ER are ubiquitinated, recognised by p97 via the UFD1-NPL4 co-factor complex, and unfolded for subsequent proteasomal degradation. As these proteins are recognised and ubiquitinated within the membrane or lumen of the ER (Krshnan, van de Weijer, & Carvalho, 2022), the segregase activity of p97 is essential to extract them and allow their degradation. The p97-UFD1-NPL4 complex extracts protein substrates in a similar manner from mitochondrial membranes during MAD (S. Xu, Peng, Wang, Fang, & Karbowski, 2011), as well as nascent polypeptides from stalled ribosomes during ribosomal quality control (Brandman et al., 2012;

Verma, Oania, Kolawa, & Deshaies, 2013), making it the most well-recognised p97 system complex. Outside of proteasomal degradation, p97-targetted substrates can be degraded by autophagy, an example being damaged lysosomes. p97 recruitment to damaged lysosomes promotes autophagosome formation (Papadopoulos et al., 2017; Papadopoulos, Kravic, & Meyer, 2020), clearing them to prevent leakage of the hydrolytic enzymes they contain. Further roles of p97 in autophagy in initiation and autophagophore maturation will be discussed in a later section, demonstrating the significance of p97 for protein and organelle turnover through both the UPS and autophagy pathways.

1.3.2 p97 in genome stability

Regulatory segregation of proteins by p97 is seen often in its chromatin-associated functions, where p97 extracts proteins that are bound to chromatin. This makes p97 key for maintenance of genomic stability (Franz, Ackermann, & Hoppe, 2016). The first identified chromatin-associated p97 substrate was the kinase Aurora B which inhibits nucleus reformation during mitosis. Its extraction from chromatin by p97 at the end of mitosis allows chromatin condensation and reformation of the nuclear envelope (Ramadan et al., 2007). In DNA replication, p97 acts to extract ubiquitinated Cdt1 licensing factor from the replisome, facilitated by its co-factors UFD1-NPL4 and FAF1, preventing over-replication (Franz et al., 2011; Franz, Pirson, et al., 2016). Later in replication, p97 extracts MCM7 from the CMG helicase during termination, facilitating the disassembly of the replisome (Maric, Maculins, De Piccoli, & Labib, 2014; Moreno, Bailey, Campion, Herron, & Gambus, 2014). The regulatory role of p97 during replication can be summarised best in its cooperation with FAF1 and the DUB USP7 to modulate the SUMO and ubiquitin modification of

DNA replication factors on chromatin, where a SUMO-high and ubiquitin-low environment promotes active replication (Franz et al., 2021).

Outside of its role in DNA replication, p97 is incredibly active during the DDR, with its phosphorylation at serine 784 upon DNA damage induction driving its localisation to DNA damage sites (Livingstone et al., 2005). In DSB repair, p97 activity is somewhat reminiscent of its role in DNA replication, where it is active at multiple stages (Torrecilla, Oehler, & Ramadan, 2017). It balances pathway choice between NHEJ and HR by mediating extraction of RNF8-mediated Lys48-ubiquitinated proteins to regulate recruitment of downstream factors (Meerang et al., 2011), as well as orchestrating the extraction of RNF8 itself (Singh et al., 2019), a crucial E3 ligase during initiation of DSB repair. In the early stages of NHEJ, it mediates 53BP1 recruitment by extracting L3MBTL1 from the binding site of 53BP1 (Acs et al., 2011), whilst in the early stages of HR, p97 extracts MRE11 nuclease from chromatin to prevent excessive DNA end resection (Kilgas et al., 2021). At the latter stages of NHEJ, the rigid Ku70-Ku80 complex that encircles the repaired DNA is remodelled and extracted by p97 (van den Boom & Meyer, 2018). Altogether, this means that inhibition of p97 radiosensitises cells by preventing repair of DSBs (Kilgas et al., 2021; Meerang et al., 2011).

p97 is also implicated in the repair of DPCs – lesions that form due to the covalent crosslinking of proteins to DNA. This can involve proteins that are in proximity to DNA becoming linked through exposure to endogenous or exogenous genotoxic agents, such as formaldehyde or UV, respectively (Lai et al., 2016) or to specific DNA lesions such as abasic sites (Sczepanski, Wong, McKnight, Bowman, & Greenberg, 2010). Specific proteins can also become crosslinked to DNA due to trapping of enzymatic intermediates, such as topoisomerases (Maede et al., 2014;

Julian Stingele, Bellelli, & Boulton, 2017). DPCs are bulky adducts that block replication (Nakano et al., 2013) and transcription (Nakano et al., 2012), so require rapid degradation of the proteinaceous adduct, often by the proteasome (C.-P. Lin, Ban, Lyu, Desai, & Liu, 2008) or a protease, such as SPRTN (Fielden et al., 2020; Maskey et al., 2017; J. Stingele et al., 2016; J. Stingele, Schwarz, Bloemeke, Wolf, & Jentsch, 2014; Vaz et al., 2016; Vaz, Popovic, & Ramadan, 2017). This reveals the protein-DNA linkage for hydrolysis by a phosphodiesterase or reduces the size of the adduct for repair by nucleotide excision repair (NER) or bypass by translesion synthesis (Julian Stingele et al., 2017). p97 aids in the repair of a number of different DPCs by unfolding the protein adduct to allow its degradation (Noireterre & Stutz, 2024). One example is in the repair of the topoisomerase I (TOP1)-DNA enzymatic intermediate termed topoisomerase I cleavage complexes (TOP1cc), where the p97 co-factor TEX264 interacts with TOP1cc to recruit p97 and the metalloprotease SPRTN, another p97 co-factor and protease. p97 unfolds TOP1 to allow its degradation by SPRTN, clearing the proteinaceous adduct to allow hydrolysis of the protein-DNA linkage by TDP1 (Fielden et al., 2020; J. Stingele et al., 2014; Vaz et al., 2017).

The p97 co-factor SPRTN is involved in replication-coupled repair of a range of DPCs, induced by formaldehyde, as well as enzymatic DPCs induced by camptothecin and etoposide, that cause TOP1ccs and topoisomerase II cleavage complexes (TOP2ccs), respectively (Fielden et al., 2020; Lopez-Mosqueda et al., 2016; Ramadan, Halder, Wiseman, & Vaz, 2016; J. Stingele et al., 2016; Vaz et al., 2017). Germline mutations in *SPRTN* cause Ruijs-Aalfs syndrome, characterised by early onset hepatocellular carcinoma and segmental progeria caused by increased genomic stability (Lessel et al., 2014). Hepatocellular carcinoma and

progeria were also observed in *SPRTN* hypomorphic mice (Maskey et al., 2014), highlighting the relevance of the SPRTN protease and, consequently, DPC clearance in cancer biology and ageing. SPRTN was shown to recruit p97 to UV-induced lesions and DPCs, with p97-mediated unfolding crucial for SPRTN-mediated proteolysis (Davis et al., 2012; Kröning, van den Boom, Kracht, Kueck, & Meyer, 2022; Mosbech et al., 2012). This is co-ordinated by the C-terminal domain of SPRTN which contains a PCNA interacting box (PIP), ubiquitin binding domain (UBZ) and SHP box responsible for SPRTN-p97 interaction (Davis et al., 2012; Mosbech et al., 2012). Some patients with Ruijs-Aalfs syndrome express SPRTN variants with the C-terminal domain truncated (Lessel et al., 2014), implicating loss of p97 recruitment via SPRTN, amongst other C-terminal associated functions, in the early onset of cancer and premature ageing.

DPC repair is regulated by modification of the proteinaceous part of the DPC, most notably by ubiquitylation and SUMOylation (Noireterre & Stutz, 2024; Ruggiano et al., 2021). In TOP1cc repair, TOP1 is modified by SUMOylation and the co-factor involved, TEX264, has a SUMO-interacting motif (SIM) that aids its repair of TOP1cc (Fielden et al., 2020). Further, a well-established pathway of SUMOylation by PIAS4 followed by ubiquitination by the SUMO-targeted ubiquitin ligase (STUbL) RNF4 directs the proteinaceous adduct of various DPCs for proteasomal degradation (J. C. Y. Liu et al., 2021; Yilun Sun et al., 2020).

PARPi-induced trapped PARP1 can be considered a DPC-like lesion as, even though PARP1 does not become covalently-bound to DNA, it is thought to block progression of the replication fork in a similar manner, with this underlying PARPi cytotoxicity (Dibitetto et al., 2024; Helleday, 2011; Murai et al., 2012; Wicks et al., 2022). Interestingly, our group previously found through mass spectrometry that p97

interacts with trapped PARP1, with following work uncovering a model of p97-mediated trapped PARP1 extraction from chromatin. This was found to be regulated in a similar fashion as other DPCs, with SUMOylation and ubiquitination by PIAS4 and RNF4, respectively, which recruits p97 via its co-factor UFD1 (Fig 7). Inhibition of p97 caused persistence of trapped PARP1 on DNA, leading to increased sensitivity of cells and patient-derived organoids to PARPi (Krastev et al., 2022).

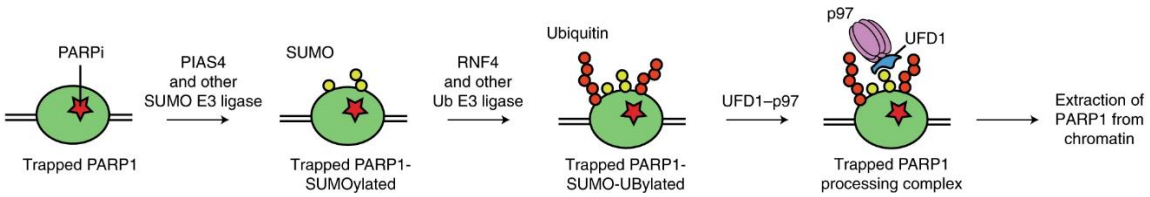

Figure 7: Model of trapped PARP1 clearance by the p97 system. This model is developed by and taken from Krastev et al (2022).

Whilst this is an interesting development in understanding trapped PARP1 repair, there are still remaining questions. Loss of proteases SPRTN and FAM111A are also associated with increased sensitivity to trapped PARP1 (Kojima et al., 2020; Saha et al., 2021), with SPRTN shown to clear 15% of trapped PARP1 during replication (Saha et al., 2021). However, the clearance of the remaining trapped PARP1, after its unfolding by p97 is unknown. Trapped PARP1 modification by PIAS4 and RNF4 is also clear, but residual modification still remains even with loss of these ligases (Krastev et al., 2022), implying other ligases and regulators are as yet unidentified. This may include other co-factors, as only UFD1 has been identified so far.

1.3.3 p97 in cancer

The role of p97 in trapped PARP1 repair clearly has exciting promise for PARPi therapy, which is furthered by an established association of p97 with cancer. By exploring the TCGA PanCancer Atlas, it is clear that p97 is altered in multiple cancers, with pancreatic and head and neck cancers showing genomic alterations

in over 5% of cases. Amplifications are the most common genomic alteration observed, although missense mutations of unknown significance are common in some cancer types (Fig 8A). The most frequently occurring missense mutation, A310T, was recorded in 4 cases, two colon and two endometrioid cancers, and was found in the D1 ATPase domain where it possibly affects p97 function, although other mutations are generally spread throughout p97 at low frequency (Fig 8B).

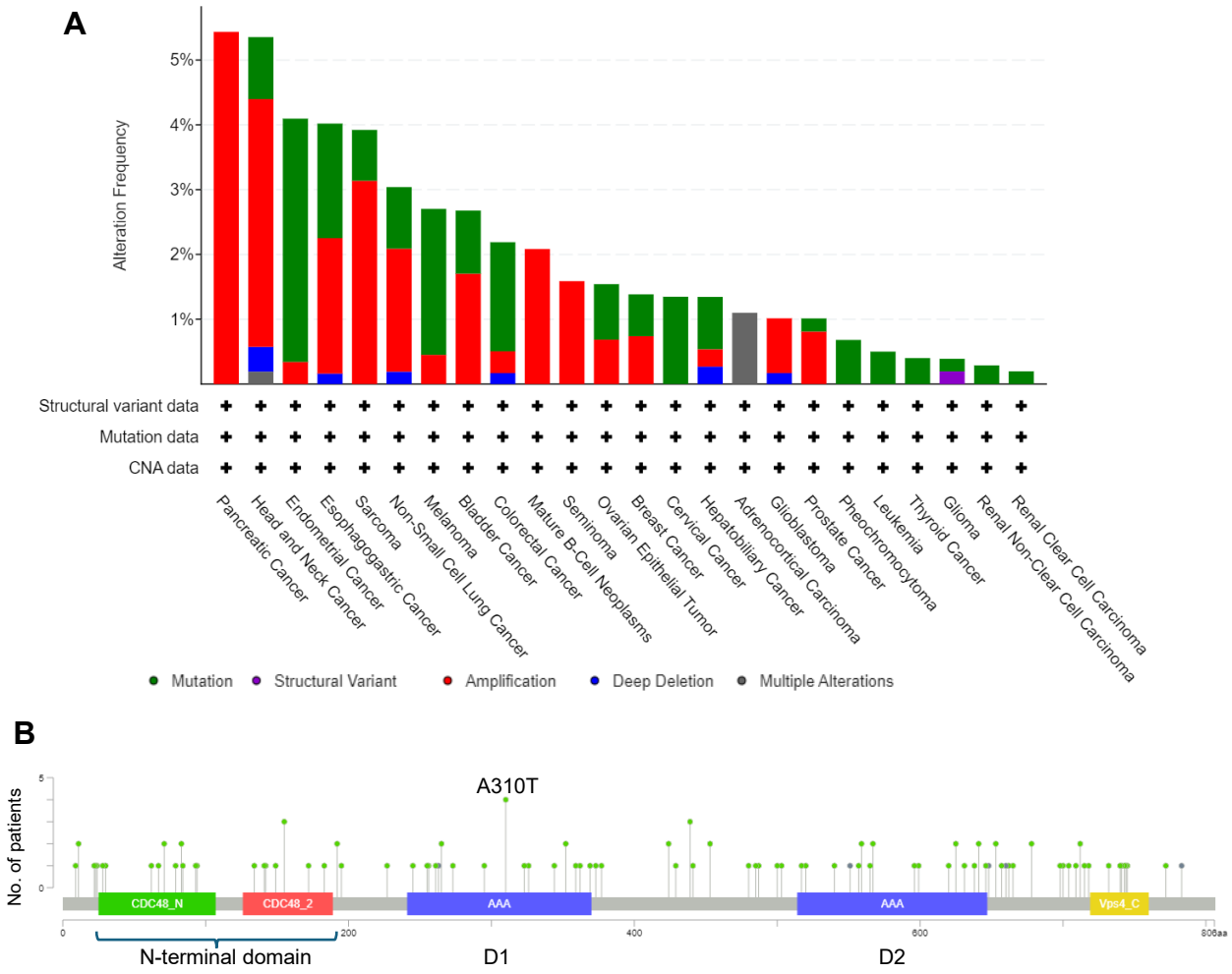

Figure 8: *p97* genomic alterations in cancer. (**A**) Frequency of *p97* genomic alteration across different types from 10967 samples taken from 10953 patients in the TCGA PanCancer Atlas. Red indicates amplification and green indicates mutation. (**B**) Diagram showing the site of mutations observed in p97 and how many patients they occurred in across the TCGA PanCancer Atlas. Green dots indicate missense mutations and grey indicate truncating mutations. The most frequent mutation is A310T which occurred in 4 patients. Plots taken from cBioPortal.

Many studies into the association of p97 with cancer have found that high levels of p97 expression correlate with poor prognosis and increased metastasis (Costantini,

Capone, Polo, Bagnara, & Budillon, 2021; Y. Cui et al., 2015; S. Yamamoto, Tomita, Hoshida, et al., 2004; S. Yamamoto, Tomita, Hoshida, et al., 2003; S. Yamamoto, Tomita, Nakamori, et al., 2003), including in cancers where PARPi-treatment is used, as summarised in Table 1. Whilst p97 has pleiotropic roles, chromatin-associated p97 function is relevant for cancer prognosis, as shown by the correlation between increased levels of chromatin-associated Ser784 phosphorylation on p97 and poorer survival in breast cancer patients receiving chemotherapy (Zhu et al., 2020).

Cancer	**Features associated with higher p97 levels**
Pancreatic	Increased malignancy of pancreatic endocrine neoplasms (S. Yamamoto, Tomita, Nakamori, et al., 2004) Increased tumorigenicity and poorer OS (Marin-Muller et al., 2013)
Breast	Higher p97 levels in cancerous compared to normal mammary epithelial cells (Y. Cui et al., 2015) Increased lymph node metastasis and poorer OS (Y. Cui et al., 2015; C. Li et al., 2021) Heightened cancer stem cell integrity and proliferation (C. Li et al., 2021)
Prostate	Worse PFS and OS (Tsujimoto et al., 2004) Increased proliferation, migration and invasion (Duscharla, Reddy Kami Reddy, Dasari, Bhukya, & Ummanni, 2018)
Ovarian	Improved PFS (Choi et al., 2020)

Table 1: A summary of the association of p97 expression with patient outcome for cancers where PARPi treatment is relevant. Adapted from Costantini et al. (2021)

Inhibitors of p97 were initially generated as a research tool, with the first being DBeQ, an inhibitor of the D1 and D2 ATPase domains that hinders both the autophagic and proteasomal-associated functions of p97 (Chou et al., 2011). This falls into the reversible, ATP-competitive class of p97 inhibitors, with two additional

classes being reversible non-ATP competitive inhibitors, which target allostery within p97 rather than the ATP-binding site itself, and covalent inhibitors (Kilgas & Ramadan, 2023). Having a broad range of inhibitors with varying target sites and mechanisms of action has helped to improve understanding of how p97 functions and may aid in clinical translation. All p97 inhibitors generally show similar phenotypes, albeit with varying potency, of accumulation of ubiquitinated substrates, induction of ERAD and unfolded protein response and anti-proliferative effects in cancer cells (Anderson et al., 2015; Magnaghi et al., 2013; Blandine Roux et al., 2021).

Development of p97 inhibitors as research tools has resulted in two inhibitors entering clinical trials for cancer therapy. The first was CB-5083, a reversible, ATP-competitive inhibitor highly selective for D2 ATPase inhibition (Anderson et al., 2015; Tang, Odzorig, Jin, & Xia, 2019). It was shown to have a high potency and anti-proliferative effects across 350 cell lines, and a panel of xenograft models of both solid and haematological tumours, due to its ability to induce ER and proteotoxic stress and G1 arrest (Anderson et al., 2015; B. Roux et al., 2021; Zhou et al., 2015). However, after entering phase I clinical trials for advanced solid tumours and multiple myeloma, it was discontinued due to ophthalmological side effects caused by an off-target effect on phosphodiesterase VI (PDE6), a regulator of phototransduction (Kilgas & Ramadan, 2023; Leinonen et al., 2021). To overcome this issue, CB-5339 was developed and entered phase I clinical trials. It has a similar potency and sensitivity profile as CB-5083 across a panel of cell lines but higher bioavailability and, crucially, 15-fold lower activity towards PDE6 (B. Roux et al., 2021).

These drugs certainly show promise in cancer therapy, with the p97-dependence of tumours over normal tissues making it an attractive target. However, as the discontinued CB-5083 clinical trial showed, off-target effects are an issue. ATP-competitive inhibitors may bind to other enzymes (Leinonen et al., 2021), and the highly pleiotropic nature of p97 activity means it is difficult to target one tumorigenic role of p97 without endangering other roles that are essential in normal tissue. Alternative strategies could come from combination therapies, such as with DNA damaging agents which show strong synergy with p97 inhibition. This was observed in an acute myeloid leukaemia mouse model where standard-of-care genotoxic agents prolonged survival when combined with p97 (B. Roux et al., 2021), and in a screen of 200 inhibitors targeting different pathways, where p97 inhibition best synergised with DNA damaging agents (Magnaghi et al., 2013). In relation to PARPi, we previously demonstrated that two p97 inhibitors, CB-5083 and CuET, enhanced sensitivity to talazoparib in cancer cells, mouse- and patient-derived organoids (Krastev et al., 2022). Alternatively, targeting co-factors or their interaction with p97 could enable specificity of inhibition. For instance, targeting SPRTN could impair the DPC-associated function of the p97 system without affecting global protein homeostasis (Kilgas & Ramadan, 2023). Some inhibitors have already been identified which inhibit p97 indirectly by targeting its co-factor NPL4, such as CuET, which impairs p97-mediated protein degradation for anti-proliferative effect towards cancer cells (Skrott et al., 2017) and thonzonium bromide, which blocks p97-NPL4 binding, inhibiting tumour growth by enhancing antitumour immunity (Nie et al., 2024). Improved understanding of p97-associated pathways is essential for developing this as a viable means of therapy. In the case of p97-trapped PARP1

activity, improved understanding of regulation through co-factor and E3 ligase activity, as well as post-p97 downstream processing is required.

1.4 Autophagy

1.4.1 Autophagy pathway

p97 is a key regulator of protein homeostasis, best described through its association with proteasomal degradation, but also acting alongside Macroautophagy (hereafter referred to as autophagy). Autophagy is an essential pathway for cellular homeostasis, where proteins and organelles are degraded and cellular material recycled, best described in relation to nutrient stress induced by starvation. It involves the formation of double-membrane vesicles, termed autophagophores, which surround cargo, and then fuse with lysosomes, resulting in cargo degradation (Morishita & Mizushima, 2019). This process can be broken down into stages: initiation, nucleation, expansion, maturation, fusion and degradation (X. Li, He, & Ma, 2020), as is summarised in figure 9.

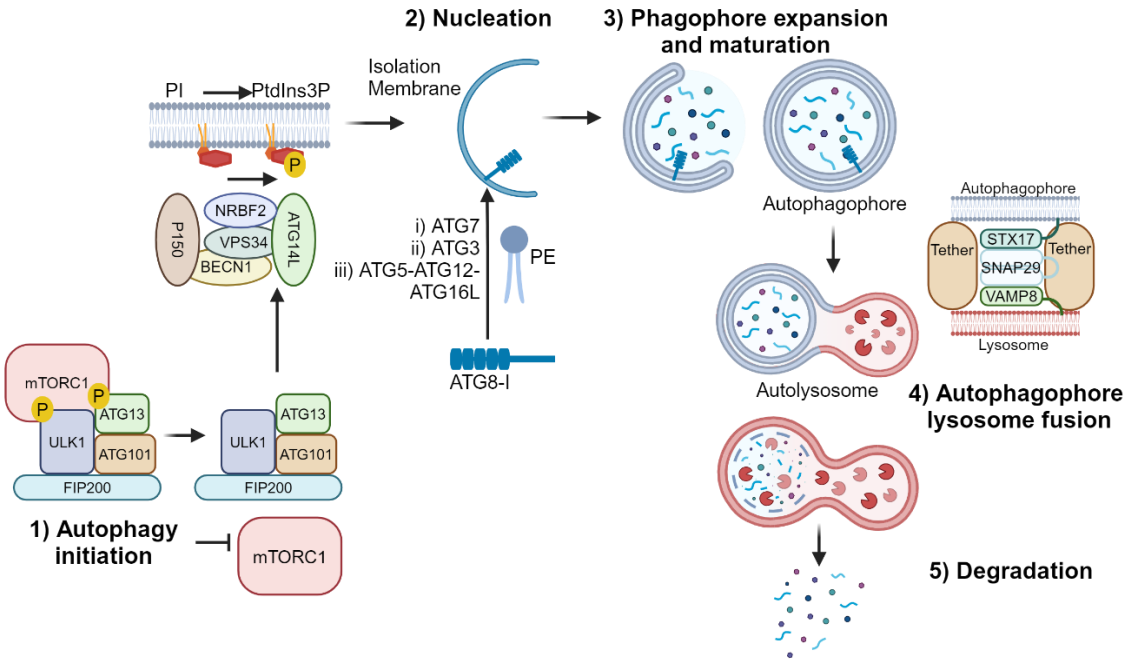

Figure 9: The autophagy pathway

During the initiation step, the ULK complex, consisting of ATG13, FIP200, ATG101 and ULK1/2, is activated by phosphorylation from upstream signalling hubs, such as AMP-activated protein kinase (AMPK) which is essential in nutrient and energy signalling. Signalling is finely balanced by opposing actions of AMPK and the autophagy-inhibitory activity of mechanistic target of rapamycin complex 1 (mTORC1), a signalling hub involved in response to a variety of autophagy-associated stressors (Jung et al., 2009; Nakatogawa, 2020). After initiation, the ULK complex mediates nucleation by phosphorylating the Beclin-1-VPS34 complex for its activation. This complex acts as a phosphatidylinositol 3-kinase (PI3K) which catalyses local formation of phosphatidylinositol-3-phosphate (PI3P) on sites of autophagophore formation, termed isolation membranes or phagophores (Axe et al., 2008; Nakatogawa, 2020). The source of isolation membranes is still unclear, with some suggesting they originate from ER-mitochondria contact sites (Hamasaki et al., 2013), whilst other evidence suggests they arise from ATG9-vesicles (H. Yamamoto et al., 2012).

The increased local concentration of PI3P serves as a platform to recruit a host of autophagy-related (ATG) genes to the isolation membrane (Nakatogawa, 2020). They co-ordinate expansion and eventual fusion of the edges of the isolation membrane into a mature autophagophore. In yeast, 40 *ATG*-genes have been described to date, with half of these having clear homologs in mammals (S. Liu, Yao, Yang, Liu, & Wang, 2023; Tsukada & Ohsumi, 1993). Phagophore expansion is still being understood, but ATG2 and ATG9 are believed to be involved, with ATG2 mediating phospholipid transport from the ER, aided by the lipid scramblase activity of ATG9 (Noda, 2021). ATG12 and ATG8 conjugation cascades, similar to ubiquitination cascades, are key during autophagophore biogenesis. ATG8 is a

ubiquitin-like protein, post-translationally cleaved at its C-terminus by ATG4 to expose a glycine residue for conjugation onto phosphatidylethanolamine (PE) lipids. This is mediated by ATG7, acting as an E1-activating enzyme, followed by ATG3, an E2-like conjugating enzyme. The ATG12-ATG5-ATG16L E3-like complex which mediates ATG8 transfer to PE is formed in a similar cascade involving ATG12 conjugation by ATG7 (E1-like) and ATG10 (E2-like) (Mizushima, Noda, et al., 1998; Mizushima, Sugita, Yoshimori, & Ohsumi, 1998). ATG8 conjugation to PE results in its tight association with the autophagophore membrane (Kabeya et al., 2000; Mizushima, 2020). In mammals, ATG8-family proteins include MAP1LC3 (hereafter referred to as LC3), GATE-16 and GABARAP (Slobodkin & Elazar, 2013). In the case of LC3, its cytosolic form, LC3-I, is converted to its PE-conjugated form, LC3-II, which associates with the autophagophore. ATG8 promotes expansion, maturation and transport of the autophagophore by regulating interaction with other core autophagy machinery proteins (Fu, Nirschl, & Holzbaur, 2014; Kraft et al., 2012; Kumar et al., 2018; Nakatogawa, 2020; Nakatogawa et al., 2012; Weidberg et al., 2011).

After the isolation membrane seals into an autophagophore, it fuses with a lysosome to form a mature degradative autolysosome. This involves Rab GTPases, tether proteins and SNARE complexes and is tightly regulated to prevent premature fusion before the autophagophore is sealed (Y. G. Zhao, Codogno, & Zhang, 2021). Syntaxin-17 is key in this process and is recruited to the autophagophore only after its closure by IRGM, which interacts with LC3 through its own LC3-interacting region (LIR) (Kumar et al., 2018). Syntaxin-17 then recruits SNAP29 and interacts with VAMP8 on the lysosome membrane to form a SNARE complex that mediates fusion, aided by tethers which promote initial capture (Itakura, Kishi-Itakura, &

Mizushima, 2012; Y. G. Zhao et al., 2021). Degradation of autolysosome contents relies on hydrolases within the lysosome, including nucleases, proteases, lipases and glycosylases. The inner autolysosome membrane is degraded alongside cargo, allowing the release of syntaxin-17 from the membrane (Tsuboyama et al., 2016). This requires acidic conditions, so V-ATPase proton pumps are essential for acidification of the autolysosome to generate degradative conditions (Yoshimori, Yamamoto, Moriyama, Futai, & Tashiro, 1991).

As previously mentioned, p97 has multiple roles throughout the autophagy pathway. During autophagy initiation, p97 scaffolds the association of the DUB ataxin-3 with Beclin-1, a component of the Beclin-1-VPS34 PI3K complex, stabilising Beclin-1 by reducing its ubiquitin-guided proteasomal degradation. p97 also promotes assembly of the remaining members of the Beclin-1-VPS34 complex, inducing autophagy (Hill et al., 2021; Z. Wang et al., 2024; Wrobel, Hill, Ashkenazi, & Rubinsztein, 2021). This acts alongside an additional autophagy-related role of p97 in maturation of autophagosomes for their fusion with lysosomes (Ju et al., 2009; Tresse et al., 2010).

1.4.2 Selective autophagy

Autophagy was initially characterised as a bulk process, where cytosolic contents are indiscriminately engulfed by the growing phagophore and degraded in the lysosome, allowing cells to survive through a period of starvation. A similar but selective process has since been described, termed selective autophagy, which permits the degradation of specific cargo, such as damaged organelles or misfolded proteins, as directed by selective autophagy receptors (SARs). SARs contain LIR motifs which facilitate its binding to LC3 and GABARAP proteins. This highly

conserved motif consists of $[W/F/Y]_0$-X_1-X_2-$[L/V/I]_3$ and usually accompanies downstream Asp, Glu, Ser or Thr residues that serve as phosphorylation sites to regulate LC3 binding (Johansen & Lamark, 2020; Rozenknop et al., 2011). Selective autophagy is often governed by ubiquitination of cargo proteins, meaning receptors commonly contain ubiquitin-binding domains that are key for bridging cargo to the LC3-containing growing autophagophore (Khaminets, Behl, & Dikic, 2016; Kirkin, McEwan, Novak, & Dikic, 2009).

The first selective autophagy process described in mammals was targeting of damaged mitochondria in mice, termed mitophagy (I. Kim, Rodriguez-Enriquez, & Lemasters, 2007). This process is initiated by Parkinson's-associated proteins (Kitada et al., 1998; Valente et al., 2004) PINK1 kinase and PARKIN E3 ligase which accumulate and catabolise phosphor-ubiquitin chains on damaged mitochondria (Kane et al., 2014; Koyano et al., 2014; Narendra, Tanaka, Suen, & Youle, 2008; Sarraf et al., 2013). SARs, such as OPTN and NDP52 (Lazarou et al., 2015), recognise these markers and bridge to LC3 on phagophores. They also aid in autophagosome biogenesis through interaction with FIP200, a component of the ULK1 complex (Lazarou et al., 2015; Vargas et al., 2019), ATG9A vesicles (Yamano et al., 2020) and ATG5-ATG12-ATG16L1 (Bansal et al., 2018). In a similar way, ubiquitination by TRIM16 governs selective autophagy of damaged lysosomes, known as lysophagy, and also interacts with core autophagy machinery to initiate autophagophore biogenesis (Kumar et al., 2017). Damaged lysosomes tagged by ubiquitination are bridged to the phagophore by the SAR p62 (Vargas, Hamasaki, Kawabata, Youle, & Yoshimori, 2023). As they contain hydrolytic enzymes, isolation and degradation of damaged lysosomes is essential for cell survival.

The irreversible nature of all forms of selective autophagy implies that it requires a high level of regulation. SARs contribute to this considerably, as do post-translational modifications (PTMs). Ubiquitination and phosphorylation of cargo have already been discussed, but further levels of regulation are achieved through receptor modification. The receptor p62 exemplifies this, with ubiquitination of its ubiquitin-binding domain promoting cargo binding (Y. Lee et al., 2017), whilst ubiquitination at its lysine 7 residue impairs its ability to oligomerise which is key for its function (Pan et al., 2016). Phosphorylation of residues N-terminal to the LIR motif in a multitude of SAR and other LIR-containing proteins has been shown to promote its association with LC3 (Johansen & Lamark, 2020). Interestingly, p97 has also been implicated in the regulation of selective autophagy, through its ability to segregate proteins from target organelle membranes and scaffold recruitment of DUBs. p97 extracts ubiquitinated mitofusins from damaged mitochondria tagged for mitophagy, shuttling these large GTPases for proteasomal degradation and preventing their activity in fusing mitochondria, to promote mitophagy (Tanaka et al., 2010). During lysophagy, recruitment of p97 and its DUB co-factor YOD1 downstream of p62 drives the removal of K48-ubquitin-labelled conjugates, driving autophagophore formation (Papadopoulos et al., 2017). This further highlights the importance of p97 across all forms of cell homeostasis.

1.4.3 TEX264

One important detail of the p97 system in relation to selective autophagy is the p97 co-factor TEX264, described earlier for its targeting of TOP1cc for p97-dependent clearance from chromatin (Fielden et al., 2020). Alongside a SHP box for its interaction with p97, TEX264 contains a LIR motif, suggesting it could function as a SAR. Indeed, two groups have descried the receptor function of TEX264 in selective

autophagy of the ER (reticulophagy), a process that occurs in response to ER stress (An et al., 2019; Chino, Hatta, Natsume, & Mizushima, 2019). Using proteomics, TEX264 was identified as a protein which is depleted under starvation or mTOR inhibition in an ATG7-dependent manner (An et al., 2019), suggesting it is degraded by autophagy, and interacts with LC3 but not an LC3 mutant unable to bind LIR-containing proteins (Chino et al., 2019), indicating it contains a LIR motif. Indeed, a C-terminal LIR motif was identified (F_{273}EEL) that governed co-localisation of TEX264 to LC3 punctate structures, characteristic of autophagosomes, and early autophagy machinery, indicating a role at the early stages of phagophore nucleation and expansion (An et al., 2019; Chino et al., 2019). More recent work has uncovered phosphorylation sites several residues downstream of the LIR motif that enhance LC3 binding (Chino et al., 2022), similar to other SARs. It was determined that TEX264 acts as a reticulophagy receptor through its N-terminal leucine-rich region (Fielden et al., 2020) which forms a transmembrane domain, bridging LC3-tagged phagophores to damaged ER membranes and proteins (An et al., 2019; Chino et al., 2019) in a ubiquitin-independent manner. This, alongside work from our group, has revealed further structural details about TEX264, such as its gyrase inhibitor (GyrI)-like domain, two SIMs and TOP1-binding site, shown in figure 10 (An et al., 2019; Chino et al., 2019; Chino et al., 2022; Fielden et al., 2020).

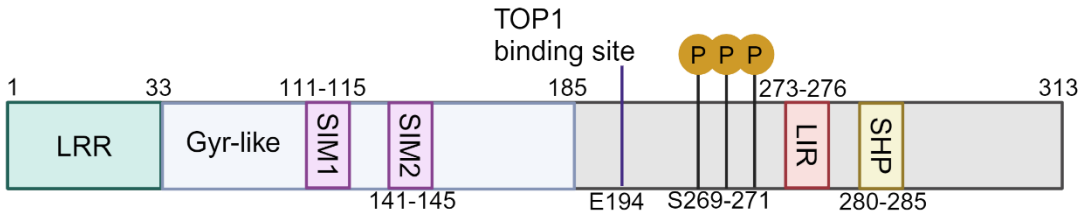

Figure 10: Schematic of TEX264 domains. "P" indicates phosphorylation sites.

As well as its localisation to the ER, TEX264 is found at the nuclear periphery. Due to its role in both DNA repair and reticulophagy, this raises the interesting question of whether its activity as a nuclear p97 co-factor and SAR may coincide in mediating selective autophagy of the nucleus (Fielden, Popovic, & Ramadan, 2022).

1.4.4 Autophagy in genome stability

So far, I have mainly described autophagy as a cytosolic process, but it is also associated with promoting genome stability. Broadly, this is observed in ageing, with a reduction in autophagic activity likely to contribute to the increase in genome instability caused by less efficient DNA repair (Ambrosio & Majello, 2020). In response to genotoxic stress caused by radiation, reactive oxygen species (ROS) and oncogenes, major sensors and signalling hubs involved in DDR signalling also activate autophagy. ATM activation in response to DSBs initiates a cascade which induces autophagy through AMPK activation and mTORC1 inhibition (Alexander et al., 2010). PARP1 also acts through AMPK activation as its hyperactivity during genotoxic stress causes a reduction in NAD+ and ATP availability, thus an increase in AMP which is sensed by AMPK (Rodríguez-Vargas et al., 2012). Transcriptional activation of various genes by TP53 also drives autophagy in response to DNA damage. This includes *ATG7*, *ULK1* and *ULK2* (Kenzelmann Broz et al., 2013), damage-regulated autophagy modulator (*DRAM1*), which encodes a lysosomal protein named for its link between DNA damage signalling and autophagy (Crighton et al., 2006), and Sestrin family genes (SESNs) which are negative regulators of mTORC1 signalling (Ambrosio & Majello, 2020; Budanov & Karin, 2008).

Autophagy regulates the DDR by influencing cell cycle progression, senescence and cell death, as well as modulating the activity of particular DDR machineries

(Ambrosio & Majello, 2020). In replicating cells, autophagy was found to be essential for recovery from oncogenic-induced replication stress by maintaining the pool of nucleotides needed for DNA replication (Vanzo et al., 2020). This is likely a result of autophagic degradation of ribosomal RNA providing substrates for dNTP synthesis (W. Chen et al., 2014; Y. Liu et al., 2018). More specific functions of autophagy in the DDR have been explored in the case of DSB repair, where loss of autophagy causes HR-deficiency. Whilst the mechanisms behind this are somewhat unclear, various studies have implicated the role of nuclear p62 in sequestering HR-regulatory proteins such as filamin A, RAD51 and RNF168. As p62 is degraded by autophagy, inhibition of autophagy causes increased p62 levels so reduced availability of filamin A, RAD51 and RNF168 and, thus, reduced HR (Cahuzac et al., 2022; Hewitt et al., 2016; Y. Wang et al., 2016).

More selective autophagic processes also associate with the DDR. For instance, the autophagic degradation of Lamin B1 and Lamin A/C, through its direct interaction with LC3 in the nucleus, was shown to mediate senescence specifically in response to oncogenic stress (Dou et al., 2015; Lenain, Gusyatiner, Douma, van den Broek, & Peeper, 2015; Y. Li et al., 2019). Loss of nuclear lamina allows extrusions of nuclear material into the cytosol, a key signal for induction of senescence. Beyond this, selective autophagy of nuclear content, referred to as nucleophagy, was recently suggested to directly clear DNA lesions. The TOP2 poison etoposide stabilises the TOP2-DNA intermediate, TOP2cc, and causes persistent DNA breaks. It was shown that etoposide induces the formation of nuclear buds and micronuclei that contain markers of the autophagic pathway, as well as TOP2 itself. This implies that the autophagic machinery could be directly involved in clearance of lesions such as TOP2cc (Muciño-Hernández et al., 2023).

Interestingly, p97 also aids in repair of TOP2cc (Y. Sun et al., 2022). As these lesions are DPCs, similar to TOP1cc, it raises the question of whether TOP1cc-associated SAR TEX264 could have an autophagic role in genome stability by responding to DPC and DPC-like lesions. Interestingly, and in parallel work to this study, we recently demonstrated a novel pathway of selective nucleophagy where TOP1cc induced by TOP1 poisons were cleared from chromatin via TEX264, utilising its p97 co-factor and SAR function (Lascaux et al., 2024). The proteinaceous TOP1 adduct as well as DNA fragments that it covalently binds to were found to localise in the lysosome, and autophagy machinery was identified at the replication fork (Lascaux et al., 2024) where TOP1cc lesions are most troubling (Sakasai & Iwabuchi, 2016), indicating selective nucleophagy can directly process these lesions. However, it is unclear whether this is a unique repair pathway or if it has relevance for other DPC and DPC-like lesions.

1.4.5 Autophagy in Cancer

Autophagy is associated with cancer, first shown by reduced Beclin-1 expression and autophagy activity in breast cancer (Liang et al., 1999). However, its role is complex, with different functions depending on cancer stage and type. Nevertheless, the general finding is that autophagy suppresses tumorigenesis but once a tumour is established, it promotes tumour growth (Hama, Ogasawara, & Noda, 2023). Autophagy association with tumorigenesis is linked to known tumour-suppressor genes such as *TP53*, a tumour suppressor mutated more frequently than any other. Particular mutants that fail to localise to the nucleus prevent its transactivating activity, described earlier, leading to suppressed autophagy through transcriptional repression of autophagy-related genes (S. Agarwal, Bell, Taylor, & Moran, 2016; Morselli et al., 2008). Suppression of autophagy may lead to

tumorigenesis through various mechanisms, including increased genome instability and accumulation of ROS through impaired mitophagy. In the development of hepatomas, p62 accumulation in autophagy-deficient cells promotes tumorigenesis by sequestering the E3 ligase KEAP1, causing accumulation of its target NRF2 that acts as a pro-proliferative transcription factor (Inami et al., 2011). However, in established tumours, likely due to their high bioenergetic demand, autophagic degradation is required to supply nutrients under metabolic and hypoxic stress (Guo, Xia, & White, 2013). This is best exemplified in KRAS-transformed tumours which have a higher basal level of autophagy. When this is impaired, abnormal mitochondria accumulate and cells experience energy depletion, leading to tumour regression in mouse models (Guo et al., 2011; S. Yang et al., 2011). This implies that autophagy could be a good target for cancer therapy.

Chloroquine (CQ) and its derivative hydroxychloroquine (HCQ) are autophagy inhibitors used against malaria with high tolerability. They induce lysosomal damage by accumulating in lysosomes, impairing autophagy at the stage of degradation. In phase II clinical trials in a variety of cancers, they have shown efficacy when used in combination with standard chemotherapy, such as in pancreatic and hepatocellular cancer patients (Arora et al., 2021; Zeh et al., 2020), and even improved symptoms when used alone, as was observed in prostate cancer patients (George et al., 2017). However, other trials show only partial or no improvement over conventional therapy, often in more advanced cancers (Hama et al., 2023; Karasic et al., 2019), even suggesting that sufficient autophagy inhibition is not achieved with CQ and HCQ (Rosenfeld et al., 2014). This raises the issue of developing improved clinically viable autophagy inhibitors. Various inhibitors have been developed for ULK1/ULK2 (Egan et al., 2015; Ren et al., 2020) and ATG7

(Huang et al., 2020), amongst others, that show high specificity, anticancer potency and synergy with other inhibitors. More recently, inhibitors that directly target protein-protein interactions have been developed to impair interaction between particular ATG proteins, such as ATG5-ATG16L1 (J. Cui et al., 2022). Whilst none of these inhibitors have entered into clinical trials yet, it is hoped that their higher specificity could improve patient outcomes compared to CQ and HCQ. Enhanced understanding of autophagy function in cancer progression and response to certain therapies could also allow the development of more specific inhibitors for certain autophagy pathways.

Whilst not tested in the clinic, combined PARPi and autophagy inhibition has been explored pre-clinically, showing promising results. In line with other genotoxic agents, numerous studies across various cancers have shown that all clinically approved PARPi enhance autophagy flux. Most studies also agree that inhibition of autophagy, either chemically or genetically, sensitises model systems to PARPi (Cahuzac et al., 2022; Elshazly, Nguyen, & Gewirtz, 2022; Y. Liu et al., 2019; Pai Bellare, Saha, & Patro, 2021; Pai Bellare & Sankar Patro, 2022; Ren et al., 2020; Santiago-O'Farrill et al., 2020; Uddin et al., 2022). This has been suggested to be ROS-dependent, with impaired PARP activity causing ROS accumulation that cannot be resolved in cells deficient in autophagy (Santiago-O'Farrill et al., 2020). Synergy between autophagy and PARP inhibition has also been linked to HR-deficiency caused by accumulated p62 in autophagy deficient cells, with activation of autophagy prior to PARPi treatment causing reduced p62 and increased BRCA1 and RAD51 foci, a marker of increased HR (Cahuzac et al., 2022). A higher level of basal autophagy has also been observed in PARPi-resistant cells, with it proposed that lower p62 levels in these cells contributes to their resistance (Uddin et al.,

2022). However, evidence presented in these studies is minimal, so further work is needed to comprehensively understand the association between autophagy and PARPi. Interestingly, the strongest evidence supporting cytoprotective autophagy is in response to talazoparib (Elshazly et al., 2022), the strongest trapping agent (Murai et al., 2014; Shen et al., 2013). Despite this, no studies have explored whether autophagy has a more direct role at trapped PARP1, as has been suggested for other nucleophagy substrates such as the nuclear lamina, TOP1cc or TOP2cc. If autophagy inhibition is to be translated to the clinic for combination therapy with PARPi, details surrounding its function in PARPi response must be elucidated.

1.5 Aims of this study

Resistance to PARPi is a major clinical challenge. Research focuses on improved detection of *de novo* resistance through biomarkers, therapeutic strategies that reduce the risk of resistance arising and treatments that overcome resistance. Therefore, it is important to investigate PARPi response and tolerance mechanisms to identify how they could be exploited. Our group recently discovered a p97-dependent mechanism for the removal of trapped PARP1, the driver behind PARPi cytotoxicity. My aim was to further understand the role of the p97 system and downstream degradation pathways in the removal trapped PARP1 from chromatin. The specific aims of this study were:

1. Identify p97 co-factor(s) that may aid p97-mediated trapped PARP1 removal from chromatin.
2. Determine how trapped PARP1 is processed after its p97-mediated extraction from chromatin.

3. Investigate the cellular consequences of impaired trapped PARP1 processing.

2. Materials and Methods

2.1 Buffers

2.1.1 10x Phosphate buffered saline (PBS)

5 L of 10x PBS (1370 mM NaCl, 27 mM KCl, 100 mM $Na_2HPO_4x2H_2O$, 18 mM KH_2PO_4) was prepared by combining the following in 4.5 L of deionised water:

400.3 g NaCl (Sigma, S9625)

10.2 g KCl (Sigma, P9541)

89 g $Na_2HPO_4x2H_2O$ (Sigma, 71645)

12.52 g KH_2PO_4 (Sigma, P0662)

After stirring until dissolved, the pH was confirmed to be between 7.3 and 7.5 before topping up the solution to 5 L.

2.1.2 10x Tris buffered saline (TBS)

5 L of 10x PBS (250 mM Tris, 1500 mM NaCl, 25 mM KCl) was prepared by combining the following in 4.5 L of deionised water:

151.4 g Trizma-base (Sigma, T6066)

438.3 g NaCl (Sigma, S9625)

9.32 g KCl (Sigma, P9541)

After stirring until dissolved, the pH was adjusted to 7.6 with 13 M HCl before topping up to 5 L. TBST was prepared by adding 1 mL of tween-20 to 1 L of 1x TBS.

2.1.3 10x Tris/Glycine buffer

5 L of 10x Tris/Glycine (250 mM Tris, 1920 mM Glycine) was prepared by combining the following in 4.5 L of deionised water:

151.4 g Trizma-base (Sigma, T6066)

720.7 g Glycine (Sigma, G7126)

After stirring until dissolved, the pH was confirmed to be between 8.3 and 8.6 before topping up the solution to 5 L.

2.1.4 5x Laemmli buffer

Laemmli buffer is used to denature and load protein samples for Western blot. 40 mL of 5x Laemmli buffer (312.5 mM Tris-HCl, 10% SDS, 50% glycerol, 12.5% β-mercaptoethanol, 0.01% bromophenol blue, pH 6.8) was prepared by mixing the following in 35 mL of deionised water:

4 g SDS (Merck, L3771)

20 mL 100% glycerol (Merck, G7757)

4 mL 3.125 M Tris-HCl (pH 6.8) prepared in advance as a 10x solution

The components were dissolved by intermittent heating in a microwave and mixing with a vortex. Once dissolved, the volume was adjusted to be 40 mL with deionised water, then 400 µL of 1% bromophenol blue was added. The solution was mixed by vortexing and 1 mL aliquots were made and stored at -20°C. Before use, 125 µL of β-mercaptoethanol was added.

2.1.5 Buffers for polyacrylamide gel preparation

500 mL of 4x separating buffer (1.5 M Tris, 0.4% SDS) was prepared by dissolving 91 g of Trizma base in 300 mL of deionised water. The pH was adjusted with 13 M HCl until reaching 8.8. 2 g of SDS was dissolved in the solution before bringing the volume to 500 mL. This was used for making the separating layer of polyacrylamide gels.

100 mL of 4x stacking buffer was prepared by dissolving 6.05 g of Trizma-base in 50 mL of deionised water. The pH was adjusted to 6.8 with concentrated HCl, then 0.4 g of SDS was added to the solution and stirred until dissolved. The volume was topped up to 100 mL. This buffer was used for making the stacking layer of polyacrylamide gels.

2.1.6 5x Tris-Acetate-EDTA buffer (TAE)

5 L of TAE (200 mM Tris, 10 mM EDTAx2H_2O, 100 mM acetic acid) was prepared by combining the following in 4.5 L of deionised water:

121.19 g Trizma-base (Sigma, T6066)

18.6 g EDTAx2H_2O

28.6 mL glacial acetic acid

After stirring until dissolved, the pH was adjusted to 8.5 with 13 M HCl before topping up the solution to 5 L.

2.1.7 Potassium phosphate buffered saline (KPBS)

1 L of KPBS (136 mM KCl, 10 mM KH_2PO_4) was prepared by combining the following in 900 mL of Mili-Q water:

10.13 g KCl (Sigma, P9541)

1.36 g KH_2PO_4 (Sigma, P0662)

After stirring until dissolved, the pH was adjusted to 7.25 using pellets of KOH before topping up the solution to 1 L. The solution was autoclaved and stored at 4°C.

2.2 Materials and reagents

The following tables list reagents and materials used in this study

Reagent	**Catalogue number**	**Supplier**
Lipofectamine RNAiMAX	13778075	Invitrogen
FuGENE HD Transfection reagent	E2311	Promega
Polyethylenimine (PEI) transfection reagent	7854	Tocris
Benzonase enzyme	71205	Merck Millipore
Veliparib	S1004	Selleckchem
Talazoparib	S7048	Selleckchem
Olaparib	S1060	Selleckchem
CB-5083	S8101	Selleckchem
Bafilomycin A1	B0025	LKT
Torin-1	14379	Cell Signalling Technology
Doxycycline	A2951,0025	PanReac AppliChem
Pen-Strep	P4333	Sigma-Aldrich
Dulbecco's Modified Eagle Medium	D6429	Merck
FluoroBrite™ DMEM	A1896702	Gibco

Opti-MEM™ Reduced Serum Medium	31985070	Gibco
Fetal bovine serum	A5256801	Thermo Fisher Scientific
Resazurin powder	R7017-1G	Sigma Aldrich
DAPI	D9542	Sigma Aldrich
LysoView™ 680	70086	Biotium
Fluoromount-G™ Mounting Medium	00-4958-02	Invitrogen
ProLong™ Glass Antifade Mountant	15898391	Invitrogen
Precision Plus Protein Dual Colour Standards	1610374	BioRad
40 % acrylamide/bisacrylamide	A3699	Merck
Tetramethylethylenediamine (TEMED)	T9281	Sigma Aldrich
Pierce anti-HA magnetic beads	88837	Thermo Fisher Scientific
GFP-Trap® Magnetic Particles M-270	gtd-20	ChromoTek
9 mm no. 1 thickness glass coverslips	10313573	Fisher scientific
NHeI-HF	R3131S	New England Biolabs
EcoRV-HF	R3195S	New England Biolabs
Q5® High-Fidelity 2X Master Mix	M0429	New England Biolabs
Quick-Load® Taq 2X Master Mix	M0271L	New England Biolabs
MycoAlert™ Mycoplasma Detection Kit	LT07-318	Lonza Bioscience
NEBuilder® HiFi DNA Assembly Cloning Kit	E5520S	New England Biolabs
Monarch® DNA Gel Extraction Kit	T1020L	New England Biolabs
QIAquick PCR Purification Kit	28104	Qiagen

NEB® Stable Competent E. coli cells	C3040H	New England Biolabs
GeneJet RNA purification kit	K0731	ThermoFisher
NucleoSpin Plasmid miniprep kit	740588	Macherey-Nagel
Duolink® In Situ PLA® Probe Anti-Rabbit PLUS	DUO92002	Sigma-Aldrich
Duolink® In Situ PLA® Probe Anti-Mouse MINUS	DUO92004	Sigma-Aldrich
Duolink® In Situ Detection Reagents FarRed	DUO92013	Sigma-Aldrich
DC protein quantification	5000111	BioRad
SuperSignal™ West Pico PLUS Chemiluminescent Substrate	34579	Thermo Scientific

Table 2: Reagents and commercial kits. Catalogue numbers and suppliers are listed.

Antibody	**Catalogue number**	**Supplier**	**Dilution**
Anti-PARP1 (E102)	ab32138	Abcam	IF 1:100, WB 1:1000, PLA 1:250
Anti-Myc (9B11)	2276	Cell Signalling	IF 1:500
Anti-γH2AX (P-Ser139)	05-636	Millipore	IF 1:250
Anti-53BP1	4937S	Cell Signalling Technology	IF 1:250
Anti-RPA32	2208	Cell Signalling Technology	IF 1:250
Anti-GFP antibody	Ab290	Abcam	PLA 1:500
Anti-V5 antibody	R96025	Novex	PLA 1:500

donkey anti-Mouse Alexa Fluor 555	A-31570	Invitrogen	IF 1:500
donkey anti-Rabbit Alexa Flour 488	A-21206	Invitrogen	IF 1:500
Anti-HA (Y-11)	sc-805	Santa Cruz	WB 1:1000
Anti-LC3B	2775S	Cell Signalling Technology	WB 1:1000
Anti-Atg7 [D12B11]	8558	Cell Signalling Technology	WB 1:1000
Anti-LAMP1	21997-1-AP	Proteintech	WB 1:1000
Anti-TEX264	Homemade	Raimundo Freire lab	WB 1:1000
Anti-Vinculin (7F9)	sc-73614	Santa Cruz	WB 1:5000
Anti-p97	10736-1-AP	Proteintech	WB 1:1000
Anti-histone H3	ab1791	Abcam	WB 1:5000
Anti-UFD1	10615-1-AP	Proteintech	WB 1:1000
Anti-RNF4	NBP2-13243	Novus	WB 1:1000
Anti-DVC1	HPA025073	Atlas	WB 1:1000
Anti-ATX3	MAB5360	Millipore	WB 1:1000
Anti-STX17	HPA001204-100UL	Sigma Aldrich	WB 1:1000
Anti-Mouse IgG (whole molecule)–Peroxidase	A9044	Sigma Aldrich	WB 1:50,000
Anti-Rabbit IgG (whole molecule)–Peroxidase	A0545	Sigma Aldrich	

Table 3: Antibodies used in this study. Catalogue number and supplier are included, as well as dilution for specific purposes.

2.3 Cell culture

2.3.1 Cell line maintenance

CAL51 (DSMZ, ACC 302), HeLa (ATCC, CCL-2), MDA-MB231 (ATCC, Htb-26) and RPE hTERT *TP53*$^{-/-}$ *BRCA1*$^{-/-}$ (a gift from Madalena Tarsounas) were maintained in Dulbecco's Modified Eagle Medium (DMEM), supplemented with 10% fetal bovine serum and 1x penicillin–streptomycin. Cells were incubated at 37°C and 5% CO_2 and passaged every 48-72 hrs to maintain at sub-confluency.

2.3.2 siRNA and plasmids used in this study

siRNA (Table 4) was used in RNA interference experiments and plasmids (Table 5) were used for transfection and generation of stable cell lines.

RNAi	**Cat. No.**	**Supplier**	**Sequence**
si*TEX264*_7 (#1)		Microsynth	CTCATCGACCTCTACCAGAAA
si*TEX264*_8 (#2)		Microsynth	CGGCTGGAGATCTACCAGGAA
si*SPRTN*_3'UTR (#1)		Microsynth	GUCAGGAAGUUCUGGUUAA
si*SPRTN*_D2 (#2)	J-015442-21-0050	Dharmacon	
si*UFD1*_5 (#1)	L-017918-00-0005	Dharmacon	
si*UFD1*_6 (#2)	SI04132583	QIAGEN	CACTGGATGATGC-AGAACTTA
si*ATXN3*_4 (#1)		Microsynth	UGCGUCGGUUGUAGGACUAAA
si*ATXN3*_3'UTR-1 (#2)		Microsynth	GGAAUGUAGGUGUCUGCUU

si*ATG7*	J-020112-05-0010	Dharmacon	CCAACACACUCGAGUCUUU
si*VCP*_7		QIAGEN	AACAGCCAUUCUCAAACAGAA

Table 4: siRNA used in this study. Supplier, catalogue number and sequence are provided where available.

Plasmid name	**Use**	**Source**
pLX313-*TP53-WT*	Backbone for generation of pLX313 plasmids	AddGene No: 118014
pLX313-*TEX264-FL*	For expression of TEX264^{WT} and generation of stable cell lines	Generated here
pLX313-*TEX264-SHP**	For expression of TEX264^{SHP*} and generation of stable cell lines	Generated here
pLX313-*TEX264-LIR**	For expression of TEX264^{LIR*} and generation of stable cell lines	Generated here
pLX313-*V5_EV*	For generation stable cell line expressing empty vector V5	Generated here
pFIRES-PURO-*FLAG-RNF4-WT*	For transient over-expression of RNF4^{WT}	(Rojas-Fernandez et al., 2014)
pFIRES-PURO-*FLAG-RNF4-M136A+R177A* (E2 binding mutant)	For transient over-expression of dominant negative RNF4 mutant	(Rojas-Fernandez et al., 2014)
pLJC5-*TMEM192*-3xHA	For generation of HeLa and CAL51 TMEM stable cell lines for lysoIP	AddGene No. 102930
pLJC6-3XHA-*TMEM192*	For creation of HeLa TEX264$^{-/-}$ TMEM stable cell line for lysoIP	AddGene No. 104434

pmCherry-*PARP1*-eGFP	For mCherry-PARP1-GFP reporter assay	Generated by genome engineering facility at WIMM
pmCherry-eGFP	Backbone for generation of pmCherry-PARP1-eGFP	AddGene No. 86639
TEX264 CRISPR/Cas9 KO Plasmid (h)	For creation of TEX264$^{-/-}$ cell lines	Santa Cruz, sc-417333
TEX264 HDR Plasmid (h)	For creation of TEX264$^{-/-}$ cell lines	Santa Cruz, sc-417333-HDR
pAmphoR envelope plasmid	For creation of lentiviral particles	Gift from Vincenzo D'Angiolella
Δ8.2R packaging plasmid	For creation of lentiviral particles	Gift from Vincenzo D'Angiolella

Table 5: Plasmids used in this study. The plasmid name, purpose and source are listed.

2.3.3 siRNA transfection

Cells were transfected with siRNA using lipofectamine RNAiMAX according to manufacturer's instructions. Briefly, siRNA and RNAiMAX were incubated in Opti-MEM™ Reduced Serum Medium at room temperature before being added to cells for 4 hrs with half the usual volume of media. After 4 hrs, media was topped up or cells were seeded, as required for the specific experimental protocol. Experiments were carried out 72 hrs after siRNA transfection.

2.3.4 Plasmid DNA transfection

Transient transfection with plasmids was carried out using FuGENE HD Transfection reagent for microscopy-based experiments, according to

manufacturer's instructions. Briefly, plasmid DNA and FuGENE were mixed in Opti-MEM™ Reduced Serum Medium and incubated for 15 mins at room temperature before adding to cells with half the usual volume of complete DMEM. After 4 hrs, cells were trypsinised and seeded as required for the specific experiment which was carried out 24 hrs after transfection. For all other experiments, Polyethylenimine (PEI) transfection reagent was used according to manufacturer's instructions. PEI and DNA were incubated in Opti-MEM™ at 37°C for 15 mins before adding to cells with half the usual volume of media without FBS. After 4 hrs, media was replaced with complete media containing FBS and penicillin–streptomycin. Experiments were performed 24 hrs after DNA transfection.

2.3.5 Generation of stable cell lines

Stable cell lines (Table 6) were sourced from published literature or generated in this study.

Cell line	Source	Details of generation
CAL51 *PARP1*$^{-/-}$ *PARP1*^{WT}-GFP	Krastev et al. (2022)	
CAL51 *PARP1*$^{-/-}$ *PARP1*^{KS}-GFP	Krastev et al. (2022)	
CAL51 *PARP1*$^{-/-}$ *PARP1*^{WT}-GFP *TEX264*^{WT}-V5	Generated here	pLX313-TEX264-FL, 600 µg/mL hygromycin
CAL51 *PARP1*$^{-/-}$ *PARP1*^{WT}-GFP EV-V5	Generated here	pLX313-V5_EV, 600 µg/mL hygromycin
CAL51 *TEX264*$^{-/-}$	Generated here	TEX264 CRISPR/Cas9 KO Plasmid (h) TEX264 HDR Plasmid (h)

CAL51 *TEX264*$^{-/-}$ *TEX264*^{WT}-V5	Generated here	pLX313-TEX264-FL, 600 µg/mL hygromycin
CAL51 *TEX264*$^{-/-}$ *TEX264*^{SHP*}-V5	Generated here	pLX313-TEX264-SHP*, 600 µg/mL hygromycin
CAL51 *TEX264*$^{-/-}$ *TEX264*^{LIR*}-V5	Generated here	pLX313-TEX264-LIR*, 600 µg/mL hygromycin
CAL51 *PARP1*$^{-/-}$ *PARP1*^{WT}-GFP *TMEM192*-3HA	Generated here	pLJC5-TMEM192-3xHA, 2 µg/mL puromycin
CAL51 *PARP1*$^{-/-}$ *PARP1*^{KS}-GFP *TMEM192*-3HA	Generated here	pLJC5-TMEM192-3xHA, 2 µg/mL puromycin
HeLa *TEX264*$^{-/-}$	Fielden et al. (2020)	
HeLa *TEX264*$^{-/-}$ *TEX264*^{WT}-V5	Generated here	pLX313-TEX264-FL, 150 µg/mL hygromycin
HeLa *TEX264*$^{-/-}$ *TEX264*^{SHP*}-V5	Generated here	pLX313-TEX264-SHP*, 150 µg/mL hygromycin
HeLa *TEX264*$^{-/-}$ *TEX264*^{LIR*}-V5	Generated here	pLX313-TEX264-LIR*, 150 µg/mL hygromycin
HeLa *TMEM192*-3HA	Lascaux et al. (2024)	
HeLa *TEX264*$^{-/-}$ *TMEM192*-3HA	Lascaux et al. (2024)	
HeLa *STX17*^{KD} *TMEM192*-3HA	Lascaux et al. (2024)	
HeLa doxycycline-inducible sh*ATG7*	Lascaux et al. (2024)	
RPE1 *hTERT TP53*$^{-/-}$ *BRCA1*$^{-/-}$	Gift from Madalena Tarsounas	

RPE1 *hTERT TP53*$^{-/-}$ *BRCA1*$^{-/-}$ Olaparib resistant	Gift from Madalena Tarsounas	

Table 6: Stable cell lines used in this study. The source is stated as well as details of their generation for those that were generated in this study.

Cells were induced to stably express TMEM192-3HA, TEX264^{WT}-V5, TEX264^{SHP*}-V5, TEX264^{LIR*}-V5 or empty vector (EV)-V5 using lentiviral transduction. Lentiviral particles were generated using HEK293T cells in a 15 cm dish transfected with transfer plasmid for the gene of interest (1.64 pmol), pAmphoR envelope plasmid (0.72 pmol) and Δ8.2R packaging plasmid (1.3 pmol) using PEI transfection reagent in a ratio of 1:3 DNA:PEI. After 72 hours, viral particles were harvested by removing the media from the cells, centrifuging at 500 g and filtering through a 0.45 µm PES filter to remove any packaging cells. 500 µL of viral mixture was mixed with 500 µL of complete DMEM containing 16 µg/mL polybrene. This mixture was added onto cells at 30-50% confluency in a 6 well-plate. Virions were also generated without transfer plasmid and added to cells in the same way to serve as a negative control for plasmid transduction. Transfer plasmids contained genes for resistance to a specific antibiotic which was added at a pre-determined optimal dose (Table 6) the day after transduction. After ~4 days, all negative control cells were dead indicating only successfully transduced cells remain in other wells. These cells were trypsinised and counted with a haemocytometer before making up a mixture of cells at 10 cells/mL in antibiotic-containing media. 100 µL was seeded per well of a 96 well-plate, meaning 1 cell should occupy each well. The plate was incubated for 1-2 weeks, with antibiotic media replaced every 4 days, until single colonies were observed in individual wells. These colonies were expanded onto 24 well-plates, then to 6 well-plates and up to T75 flasks. Several clones were propagated, validated and frozen for each cell line. Validation was by Western blot to compare

protein level to endogenous level and by immunofluorescence to ensure proper cell localisation and fluorescence, where appropriate.

CAL51 *TEX264*$^{-/-}$ were created by CRISPR/Cas9 knockout of *TEX264* using two plasmids purchased from Santa Cruz, one containing a pool of plasmids encoding guide RNA against TEX264 and Cas9 and another homology-directed repair plasmid encoding for puromycin resistance. 2.5 µg of each plasmid was transfected into CAL51 cells using FuGENE at a ratio of 1:3 DNA to FuGENE. Transfection was carried out as already described. After 3 days, media containing 2 µg/mL puromycin was added to transfected cells as well as a non-transfected negative control. After all negative control cells had died, single cell clones were generated and expanded as described above for generation of other stable cell lines. A number of clones were validated for loss of TEX264 expression by Western blot.

2.4 Molecular and cellular biology techniques

2.4.1 Generation of plasmid DNA by molecular cloning

To generate lentiviral plasmids expressing C-terminal V5-tagged TEX264^{WT}, TEX264^{SHP*}, TEX264^{LIR*}, TEX264 sequences were cloned into a pLX313 backbone which contained a V5-tag (AddGene, #118014). The backbone plasmid contained an insert encoding p53 which was first removed by restriction digest with NHeI-HF and EcoRV-HF in CutSmart buffer (NEB). The restriction digest reaction was carried out at 37°C for 30 mins, then the DNA mixture was resolved on a 1% agarose gel at 100 V for 1 hr. The band corresponding to the linear backbone with p53 insert removed was cut from the gel and underwent gel extraction using the Monarch® DNA Gel Extraction Kit to purify the backbone. TEX264 inserts were PCR amplified from TEX264^{WT} or TEX264^{SHP*} plasmids previously generated (Fielden et al., 2020),

or from TEX264^{LIR*} (Chino et al., 2019) using primers listed in Table 7. The mutant variants encode for the following point mutations are as follows: SHP* G280R, G282R, L284A; LIR* F273A.

Oligo	**Sequence**	**Purpose**
TEX-pLX313_Fwd	aggtgtcgtgaggctagcatgtcggacctgctactactggc	Generation of pLX313-TEX264^{WT}, -TEX264^{SHP*}, -TEX264^{LIR}
TEX-pLX313_Rev	gataggcttaccgatatcctccttgcccttctcaggggc	Generation of pLX313-TEX264^{WT}, -TEX264^{SHP*}, -TEX264^{LIR}
V5_pLX313_Fwd	ccatttcaggtgtcgtgaggatgggtaagcctatccctaaccctctcctcggt	Generation of pLX313-V5_EV
V5_pLX313_Rev	aaccctctcctcggtctcgattctacgtagatcggtaagcctatccctaa	Generation of pLX313-V5_EV

Table 7: Primers used for generation of plasmids. The sequence and purpose of each primer is listed.

The PCR mix was prepared using 0.5 µM of each primer, Q5® High-Fidelity 2X Master Mix and 0.5 µL of template DNA. PCR conditions (Table 8) were chosen with an extension time to account for template DNA length and annealing temperature to account for primer melting temperature (Tm).

	98°C, 30 seconds
35 cycles	98°C, 10 seconds
	60°C, 30 seconds

	72°C, 30 seconds
	72°C, 120 seconds

Table 8: PCR conditions for molecular cloning.

Amplicons were validated by running a small sample on a 1% agarose gel, then the insert was purified from the mixture using a QIAquick PCR Purification Kit. Inserts were ligated into pLX313 using NEBuilder® HiFi DNA Assembly. 20 femtomole of backbone and 40 femtomole of insert were combined with 2x NEB builder to 10 µL, then heated at 50°C for 30 mins. To generate pLX313-V5_EV, two overlapping oligos (Table 7) were ligated into pLX313 that would insert a STOP codon after the V5 tag. Ligated plasmids were transformed into NEB® Stable Competent E. coli cells with heat shock and spread on agar plates containing 100 µg/mL ampicillin. After incubating overnight at 37°C, 10-20 colonies were picked from each plate and underwent colony PCR to identify clones containing the correct plasmid. Colony PCR was carried out using the same primers as were used to amplify the insert but in Quick-Load® Taq 2X Master Mix. Positive clones were identified by running the PCR output on 1% agarose gel, then those clones were amplified overnight in LB and the plasmid isolated by miniprep, using the NucleoSpin Plasmid miniprep kit. Plasmids sequences were confirmed by sequencing at Source BioScience, Oxford, UK.

2.4.2 Colony formation assay

Colony formation assays were used to assess cell survival. Cells were seeded in 6 well-plates at 1000 cells/well for WT and 1500 cells/well for *TEX264*$^{-/-}$ cells, with triplicate wells for each condition. After 16 hrs, media containing drug treatment was added to each well for the time described for each experiment, then drug media was washed, and colonies were allowed to grow in recovery media for 6-10 days until

colonies were ~50 cells in diameter. Wells were washed with PBS, then fixed in 100% methanol for 10 mins before staining in crystal violet (1.23 mM crystal violet, 1% formaldehyde, 1% methanol, 1x PBS) for at least 10 mins until colonies were dark purple. Excess crystal violet was washed out of plates, then the plates were dried before being scanned and counted using GelCount (Oxford Optronix). Colony counts were normalised by dividing by the average number of colonies in the untreated wells.

2.4.3 Resazurin cell viability assay

500-1000 cells/well were seeded in a black well, clear bottom 96 well-plate with each condition seeded in triplicate. After 16 hours, treatment media was added for the time stated in figure legends. Media containing 30 µg/mL resazurin was added for 4 hrs before taking fluorescence measurements. Resazurin media was added to 3 empty wells to serve as a blank. Fluorescence was measured at 570 nm using a plate reader. Higher fluorescence is due to greater reduction of resazurin dye to the highly fluorescent resorufin dye by higher metabolic activity, indicating more live cells in the well. The average fluorescence detected in the blank sample was subtracted from each reading to normalise for background fluorescence.

2.4.4 Immunofluorescence

Cells were seeded and grown on 9 mm no. 1 thickness glass coverslips in 6 well-plates to 70-90% confluency. After drug treatment, coverslips were washed once with PBS. In all immunofluorescence experiments, cells underwent detergent pre-extraction before fixation to wash out all proteins not bound to chromatin. Pre-extraction buffer (25 mM HEPES, pH 7.5, 50 mM NaCl, 1 mM EDTA, 3 mM $MgCl_2$, 300 mM sucrose and 0.5% (v/v) Triton X-100) was added on ice for 2-2.5 mins,

before washing once with the same buffer without Triton X-100. Cells were fixed for 15 mins on ice with 4% formaldehyde in PBS. Coverslips were blocked with 5% BSA for 1 hr at 37°C, then sequentially incubated with antibodies diluted in 2.5% BSA for 1 hr at room temperature. Antibodies used were anti-PARP1, anti-myc, anti-γH2AX, anti-RPA, anti-53BP1, donkey anti-Mouse Alexa Fluor 555, and donkey anti-Rabbit Alexa Flour 488. Images were acquired using either the Andor Dragonfly confocal or Nikon Ni-E widefield microscopes and analysed with custom CellProfiler pipelines to count foci and measure signal intensity.

2.4.5 Proximity ligation assay

Proximity ligation assay (PLA) was performed using the Duolink® In Situ PLA® kits, following the manufacturer protocol. CAL51 cells stably expressing both PARP1-GFP and TEX264-V5 were seeded and grown on glass coverslips to 70-90% confluency. After treatment, cells were fixed with 4% formaldehyde in PBS for 10 mins, then permeabilised with 0.25% triton X-100 for 10 mins. After 3 washes in buffer A (150 mM NaCl, 10 mM Tris pH 7.4, 0.05% Tween 20), cells were blocked in the provided blocking reagent. Further washes in buffer A were followed by incubation with anti-GFP and anti-V5 primary antibodies (1:500). Coverslips were then incubated with PLA PLUS and MINUS probes. Cells were incubated with ligase followed by polymerase, with washes in buffer A between each step. Coverslips were then washed twice with wash buffer B (100 mM NaCl, 250 mM Tris pH 7.5) before staining with DAPI (1:1000) for 10 mins. Finally, coverslips were washed twice with buffer A and once with 0.01x buffer B before mounting using ProLong™ Glass Antifade Mountant. Images were taken using the Leica DMi8 SP8 FALCON with 63 x lens with a 1.4 NA and water immersion. Images were acquired in 2048 x

2048-pixel format at 8-bit. Analysis was carried out using ImageJ and a bespoke pipeline on CellProfiler.

2.4.6 mCherry-PARP1-GFP reporter assay

Cells were transfected with pmCherry-*PARP1*-eGFP using FuGENE for 24 hrs before the assay began. For fixed imaging, cells were seeded in 6 well-plates onto glass coverslips as described for immunofluorescence. After treatment, coverslips were washed once in PBS and fixed with 4% formaldehyde in PBS for 15 mins at room temperature. Cells were washed 3 times with 0.01% BSA in PBS, then incubated with DAPI diluted 1:10,000 in PBS for 30 mins in the dark. Coverslips were washed 3 times with 0.01% BSA in PBS, then mounted on glass slides using ProLong™ Glass Antifade Mountant. Cells were imaged on the confocal Leica DMi8 SP8 FALCON and analysed using ImageJ. Quantification was performed manually by counting the number of red cytosolic puncta per cell.

For live cell imaging, cells transfected to express mCherry-PARP1-GFP were seeded in 35 mm glass bottom dishes. LysoView™ 680 was added 20 mins prior to beginning the live imaging assay. Regular DMEM was washed out with PBS and replaced with FluoroBrite™ DMEM which contains no phenol red to prevent background fluorescence signal. Confocal images were captured on an Olympus IXplore Spin-SR microscope using a 50 µm pinhole spinning disc. A 60x/1.3 NA Lens was used, and images were obtained using a Hamamatsu ORCA fusion BT camera. 12 µm Z-stacks were captured using a z spacing of 0.8 µm, over a 4-hour time course at 35 second intervals.

2.4.7 Preparation of whole cell lysate

Cells were harvested by scraping and centrifuged at 400 g for 3 mins at 4°C. The cell pellet was washed by resuspending in ice cold PBS before centrifugation. The cell pellet was then resuspended in RIPA lysis buffer (10 mM Tris-HCl pH 8.0, 1 mM EDTA, 0.5 mM EGTA, 1% Triton X-100, 0.1% sodium deoxycholate, 0.1% SDS, 140 mM NaCl) containing inhibitors indicated in the Table 9.

Chemical	**Source**	**Target**	**Working conc**
Na_3VO_4	Sigma 56508 /450243	Tyr, ATP and alkaline phosphatase	1 mM
$Na_2P_2O_7$	Sigma 221368	Ser/Thr phosphatase	2 mM
NaF	Sigma S7920	Acid phosphatase	10 mM
Leupeptin	Santa Cruz sc-295358a	Ser, Thr, Cys protease	1 µg/mL
Pepstatin	Sigma 11524488001	Aspartic protease	1 µg/mL
Aprotinin	Sigma A1153	Serine protease	10 µg/mL
PMSF	Sigma P7626	Serine protease	0.1 mM
N-Ethylmaleimide (NEM)	Sigma E3876	Cysteine peptidases /DUBs	10 mM

Table 9: Protease and phosphatase inhibitors. Source, target and working concentration are indicated for use in preparation of lysates and other protein samples.

The volume of lysis buffer used was roughly double the volume of the cell pellet. Lysis was performed for 10 mins on ice, then the lysate was sonicated at 4°C for 10 cycles of 30 seconds on and 30 seconds off in a BioRuptor pico. The sample was centrifuged at 20,000 g for 10 mins to pellet any debris or membrane components and the supernatant was stored as lysate. Lysate protein concentration was

determined by detergent compatible (DC) assay according to manufacturer's instructions. 2 µL of sample was loaded into a well of a 96 well-plate. 20 µL alkaline copper tartrate was diluted in 1 mL surfactant solution and 25 µL of this mixture was added to each well. 200 µL Folin reagent was added to each well and the plate was incubated in the dark at room temperature for 15 mins before absorbance was read at 650–750 nm on ClarioStar plate reader. Samples were measured in duplicate, with 2 blank wells containing no sample to eliminate background signal. A range of BSA concentrations were used to generate a standard curve to determine sample protein concentration from absorbance. Between 10-100 µg of protein, depending on the nature of the assay and sensitivity of the antibody for the target protein, was prepared for Western blot detection by dilution of lysate with 5x Laemmli buffer.

2.4.8 Western blot

Western blots were used to separate and detect proteins in lysoIP, immunoprecipitation and whole cell lysate experiments. 5-18% gradient polyacrylamide gels were prepared in house by preparing solutions for 5%, 18% and stacking gels. Glass plates were setup in the casting chamber. Using one stripette, the 5% solution, then the 18% mixture was taken up, drawing a bubble through the solutions to create the gradient. This was added between the glass plates and 100% isopropanol added on top to prevent the gel drying out during polymerisation. After the separating layer had polymerised, the stacking layer was added on top with a comb added to create wells during polymerisation. The acrylamide solutions were prepared according to Table 10.

Reagent	**5%**	**18%**	**Stacking**
Deionised water	6.93 mL	1.73 mL	4.89 mL

4 x separating buffer	3 mL	3 mL	2 mL
40 % acrylamide/bisacrylamide	2 mL	7.2 mL	1.07 mL
10 % ammonium persulfate	60 µL	60 µL	40 µL
TEMED	16 µL	16 µL	16 µL

Table 10: Components for preparation of 4 polyacrylamide gels.

Samples, prepared with Laemmli buffer as described for specific protocols, and Precision Plus Protein Dual Colour Standards were loaded into gels setup in the mini-PROTEAN system (BioRad). SDS-PAGE was run in running buffer (1x Tris-glycine, 0.1% SDS) at 50 V until samples entered the separating gel, then at 100 V. Proteins were transferred onto PVDF membrane by wet transfer using the Mini Trans-Blot® Cell system (BioRad) in ice-cold transfer buffer (1x Tris-glycine, 20% methanol, 0.025%) at 100 V for 75 mins. Transfer was kept at 4°C using frozen ice packs and carried out in the cold room to maximise efficiency and quality of protein transfer, especially of larger proteins. Membranes were blocked 5% milk in TBST for 30 mins, then incubated at 4°C overnight in primary antibodies in 2.5% BSA dissolved in TBST. Membranes were washed twice in TBST for 15 mins before incubating at room temperature in HRP-labelled secondary antibodies, according to species, prepared in 2.5% milk in TBST. After washing twice for 10 mins in TBST, protein signals were visualised by adding SuperSignal™ West Chemiluminescent Substrate for 5 mins. Pico PLUS or femto maximum sensitivity substrates were used depending on the amount of protein to be detected. Protein signals were imaged using the iBright imaging system (Thermo-Fisher Scientific) and analysed using the iBright Analysis Software to prepare images, with ImageJ used to quantify signal intensity.

2.4.9 Immunoprecipitation of intact lysosomes (LysoIP)

Cells were generated to stably express TMEM192-3HA. These cells, as well as parental control cells, were seeded on 15 cm dishes to be sub-confluent at the time of treatment. After treatment, cells were washed and harvested in KPBS by scraping. After cell pellet resuspension in KPBS, 2.5% was taken as an input sample and lysed in RIPA buffer as described for preparation of whole cell lysate. Cells were homogenised with 15 strokes in a Dounce homogeniser to lyse cells and release intact cellular organelles. Cytosolic organelles including lysosomes were isolated in the supernatant by centrifugation at 1000 g for 2 mins. Anti-HA magnetic beads were prepared in advance by blocking in 5% BSA for 1-2 hrs on a rotating wheel at 4°C. Supernatant was loaded onto anti-HA magnetic beads and incubated for 15 mins on a rotating wheel at 4°C. Beads were washed 5 times for 3 mins in KPBS on the wheel, then eluted in 2x Laemmli at 95°C for 10 mins. Elution and input samples were loaded onto SDS-PAGE gels for protein separation and detection by Western blot.

2.4.10 Co-immunoprecipitation from chromatin fraction

CAL51 cells expressing PARP1-GFP and CAL51 WT control cells were seeded on 15 cm dishes to sub-confluency at the time of treatment. After treatment, cells were washed on the plate once in PBS, then harvested in PBS containing 3 mM EDTA by scraping. Cells were pelleted by centrifugation at 400 g for 3 mins at 4°C. To lyse cells and isolate the nuclear pellet, cells were resuspended in twice the pellet volume of buffer A (10 mM HEPES pH 7.45, 10 mM KCl, 340 mM sucrose, 3 mM EDTA, 10% glycerol, protease and phosphatase inhibitors, NEM), then triton X-100 was added to a final concentration of 0.1%. This mixture was incubated on ice for 5

mins at 4°C. The nuclear pellet was isolated by centrifugation at 300 g for 3 mins and washed twice in buffer A without triton. A volume of buffer B (3 mM EDTA, 0.2 mM EGTA, 5 mM HEPES pH 7.9, protease and phosphatase inhibitors, NEM) equal to the pellet size was added to the nuclear pellet which was resuspended gently by flicking the tube. The mixture was incubated on ice for 10 mins, then centrifuged at 1700 g for 3 mins to isolate chromatin. To remove membrane contamination, the chromatin pellet was washed twice with buffer B containing 0.5% triton and incubated for 15 mins on a rotating wheel at 4°C. The pellet was then washed with benzonase buffer (50 mM Tris-HCl pH 7.9, 100 mM NaCl) and finally with benzonase buffer containing 10 mM $MgCl_2$. The pellet was isolated between washes by centrifugation at 5000 g for 5 mins. Chromatin was digested for 1 hr at 4°C with rotation with 125 U/mL benzonase in 200-500 µL (volume dependent on pellet size) benzonase buffer containing 10 mM $MgCl_2$, protease and phosphatase inhibitors and NEM. After 1 hr of digestion, the supernatant was cloudy, and the pellet had disappeared indicating digestion of soluble chromatin. The soluble chromatin fraction in the supernatant was isolated by centrifugation at 20,000 g for 10 mins. 25 µL of sample was reserved as an input sample, which was prepared for analysis by Western blot by addition of 25 µL of 2x Laemmli buffer and boiling at 95°C for 10 mins. Ethidium bromide was added to the remainder of the sample to a concentration of 50 µg/ml to reduce unspecific binding to the beads. GFP-trap beads were prepared in advance by blocking in 5% BSA in IP wash buffer (50 mM Tris-HCl pH 7.4, 150 mM NaCl, 0.5 mM EDTA) without triton X-100 or any inhibitors. After washing beads in IP wash buffer to remove BSA, samples were loaded onto 8 µL of beads per sample and incubated for 3 hrs at 4°C with rotation. Beads were washed 3 times for 15 mins with IP wash buffer (50 mM Tris-HCl pH 7.4, 150 mM

NaCl, 0.5 mM EDTA, 0.05% triton X-100, protease and phosphatase inhibitors, NEM), before elution with 2x Laemmli buffer and boiling at 95°C with shaking. Samples were run on SDS-PAGE gels for protein separation and detection by Western blot.

2.4.11 RNA extraction and RNA-sequencing

For RNA-sequencing experiments, RNA was extracted from HeLa and CAL51 WT and *TEX264*$^{-/-}$ cells at 80% confluency in a well of a 6 well-plate. GeneJet RNA purification kit was used with RNA extraction carried out according to manufacturer's instructions. Briefly, cells were lysed by resuspending in lysis buffer supplemented with β-mercaptoethanol and passed through a 20-gauge syringe several times. Ethanol was added to the lysate, which was then added to the purification column. The column was centrifuged for 1 min at 12,000 g, allowing the lysate to pass through and RNA to bind to the silica membrane. The membrane was washed with wash buffer 1, then twice with wash buffer 2, with centrifugation to wash the membrane. The column was transferred to a sterile microcentrifuge tube and RNA was eluted with nuclease-free water. RNA was quantified by nano-drop to ensure the concentration was higher than 20 ng/μL and both the 260/230 and 260/280 ratios were above 2.0 to indicate sufficient purity. 3 biological repeats were sent to Novogene for sequencing, RNA sample quality control, mRNA library preparation (polyA enrichment), Illumina Sequencing and bioinformatic analysis. Bioinformatic analysis performed by Novogene included: (i) data quality control and filtering, (ii) mapping to reference genome GRCh38/hg38, (iii) gene expression quantification and correlation analysis, (iv) differential expression analysis, (v) enrichment analysis and (vi) gene set enrichment analysis.

2.4.12 Data presentation and statistical analysis

Image data analysis and representation was carried out using CellProfiler™ (Broad Institute, https://cellprofiler.org/) and ImageJ (NIH, https://imagej.net/Fiji/Downloads). Images are shown with scale bars of 10 μm unless otherwise stated. Graphs were plotted and statistical analysis was performed using Prism v10 (GraphPad Software, https://www.graphpad.com). All experiments were performed at least 2 times, with number of replicates indicated in the figure legends. Error bars represent SEM. Tukey box plots are as standard, where centre line equals the median, box indicates the interquartile range and whiskers indicates 1.5x interquartile range. Statistical tests (Student's t-test, one-way ANOVA, two-way ANOVA) used are indicated in the figure legends. Asterisks are used to indicate p values ($p>0.05$ = ns, $p\leq0.05$ = *, $p\leq0.01$ = **, $p\leq0.001$ = ***, $p\leq0.0001$ = ****).

3. Results: Identification and validation of p97 co-factor TEX264 in cellular response to PARP1 trapping

Similar to other DPC and DPC-like adducts, cytotoxic trapped PARP1 can be cleared from chromatin by the p97 system. This has previously been detected by chromatin co-immunoprecipitation which determined that p97 localises to trapped PARP1 through sequential SUMOylation and ubiquitination, with inhibition of p97 causing an accumulation of trapped PARP1 in chromatin fractions (Krastev et al., 2022). However, due to its pleiotropic roles, the p97 system relies on a series of co-factors to regulate interaction with its substrates and give p97 specificity of function (Buchberger et al., 2015; Meyer, Bug, & Bremer, 2012). To better understand the function of the p97 system in regulating trapped PARP1 and how this could be therapeutically targeted whilst restricting effects on the pleiotropic roles of p97, we first sought to investigate which co-factors may be involved in this process.

3.1 p97 inhibition increases PARP1 trapping

PARPi affect both the catalytic activity of PARP1 and cause it to become trapped on chromatin, with the latter being the source of cytotoxicity (Murai et al., 2012). To explore PARP1 trapping levels, I established an immunofluorescence assay to screen exclusively for chromatin-bound trapped PARP1. Cells were treated with a low dose of the alkylating agent methyl methanesulfonate (MMS) to induce abasic sites that recruit PARP1, and PARPi talazoparib, which is known to be one of the strongest inducers of trapped PARP1 (Murai et al., 2014; Shen et al., 2013). This caused levels of trapped PARP1 that can be detected by immunofluorescence with detergent pre-extraction to exclude any proteins not tightly bound to chromatin. To verify the effectiveness of this assay, previously generated CAL51 *PARP1*$^{-/-}$ cells

were used in which either PARP1^{WT} or trapping deficient PARP1$^{del.p.119K120S}$ had been introduced (Krastev et al., 2022). K119 and S120 are both key DNA-contacting residues in the second zinc finger domain of PARP1 (Ali et al., 2012) whose mutation impairs its ability to trap PARP1 on DNA and, thus, induces resistance to talazoparib (S. J. Pettitt et al., 2018). Trapping conditions (talazoparib and MMS treatment) induced clear trapped PARP1 foci in PARP1^{WT} cells, whereas expression of the trapping deficient PARP1$^{del.p.119K120S}$ ablated this signal down to untreated levels (Fig 11A, B), validating the use of this assay for detecting trapped PARP1.

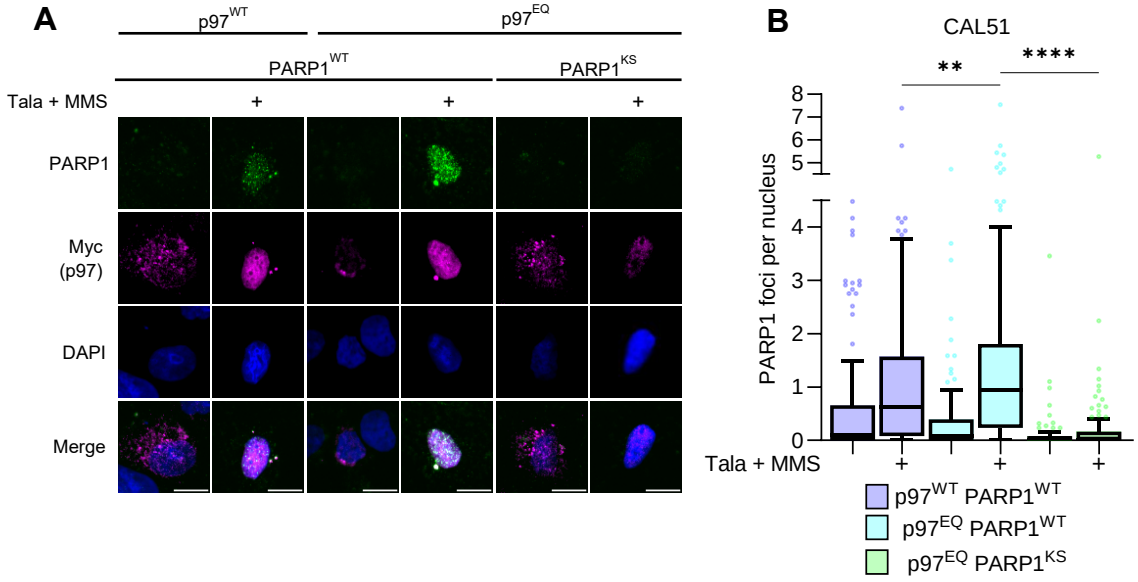

Figure 11: Impaired p97 activity causes increased trapped PARP1. (**A and B**) Immunofluorescence with detergent pre-extraction to detect trapped PARP1 foci upon treatment with talazoparib (200 nM) and MMS (0.01%). Cells stably expressing either PARP1^{WT}-GFP or DNA-binding mutant PARP1$^{del.p.119K120S}$-GFP (PARP1^{KS}), and transiently expressing either myc-tagged p97^{WT} or dominant negative catalytically dead p97^{E578Q} (p97^{EQ}). Images (**A**) have 10 µm scale bar. Quantification (**B**) is from 3 biological repeats with >100 cells total, showing mean and SEM. Statistical analysis by one-way ANOVA. Published in Krastev et al. (2022).

To validate previous work which demonstrated the accumulation of trapped PARP1 by biochemical chromatin fractionation, I overexpressed either myc-tagged p97^{WT} or dominant-negative ATPase-deficient p97^{E578Q} which is unable to process its substrates (Krastev et al., 2022; Ye, Meyer, & Rapoport, 2003). Not only was there a considerable increase in trapped PARP1 foci upon expression of the ATPase-

deficient p97 mutant (Fig 11A, B), but these foci co-localised with $p97^{E578Q}$-myc foci, as detected by myc-tag immunostaining (Fig 11A). This indicates that the catalytically dead mutant strongly localises and accumulates on trapped PARP1 lesions, confirming the role of p97 in actively processing trapped PARP1 to remove it from chromatin. Overall, this established that this assay is sufficient for investigating factors which play a key role in the regulation of PARPi-induced trapped PARP1.

3.2 Loss of TEX264 causes increased PARPi-induced trapped PARP1

Having established an assay for the detection of trapped PARP1 levels, I aimed to further explore which p97 co-factors may aid in the extraction of trapped PARP1 from chromatin. By RNA interference (RNAi), several p97 co-factors (UFD1, SPRTN, Ataxin-3, TEX264), known to aid in removal of DNA-bound proteins, were depleted in two TNBC cell lines (CAL51 and MDA-MB231) (Fig 12). In our previous work, UFD1 has been shown to recognise ubiquitylated trapped PARP1 to mediate p97 recruitment, with UFD1 depletion causing PARP1 accumulation on chromatin under trapping conditions as shown by biochemical cellular fractionation (Krastev et al., 2022). Indeed, depletion of UFD1 induced a 2.3- and 1.5-fold increase in trapped PARP1 levels visualised by immunofluorescence in CAL51 and MDA-MB231, respectively (Fig 12). This further confirms the sensitivity of this assay and acts as a positive control.

SPRTN, a metalloprotease that acts with p97 to digest the proteinaceous adduct of DPCs during DNA replication (Fielden et al., 2020; Kröning et al., 2022; J. Stingele et al., 2016; Vaz et al., 2016), has been previously implicated in the cellular response to PARPi. SPRTN deficient cells were found to be hypersensitive to

talazoparib, but not non-trapping PARPi veliparib, due to delayed removal of trapped PARP1 from chromatin (Saha et al., 2021). Despite this, I observed only a marginal increase in trapped PARP1 levels upon its depletion and this wasn't consistent over different siRNA sequences and cell lines (Fig 12). Saha et al. (2021) calculated that SPRTN may only be responsible for the clearance of 15% of trapped PARP1 and may only be acting during DNA replication, so it is unsurprising that only a marginal effect on global trapped PARP1 foci is detected by our immunofluorescence assay. Further, conflicting work suggests that SPRTN is inactive towards trapped PARP1, and SPRTN-deficient cells are not hypersensitive to PARPi (Kojima et al., 2020; Maskey et al., 2017). Altogether, this suggests SPRTN is not essential for p97-mediated trapped PARP1 processing.

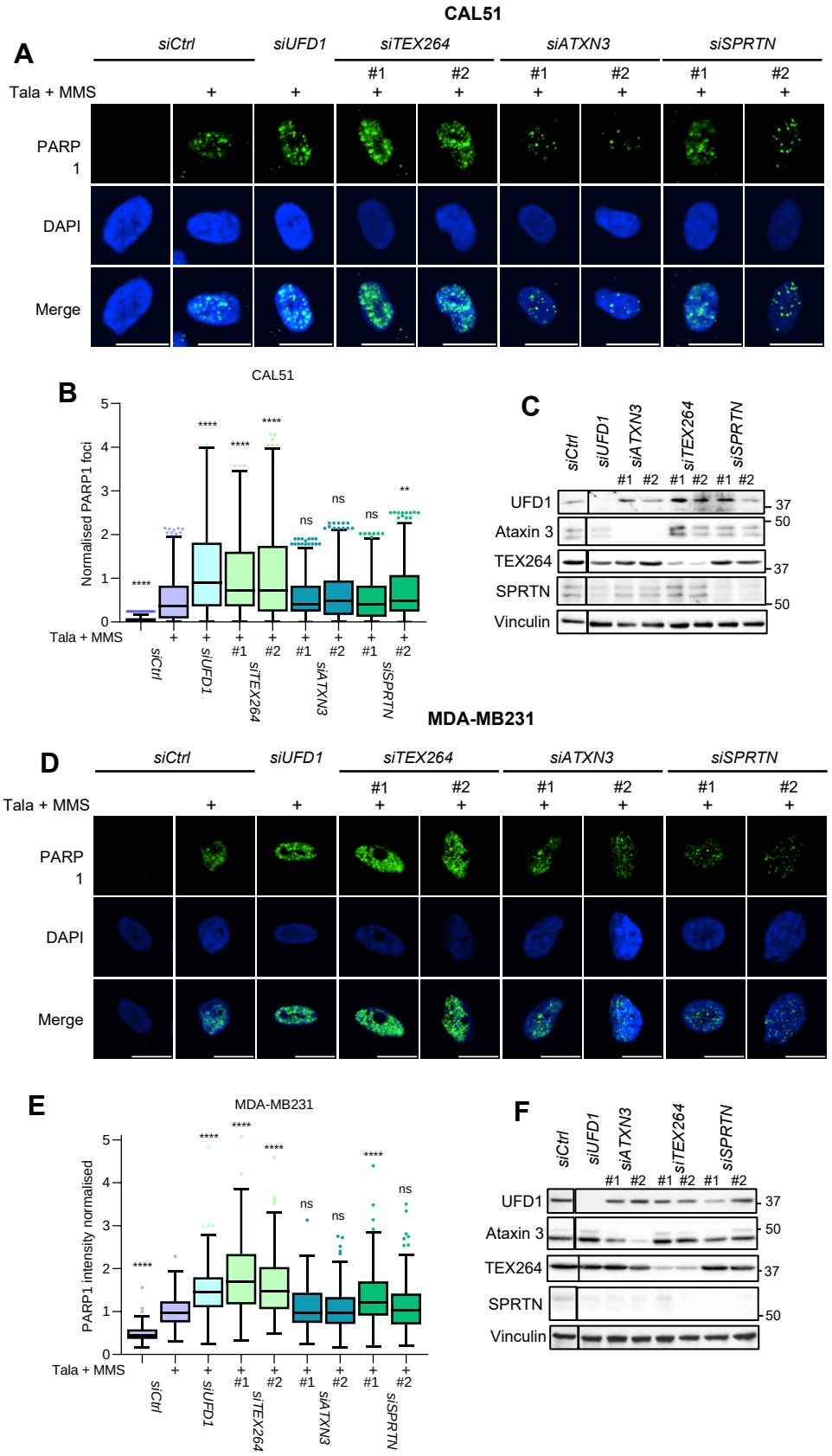

Figure 12: Screen of p97 co-factors for regulation of PARP1 trapping. (A and B) Immunofluorescence with detergent pre-extraction to detect trapped PARP1 foci in cells depleted of the indicated p97 co-factor. Images in (**A**) and quantification in (**B**). Scale bar is 10 µm. Tukey box plot

of 6 biological repeats with >600 cells and statistical analysis by one-way ANOVA. (**C**) Immunoblots validating depletion of indicated co-factors in (A) and (B). (**D, E and F**) as in (A), (B) and (C), respectively, but in MDA-MB231 cells over 3 biological repeats with >150 cells.

Ataxin-3 is a p97-associated DUB involved in DDR, specifically at DSBs where it counteracts RNF4 activity (Pfeiffer et al., 2017) and acts on RNF8 (Singh et al., 2019) to determine DSB repair pathway choice. The recruitment of ataxin-3 to DSB sites is dependent in part on PARylation (Pfeiffer et al., 2021) and loss of ataxin-3 hypersensitizes cells to PARPi (Pfeiffer et al., 2017), highlighting an association between ataxin-3 and PARP1. Despite this, depletion of ataxin-3 had no impact on trapped PARP1 levels (Fig 12).

The final co-factor tested for accumulation of trapped PARP1 was TEX264. Only recently characterised as both a p97 co-factor (Fielden et al., 2020), reticulophagy receptor (An et al., 2019; Chino et al., 2019) and nucleophagy receptor (Lascaux et al., 2024), the most well understood role of TEX264 in the nucleus is to bridge p97 to TOP1cc and aid in its clearance from chromatin (Fielden et al., 2020; Lascaux et al., 2024). TOP1cc cause cell cytotoxicity through their ability to block and lead to DSB at both transcription (Capranico et al., 2007; Cristini et al., 2016; Sordet et al., 2009) and replication forks (Pommier et al., 2006; R. G. Shao et al., 1999), with their repair by TEX264 highly replication-associated (Fielden et al., 2022; Fielden et al., 2020; Lascaux et al., 2024). This is reminiscent of PARPi-induced trapped PARP1 which induces cell death through physical obstruction of DNA-based processes, most notably DNA replication (Helleday, 2011; Murai et al., 2012; Petropoulos et al., 2024) resulting in replication stress and accumulation of DNA damage in replicating cells (Michelena et al., 2018). Strikingly, TEX264 was the only co-factor tested to cause a considerable increase in trapped PARP1 levels in all cell lines, with roughly a 2- and 1.7-fold increase in CAL51 and MDA-MB231, respectively (Fig 12). A 1.6-

fold increase in trapped PARP1 was also observed in HeLa cells after *TEX264* knockout by CRISPR/Cas9 (Fig 13A, B). Trapped PARP1 levels were raised to a similar extent as with UFD1 depletion, implying a role of TEX264 in the regulation of trapped PARP1 that compares to UFD1-mediated p97-dependent extraction.

3.3 TEX264 loss hypersensitizes cells to talazoparib (trapping) but not veliparib (non-trapping) PARPi

TEX264 plays a role in response to PARP1 trapping, with its loss causing a substantial increase in trapped PARP1 levels. I next wanted to explore if this trapping increase translates to a change in sensitivity to PARPi under extended treatment times and without the presence of an alkylating agent. I generated CRISPR/Cas9 *TEX264* knockout (*TEX264*$^{-/-}$) cells in CAL51 and used HeLa *TEX264*$^{-/-}$ cells that had been previously generated (Fielden et al., 2020) and showed the same accumulation of trapped PARP1 as was observed with other cell lines (Fig 13A, B). These were treated for 24 hrs with talazoparib and subjected to colony formation assay to assess cell survival. Remarkably, in both cell lines, loss of TEX264 lead to a considerable increase in sensitivity to talazoparib, with approximate IC50 values reduced from 180 nM to 40 nM in HeLa and 50 nM to 10 nM in CAL51 cells upon TEX264 loss (Fig 13C-G). All PARPi inhibit catalytic activity of PARP1, but the predominant cause of cytotoxicity is through PARP1 trapping, with strong correlation between the potency of a PARPi and its ability to drive entrapment of PARP1 on DNA (Helleday, 2011; Murai et al., 2012). To distinguish whether hypersensitivity in *TEX264*$^{-/-}$ cells is linked with catalytic inhibition or PARP1 trapping, I performed colony formation assays with veliparib. Whilst its ability to inhibit PAR synthesis, a measure of catalytic inhibition, is only slightly poorer than talazoparib, sensitivity to veliparib is only observed at μM doses compared to the

nM doses required to elicit talazoparib sensitivity. This is due to the inability of veliparib to trap PARP1 on DNA, compared to talazoparib which is a far more potent trapper (Murai et al., 2012; Murai et al., 2014; Shen, Aoyagi-Scharber, & Wang, 2015; Shen et al., 2013). When *TEX264*$^{-/-}$ cells undergo extended treatment with veliparib, they display no change in sensitivity compared to WT cells, with approximate IC50 increasing from 40 nM to 50 nM in HeLa and a marginal decrease from 50 nM to 35 nM in CAL51 when comparing WT to *TEX264*$^{-/-}$ cells (Fig 14). Therefore, in accordance with the loss of TEX264 causing increased PARP1 trapping, *TEX264*$^{-/-}$ cells seem to be specifically sensitive to trapping PARPi compared to non-trapping. This implies a role of TEX264 in regulating sensitivity to PARPi through an ability to restrict the accumulation of trapped PARP1, rather than through any link to PARP1 catalytic activity.

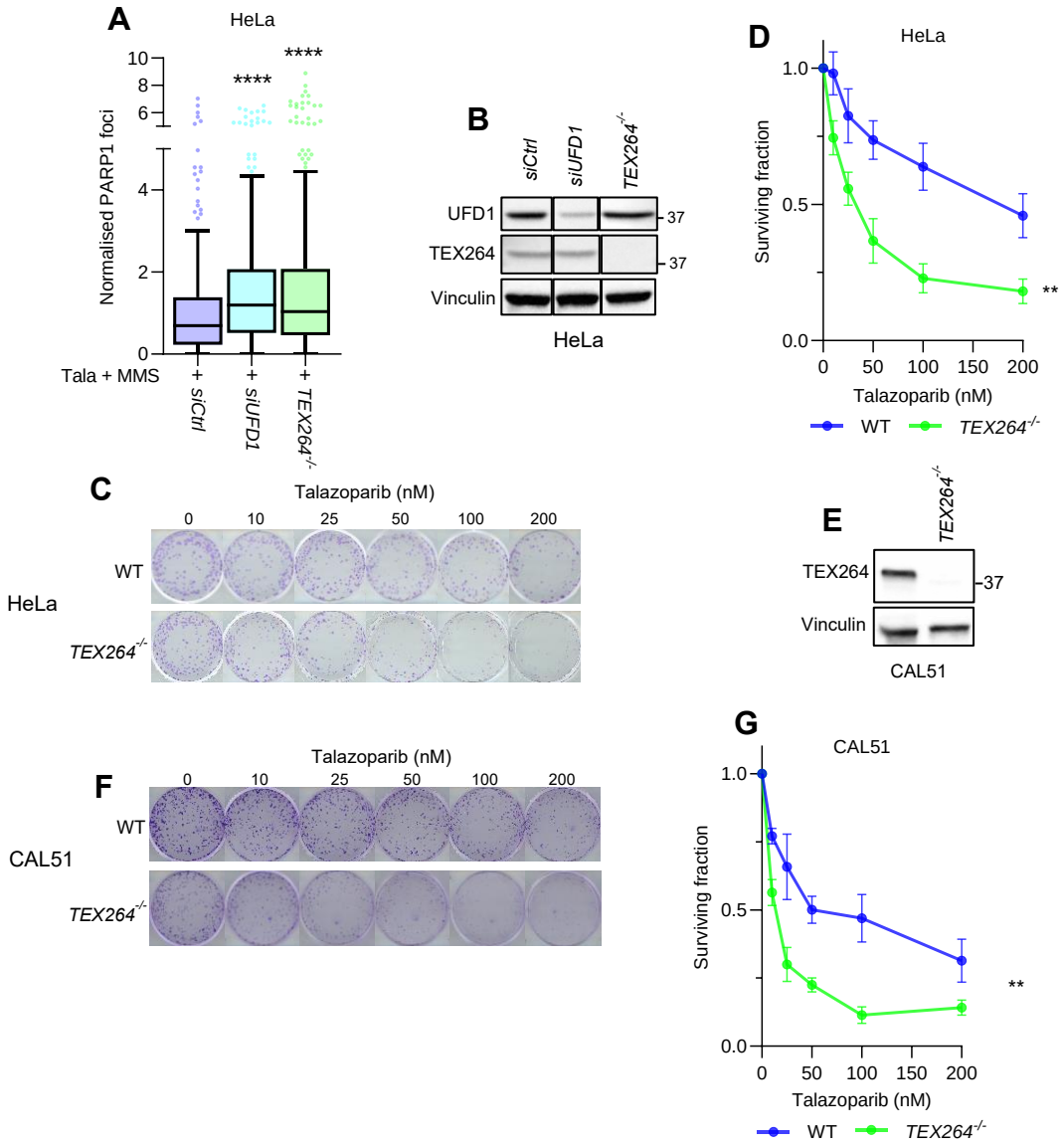

Figure 13: TEX264 loss hypersensitises cells to talazoparib. (**A**) Quantification of immunofluorescence with detergent pre-extraction to detect trapped PARP1 foci in HeLa cells either depleted of UFD1 by siRNA or with *TEX264*-knock out by CRISPR/Cas9. Tukey box plot of >275 cells from 3 biological repeats. One-way ANOVA. (**B**) Validation of UFD1 depletion for (A) and *TEX264*$^{-/-}$. (**C and D**) Images (**C**) and quantification (**D**) of colony formation assays in HeLa WT and *TEX264*$^{-/-}$ cells treated with talazoparib over 5 biological repeats. Mean +/- SEM and stats by paired t-test. (**E**) Immunoblotting validating knockout of *TEX264* in CAL51 *TEX264*$^{-/-}$ cells. (**F and G**) as in (C) and (D) showing colony formation assays in CAL51 cells over 3 biological repeats.

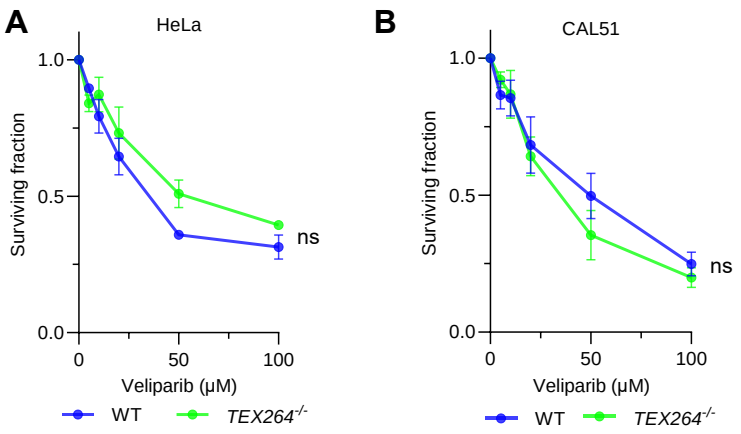

Figure 14: TEX264 loss has no effect on sensitivity to non-trapping PARPi. (**A and B**) Colony formation assays in HeLa (**A**) and CAL51 (**B**) WT and *TEX264*$^{-/-}$ cells upon treatment with veliparib. N=3 in (A) and N=4 in (B) with mean +/- SEM displayed. Statistical analysis by paired t-test.

3.4 Concluding remarks

The recently discovered ability of p97 to extract cytotoxic trapped PARP1 from chromatin could result in clinical advancements in relation to resistance, whereby targeting this mechanism of trapped PARP1 clearance hypersensitises cancer cells or re-sensitises resistant cells to PARPi. However, the pleiotropic roles of p97 make this challenging to target without seeing further off-target effects. Here, I have identified a p97 co-factor that regulates PARP1 trapping, with its loss hypersensitising cancer cells to PARPi. This effect is seen only in the context of PARP1 trapping and not with other PARPi that induce only catalytic inhibition. This represents a potential for impairing trapped PARP1 clearance in a more specific manner than global p97 inhibition. Further exploration of the role of TEX264 in this pathway is, therefore, essential.

4. Results: TEX264 acts as a selective autophagy receptor and p97 co-factor to mediate trapped PARP1 processing

In its chromatin-related role, TEX264 aids in repair of TOP1cc (Fielden et al., 2020; Lascaux et al., 2024). Due to the essential function of both TOP1 and PARP1 in maintaining processivity and fidelity of DNA replication (Bryant et al., 2009; Hanzlikova et al., 2018; Ho et al., 2022; Pommier, Nussenzweig, Takeda, & Austin, 2022), both TOP1cc and trapped PARP1 cause cytotoxicity through their ability to block DNA replication (Murai et al., 2012), causing eventual fork collapse and DSB formation (Helleday, 2011; Pommier et al., 2006). TEX264 repairs TOP1cc through its direct interaction and recruitment of p97 and SPRTN to unfold and cleave the DNA-bound TOP1, respectively (Fielden et al., 2020). Recently, our group also discovered an alternative SPRTN-independent function of TEX264 at TOP1cc lesions, where it acts as a SAR to direct them for repair by selective nucleophagy (Lascaux et al., 2024). Due to the similarities of TOP1cc and trapped PARP1 lesions and having shown that TEX264 promotes PARPi tolerance by regulating accumulation of trapped PARP1, I hypothesised that TEX264 may also be acting at trapped PARP1 lesions.

4.1 TEX264 interacts with PARP1 under trapping conditions in a spatially dynamic manner

To investigate whether TEX264 acts at trapped PARP1 lesions, I explored two previously published interactomes of TEX264, as determined by mass spectrometry (An et al., 2019; Fielden et al., 2020). PARP1 is identified in both data sets. In fact, in untreated conditions, PARP1 is the 169th most abundant protein out of over 1100 total proteins in the TEX264 interactome (Fielden et al., 2020) (Fig 15A). Whilst this implies the existence of a TEX264-PARP1 interaction, the relevance of this on chromatin or, more specifically, at trapped PARP1, remains unclear. To investigate this, I performed

immunoprecipitation of GFP-tagged PARP1 under native conditions from chromatin fractions in CAL51 cells with CRISPR/Cas9 *PARP1*-knockout stably expressing GFP-tagged PARP1 (hereafter referred to as PARP1-GFP cells) (Fig 15B, C). As in chapter 3, trapping conditions were generated through treatment with talazoparib and low dose MMS. p97 is known to interact with PARP1 specifically under trapping conditions (Krastev et al., 2022), so detection of this serves as a positive control. TEX264 interaction was also detected strongly and shown to be specific due to its absence in CAL51 WT cells. Whilst less striking than with p97, TEX264 interaction with PARP1 increased ~1.4-fold under trapping conditions (Fig 15B, C). This implies that TEX264 interacts with PARP1 and accumulates at trapped PARP1 lesions.

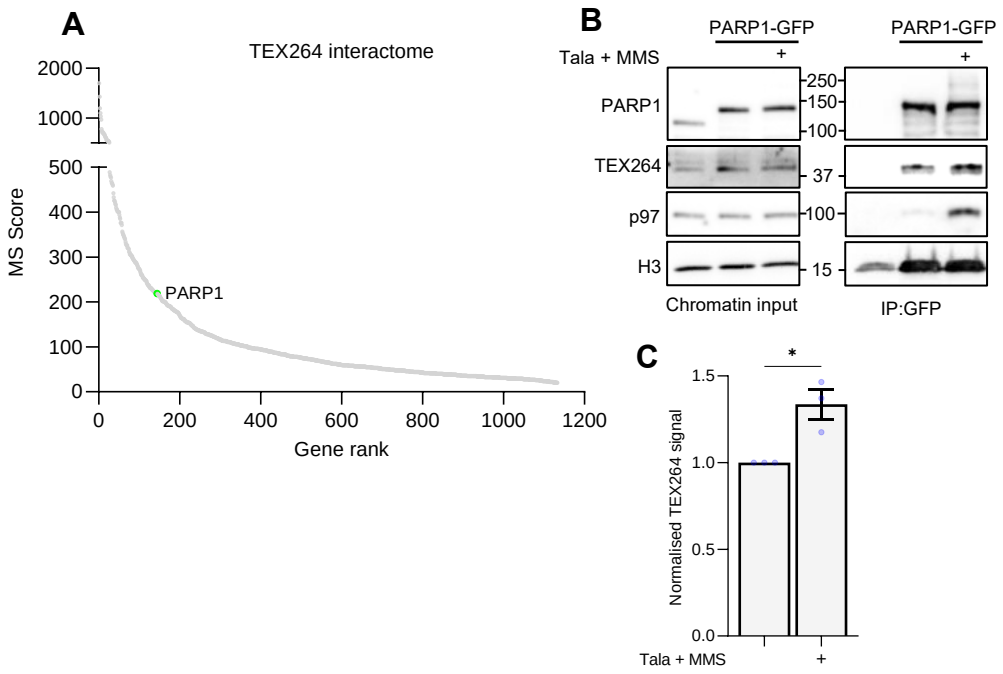

Figure 15: TEX264 interacts with trapped PARP1. (**A**) TEX264 interactome determined by mass spectrometry by Fielden et al. (2020). PARP1 is labelled in green. (**B**) Co-immunoprecipitation of GFP in CAL51 cells stably expressing PARP1-GFP after treatment with talazoparib and MMS for 3 hrs. (**C**) Quantification of TEX264 signal in (B) from 3 repeats with statistical analysis by t-test.

To further explore TEX264-PARP1 interaction outside of the chromatin context, I carried out a PLA. This allows highly sensitive *in situ* detection of protein-protein

interactions up to 40 nm distance (Alam, 2022; Gullberg et al., 2004; Söderberg et al., 2006), permitting visualisation of where the interaction is occurring. I modified CAL51 PARP1-GFP cells, as used in immunoprecipitation experiments, to stably express V5-tagged TEX264, and performed PLA between GFP and V5. All negative controls, either with empty vector V5 or with either primary antibody excluded, showed no PLA signal, demonstrating the specificity of this assay for detecting interacting PARP1 and TEX264 (Fig 16A). In accordance with mass spectrometry data, the PLA signal is detected in untreated conditions (Fig 16B, C). Physiologically, TEX264 is present in the cytosol, nucleus and on the chromatin whilst PARP1 predominantly localises to the nucleus (Vyas, Chesarone-Cataldo, Todorova, Huang, & Chang, 2013). Accordingly, the PLA signal seems to be predominantly nuclear and accumulate around the nuclear periphery, where TEX264 is known to localise (Fielden et al., 2020). PLA signal is increased by PARPi treatment, across the whole cell and, in agreement with co-immunoprecipitation experiments, in the nucleus. Strikingly, an increase in cytosolic signal is also observed upon treatment (Fig 16B, C). This implies that the PARP1-TEX264 interaction is spatially dynamic depending on PARPi treatment. Considering the predominantly nuclear localisation of PARP1, it is surprising to see such a strong cytosolic interaction of TEX264-PARP1 after PARPi treatment.

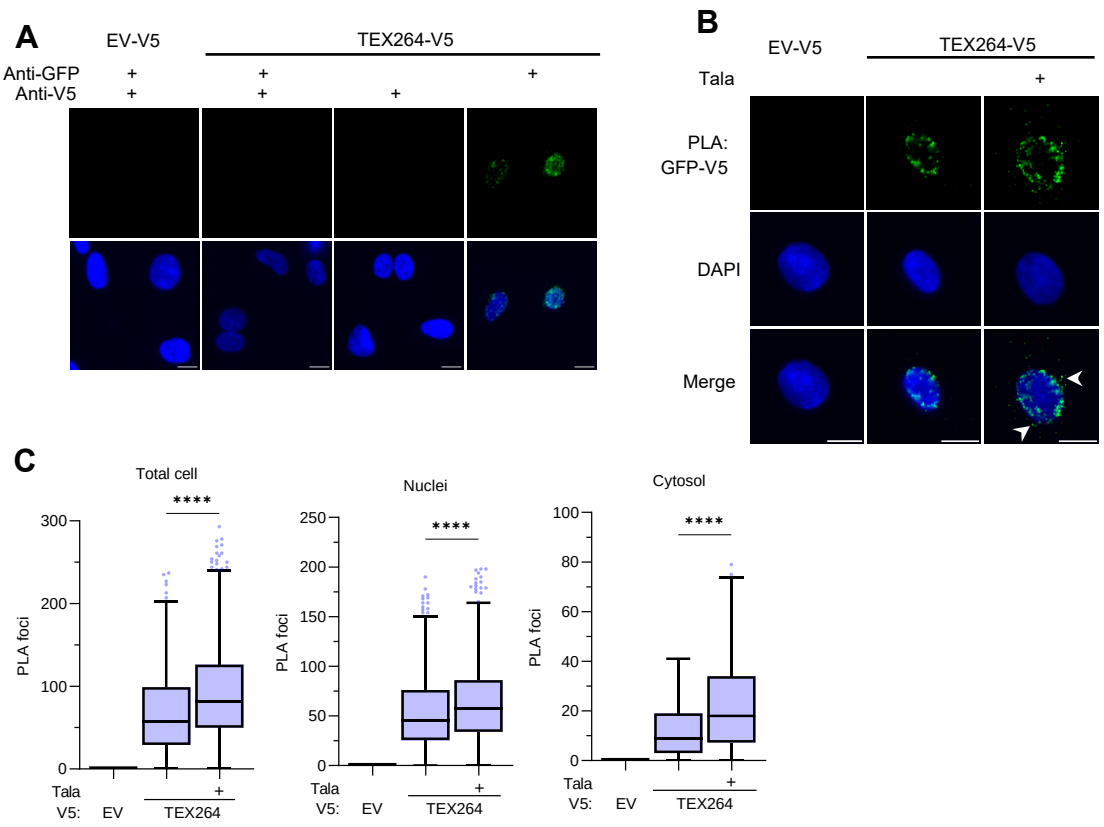

Figure 16: TEX264 interaction with trapped PARP1 is spatially dynamic after PARPi treatment. (**A and B**) Proximity ligation assay (PLA) between GFP and V5 in CAL51 cells stably expressing PARP1-GFP and either TEX264-V5 or empty vector (EV)-V5. (**A**) shows PLA negative controls with either primary antibody excluded. (**B**) includes talazoparib treatment of 200 nM for 3 hrs with scale bar of 10 µm. White arrows indicate cytosolic PLA signal. (**C**) Quantification of PLA. Quantification is of foci in whole cell, cytosol or nuclei as shown by Tukey box plot with statistical analysis by one-way ANOVA.

4.2 Autophagy machinery is upregulated by and interacts with trapped PARP1

The localisation of TEX264 in both the nuclear periphery and the ER is believed to be key for its role as a SAR for reticulophagy (An et al., 2019; Chino et al., 2019) and selective nucleophagy of TOP1cc (Lascaux et al., 2024). Selective autophagy relies on these receptors to bridge specific substrates to ATG8 family proteins in a growing autophagosome which, once fully formed, will transport substrates into the cytosol for

fusion with a lysosome for substrate degradation (Johansen & Lamark, 2020; Vargas, Hamasaki, Kawabata, Youle, & Yoshimori, 2023). Due to the cytosolic nature of selective autophagy, I postulated that the cytosolic PARP1-TEX264 signal we observed is related to the crucial role of TEX264 as a SAR.

I first turned to a published mass spectrometry data set using Apex2-mediated proximity labelling around trapped PARP1 (Krastev et al., 2022). PARP1 fused to Apex2 was introduced into CAL51 *PARP1*$^{-/-}$ cells, allowing biotinylation of proteins in close proximity to PARP1. Biotinylated proteins are isolated and analysed by mass spectrometry to form a comprehensive picture of the PARP1 interactome either in trapping conditions, with talazoparib and low dose MMS, or with MMS alone. Interestingly, gene set enrichment analysis identified autophagy as the 8th most significant term for interaction with trapped PARP1 (Fig 17A). To further explore this, I probed the dataset of 360 PARP1-interacting proteins for autophagy-related proteins using a published, annotated autophagy signature (Bordi et al., 2021). Strikingly, 22 autophagy-related proteins were identified in the PARP1 proteome. Autophagy core machinery proteins were over-represented, with 11 proteins identified, including ATG16L1 which has both a high PSM ratio, indicating increased interaction upon PARP1 trapping, and a moderately high MS score, indicating high abundance (Fig 17B). Existing as part of a colossal ~800 kDa complex in cells, ATG16L1 is an essential component of the autophagy machinery. Its multifaceted roles include LC3-phagophore conjugation via recruitment of the ATG5-ATG12 E3 ligase-like enzyme, facilitation of phagophore growth and autophagosome maturation (Gammoh, 2020). The interaction of PARP1 with such a key factor during autophagophore formation implies that PARP1 may localise to autophagophores during their formation. Another 5 proteins identified are regulators of mTOR, a major signalling pathway in the

regulation of autophagy flux, including MTOR itself which is increased under trapping conditions. Many negative regulators of autophagy are identified and seem to have decreased interaction with PARP1 under trapping conditions, including RHEB (Sciarretta et al., 2012) and IGF2BP1(Williams et al., 2022) (Fig 17B). Altogether, this indicates a likelihood that autophagy is involved directly at trapped PARP1 lesions, and that autophagy flux may be modulated by trapping conditions.

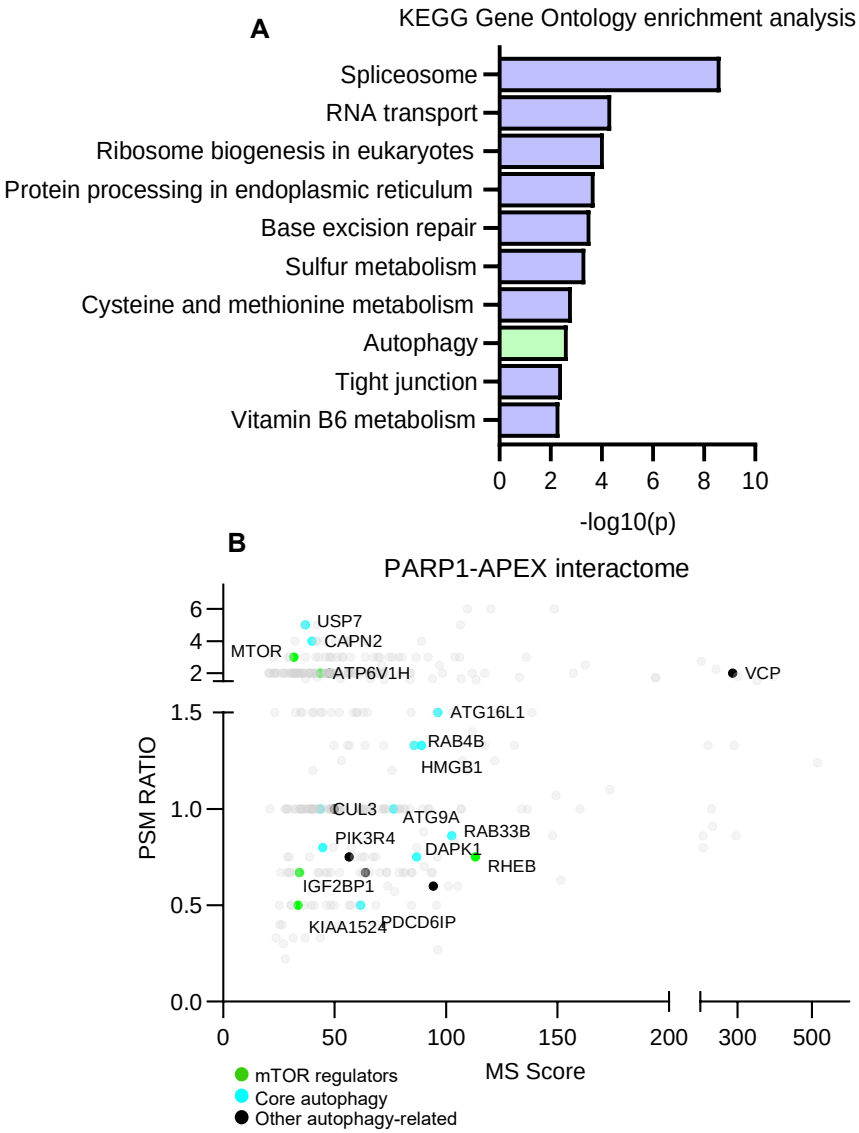

Figure 17: Autophagy factors detected in trapped PARP1 interactome. Mass spectrometry data from Krastev et al. (2022) of PARP1 interactions that are enriched under PARP1-trapping conditions (Tala + MMS) by PARP1^{WT}–Apex2–eGFP proximity labelling. (**A**) Gene sets identified by KEGG gene set enrichment analysis. Autophagy is the 8th most significantly enriched gene set. (**B**) PARP1 interactome with autophagy-related genes (Bordi et al., 2021) labelled. Higher PSM ratio indicates increased interaction upon PARP1 trapping.

To further validate the relevance of autophagy in trapped PARP1 response, I carried out RNA-seq of CAL51 cells after extended treatment with talazoparib. As expected, gene set enrichment analysis reveals PARPi-induced upregulation of genes related to DNA damage repair, replication stress, apoptosis, G1/S cell cycle checkpoint and mitotic checkpoint (Fig 18A). Specific top hits related to this include *CDKN1A* and *BTG2*, involved in DNA damage-induced p53-dependent G1/S checkpoint signalling (Chang et al., 2002); *MDM2*, a p53 regulator which also has p53-independent roles in regulation of DNA synthesis and repair (Nag, Qin, Srivenugopal, Wang, & Zhang, 2013); and *BAX*, a pro-apoptotic protein (Youle & Strasser, 2008) (Fig 18B). To investigate any modulation of autophagy-related genes, I once again probed with the comprehensive gene list used in mass spectrometry analysis (Bordi et al., 2021). Upon treatment with PARPi, 31 autophagy-related genes are significantly upregulated (by p value) with 9 of these significantly upregulated when using more stringent analysis (adjusted p value). The most significantly upregulated genes mainly consist of core autophagy machinery, namely *TP53INP1*, *DRAM1*, *PMAIP1*, *MYO6*, *EI24* and negative regulators of mTOR signalling, so positive regulators of autophagy, *SESN1* and *SESN2* (Fig 18B). *DRAM1* and *SESN* genes are well-established to be transcriptionally activated by p53 under genotoxic stress conditions to promote autophagy (Ambrosio & Majello, 2020). This is a markedly similar finding to proteins identified as interacting with trapped PARP1 and once again indicates increased autophagy flux after treatment. In accordance with this, numerous studies show upregulation of autophagy in cells and patient-derived xenografts treated with PARPi (Arun, Akar, Gutierrez-Barrera, Hortobagyi, & Ozpolat, 2015; Cahuzac et al., 2022; Elshazly et al., 2022; Y. Liu et al., 2019; Pai Bellare et al., 2021; Pai Bellare & Sankar Patro, 2022; Santiago-O'Farrill et al., 2020; Uddin et al., 2022). Whilst this supports a

role of autophagy in trapped PARP1 repair, various explanations have recently been tendered for the importance of autophagy upregulation upon PARPi treatment, including PARPi-induced upregulation of PTEN to promote cytoprotective autophagy (Santiago-O'Farrill et al., 2020) and decreased nuclear localisation of p62 causing upregulated HR (Cahuzac et al., 2022). However, when considering not only the upregulation of autophagy genes by RNA-seq, but also the interaction of many autophagy core machinery proteins with trapped PARP1 by mass spectrometry, it is worth considering that autophagy is playing a more direct role in the processing of trapped PARP1 upon talazoparib treatment.

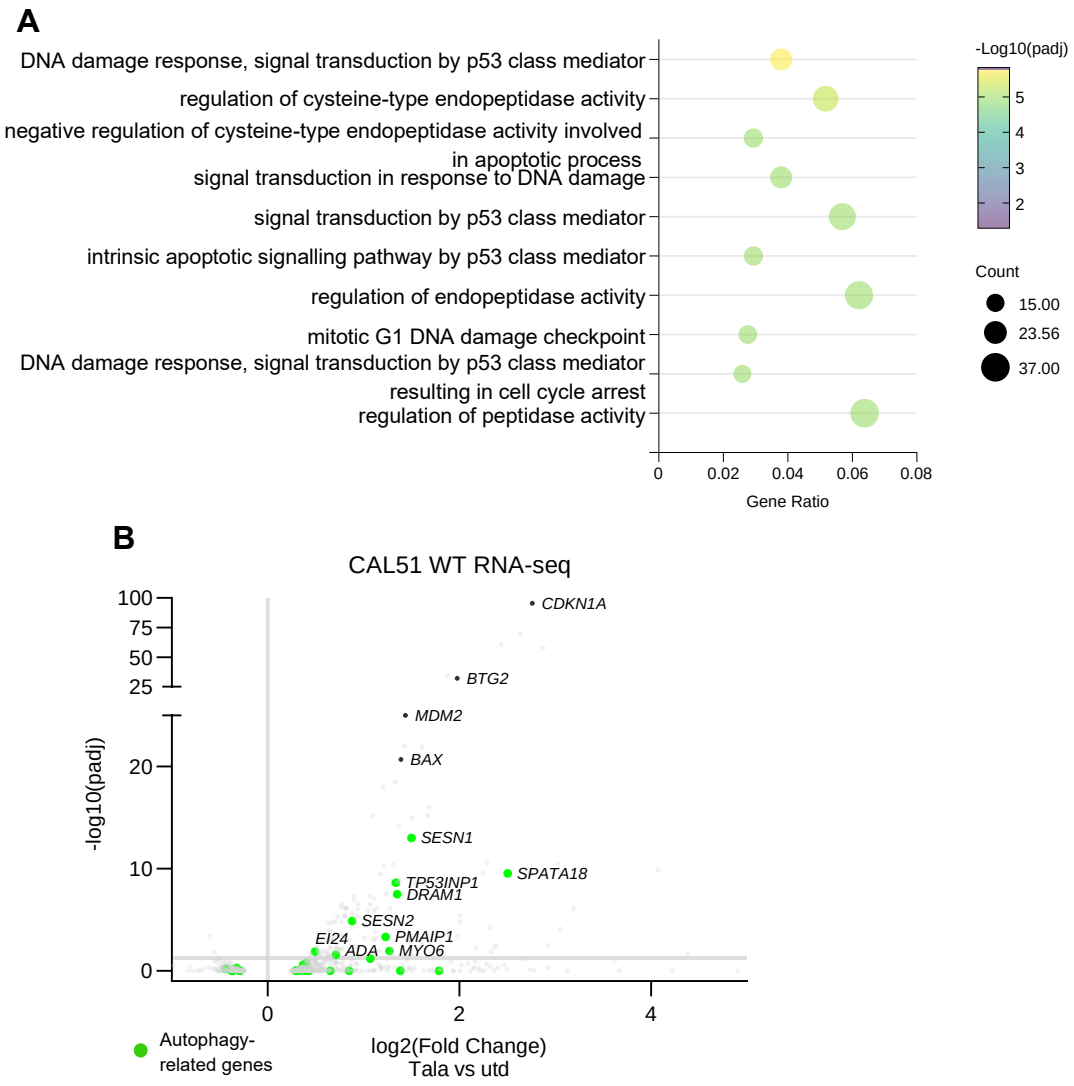

Figure 18: Autophagy is upregulated by PARPi treatment in RNA-seq. RNA-seq performed in CAL51

cells after 100 nM talazoparib treatment for 24 hrs compared to untreated. (**A**) Top gene sets identified by gene set enrichment analysis. Size of points indicates number of genes from each gene set whilst colour indicates level of significance. (**B**) Volcano plot showing differential gene expression in CAL51 cells comparing talazoparib treatment to untreated by RNA-seq. Relevant genes are labelled including autophagy-related genes identified from a previously described autophagy signature (Bordi et al., 2021). Grey line showing adjusted p value of 0.05.

4.3 Trapped PARP1 is directly processed by selective autophagy

Having established the PARPi-induced upregulation of autophagy-related genes and the interaction of core autophagy machinery with trapped PARP1, I sought to understand the role of autophagy in trapped PARP1 response. I hypothesised that trapped PARP1 could be processed by autophagy, meaning PARP1 would become localised to the lysosome under trapping conditions. To detect lysosome substrates, I performed immunoprecipitation of intact lysosomes (lysoIP) (Abu-Remaileh et al., 2017). A construct for the expression of HA-tagged TMEM192, a protein localised to the lysosome (Schröder, Wrocklage, Hasilik, & Saftig, 2010), was introduced to cells. Intact lysosomes were isolated over HA beads from cell extract generated by homogenisation to isolate and preserve the integrity of organelles (Abu-Remaileh et al., 2017). Cells were treated with bafilomycin A1, an autophagy inhibitor that neutralises the low pH of lysosomes, to prevent the degradation of lysosomal contents, allowing them to be detected by immunoblotting (Fig 19A). LAMP1, a resident lysosome marker (Abu-Remaileh et al., 2017), and LC3-II, incorporated in the autophagophore membrane (Kabeya et al., 2000), were both isolated in cells expressing TMEM192-3HA, but not in parental cells (Fig 19B, C), demonstrating the specificity of this technique for isolating lysosome-localised proteins. PARP1 was detected in lysosomes from both HeLa and CAL51 cells. Strikingly, PARP1 seemed to accumulate much more in lysosomes under trapping conditions in both HeLa and CAL51 cells (Fig 19B, C). In cells expressing either PARP1^{WT} or DNA-binding mutant

PARP1$^{del.p.119K120S}$ which cannot become trapped on DNA, only PARP1^{WT} accumulated in the lysosome under trapping conditions. Despite lower expression of PARP1$^{del.p.119K120S}$ in whole cell extract, even when the lysosomal level was normalised to whole cell level across 7 biological repeats, we observed a robust reduction in lysosomal PARP1$^{del.p.119K120S}$ compared to PARP1^{WT} (Fig 19D). Altogether, this implies that trapped PARP1 can be processed in the lysosome and that this lysosomal accumulation of PARP1 is specific to trapping, and not indirect effects of PARPi.

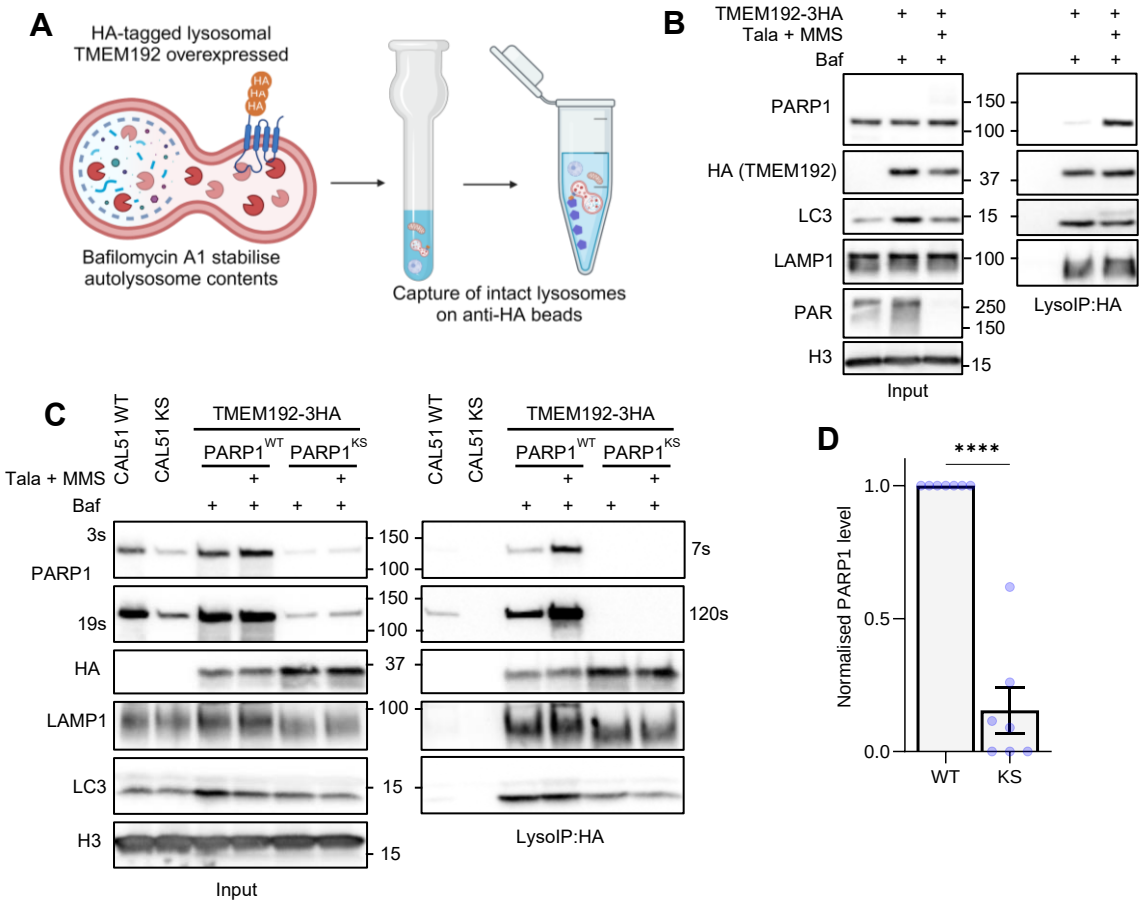

Figure 19: PARP1 accumulates in the lysosome under trapping conditions. (**A**) Schematic showing methodology of LysoIP, whereby TMEM192-3HA is immunoprecipitated from cells treated with Bafilomycin A1 to isolate intact lysosomes. (**B**) LysoIP in HeLa cells to detect PARP1 accumulation in the lysosome under PARP1 trapping conditions. (**C**) As in (A) but in CAL51 cells stably expressing either PARP1^{WT} or DNA-binding mutant PARP1del.p.119K120S (PARP1^{KS}). (**D**) Quantification of (C) from 7 biological repeats. Lysosomal PARP1 signal intensity is normalised by dividing by input PARP1 signal and lysoIP HA signal. Statistical analysis by unpaired t-test.

As an alternative to lysoIP for validation of trapped PARP1 processing by the lysosome, I turned to a modified mCherry-GFP reporter assay. Previously used to measure autophagy flux with a dual tagged mCherry-GFP LC3, this construct was modified to transiently express mCherry-PARP1-GFP. In most cellular compartments, including the nucleus, both mCherry and GFP fluoresce and co-localise. However, in the acidic environment of the lysosome, GFP is quenched so only the mCherry signal is observed (Kimura, Noda, & Yoshimori, 2007) (Fig 20A). This allows the visualisation of substrates and detection of their lysosome localisation in both fixed and live imaging. In fixed imaging, the majority of the mCherry and GFP signal was in the nucleus, as expected (Fig 20B). However, under trapping conditions, red puncta were seen outside the nucleus. The absence of green signal in these cytosolic red puncta confirmed their lysosomal localisation. As a control, treatment with Bafilomycin to neutralise lysosomal pH, preventing GFP quenching, converted these red-only buds to both red and green (Fig 20B, C). This technology was combined with lysoView, a lysosomal dye, by live imaging to track how both lysosome and PARP1 dynamics are affected by treatment (Fig 20D). Interestingly, upon treatment with talazoparib and MMS, lysosomes seemed to congregate around the nuclear envelope. After around 20 minutes of treatment, red puncta could be seen to emerge from the nucleus and localise with lysosomes. This appeared only red and not both red and green, further confirming that the PARP1 puncta localised within the lysosome and not simply in close proximity to it. Within 16 minutes of the puncta emerging from the nucleus and localising to lysosomes, it disappeared, and the lysosomes dispersed, indicating degradation of the puncta in the lysosome (Fig 20D). Altogether, this demonstrated visually that trapped PARP1 is processed in the lysosome.

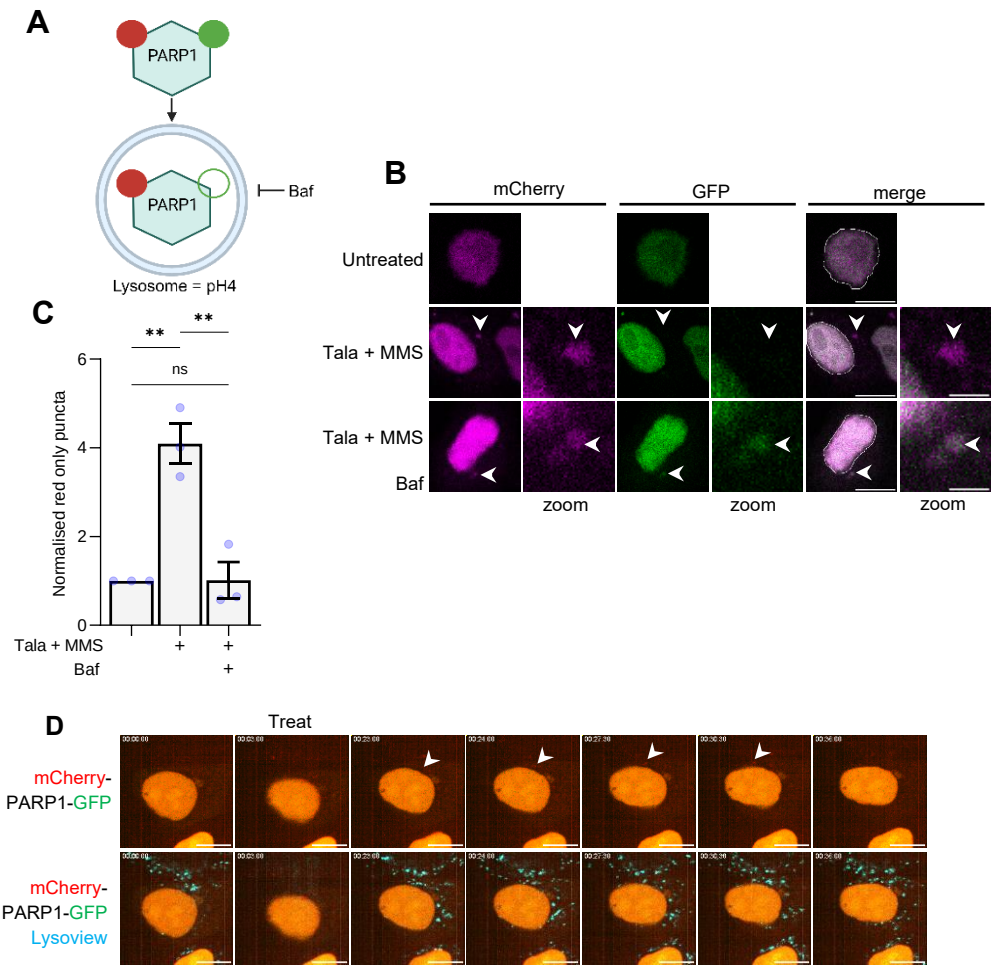

Figure 20: Trapped PARP1 is processed by the lysosome. (**A**) Schematic showing methodology of mCherry-GFP reporter assay. PARP1 tagged with mCherry and GFP is transiently expressed in cells and visualised by either fixed of live imaging. GFP is quenched in acidic environments so only the red signal is detected in the lysosome. This can be reversed by treatment with bafilomycin A1 which neutralises the lysosome. (**B**) Fixed images and (**C**) quantification from mCherry-PARP1-GFP reporter assay in cells either untreated, with Tala + MMS or combined with Bafilomycin A1 (50 nM). Statistical analysis by one-way ANOVA. Zoom images showing puncta indicated by white arrows. Scale bar 2 µm in zoom panels. (**D**) Images from live cell imaging of HeLa cells transfected with lysosome reporter mCherry-PARP1-GFP and stained with lysoView 680. Time stamps indicate time since imaging began, with Talazoparib + MMS treatment added at 3 minutes.

Combined with earlier data showing the interaction of trapped PARP1 with autophagy machinery and PARPi-induced upregulation of autophagy by RNA-seq and in previous literature (Elshazly et al., 2022), selective autophagy is likely to target trapped PARP1 for degradation in the lysosome. Selective autophagy relies upon conjugation of

lipidated LC3 to the inner concave surface of the growing phagophore (Vargas et al., 2023), as performed by a cascade of enzymes, similar to ubiquitination, such as the E1-like enzyme ATG7 (Slobodkin & Elazar, 2013). SARs are then able to bridge substrates to the phagophore via their LIR (Stolz, Ernst, & Dikic, 2014). To test the role of autophagy in transport of PARP1 to the lysosome, I depleted ATG7 to prevent LC3 membrane conjugation and performed lysoIP to detect levels of PARP1 in the lysosome under trapping conditions. Strikingly, depletion of ATG7 reduced PARPi-induced accumulation of PARP1 in the lysosome ~4-fold (Fig 21A, B). Evidently, lipidation of LC3 is essential for lysosomal processing of trapped PARP1. In further validation of this, the same effect on lysosomal PARP1 levels was observed when autophagosome-lysosome fusion is inhibited through the depletion of syntaxin-17 (Fig 21C, D) (Itakura et al., 2012). Overall, this demonstrates that trapped PARP1 is processed by autophagy directly.

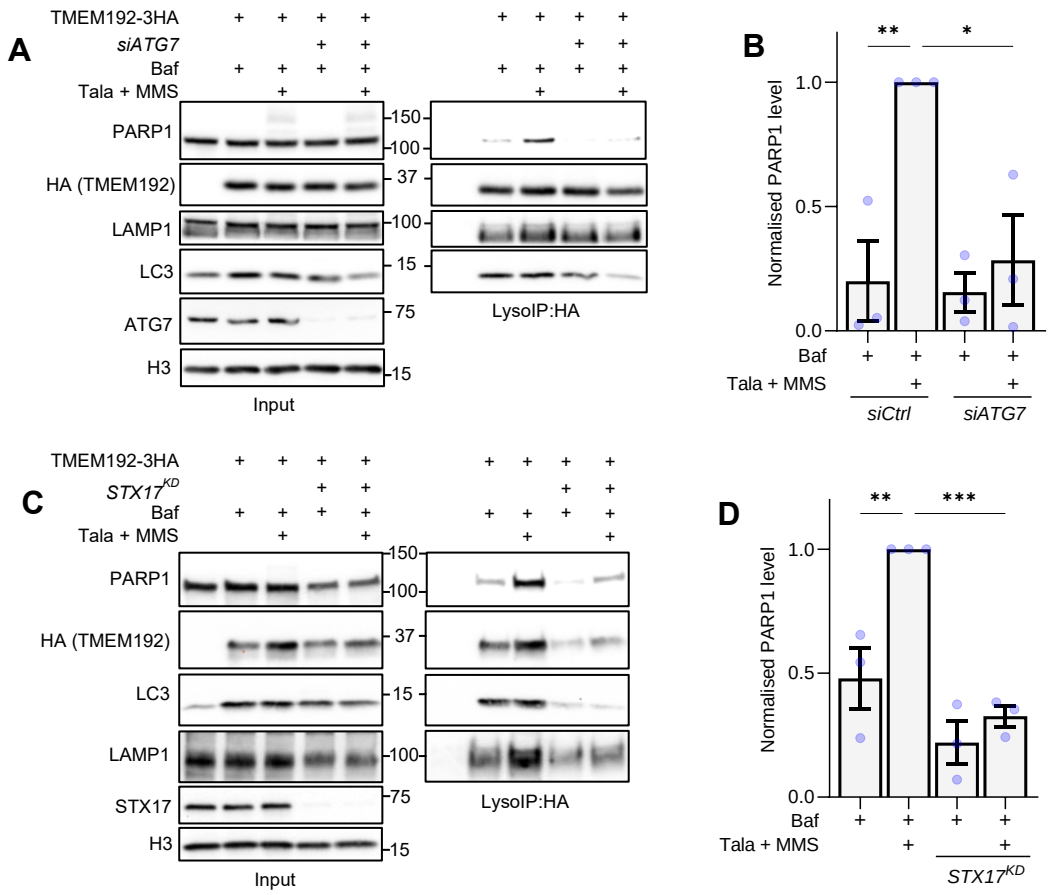

Figure 21: Autophagy mediates PARP1 processing in the lysosome. (**A**) LysoIP in HeLa cells with depletion of ATG7 by siRNA, with siRNA against luciferase as a control. (**B**) Quantification of (A) from 3 repats with statistical analysis by one-way ANOVA. (**C**) LysoIP in HeLa cells with stable knockdown of syntaxin-17 (*STX17^{KD}*). (**D**) Quantification of (C) across 3 repeats with quantification by one-way ANOVA.

4.4 Autophagosomal processing of trapped PARP1 is TEX264-dependent

Selective autophagy heavily depends upon SARs, such as TEX264 described in reticulophagy (An et al., 2019; Chino et al., 2019). TEX264 contains a LIR domain, crucial for its activity in autophagy by interacting with LC3, and a SHP box, essential for its p97 co-factor function (Fig 22A). Due to its interaction with trapped PARP1, both on chromatin and in the cytosol, I postulated that TEX264 acts as a SAR for the autophagosomal processing of trapped PARP1. In accordance with this, PARPi-induced accumulation of PARP1 in the lysosome was considerably depleted by CRISPR/Cas9 knockout of *TEX264* (Fig 22B). To test if this is due to the SAR function

of TEX264, I complemented *TEX264*$^{-/-}$ cells with a TEX264 variant containing a mutation in its LIR domain (TEX264^{LIR*}). Unlike complementation with TEX264^{WT} which was able to rescue the reduction of lysosomal PARP1, expression of TEX264^{LIR*} failed to restore PARP1 levels (Fig 22B, C). This supports the hypothesis that selective autophagy of trapped PARP1 is mediated by TEX264 acting as a SAR.

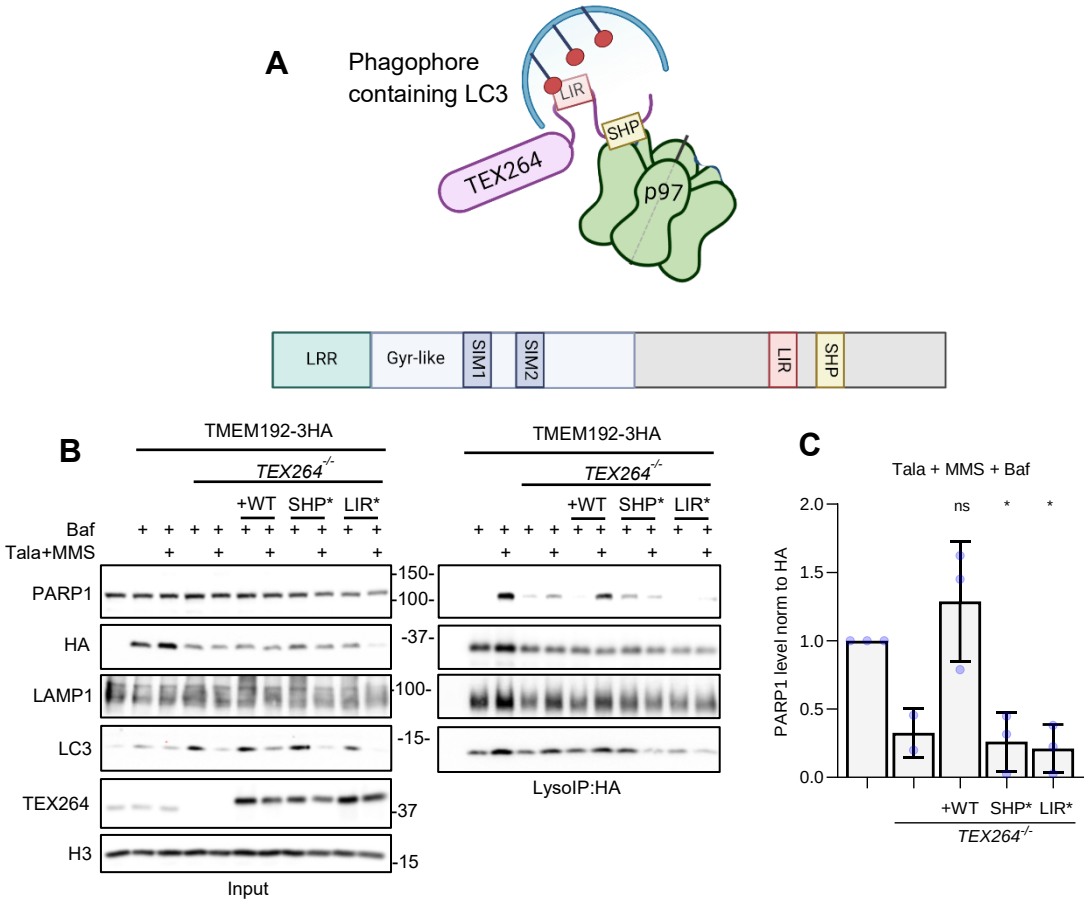

Figure 22: Processing of trapped PARP1 by autophagy is mediated by TEX264. (**A**) Schematic showing domain structure of TEX264 with a focus on the LC3-interacting region (LIR) and p97-binding domain (SHP). (**B**) LysoIP in HeLa WT or *TEX264*$^{-/-}$ cells stably expressing TMEM192-3HA. TEX264-V5 variants are transiently expressed where indicated. (**C**) Quantification of (B) from 3 repeats, except for *TEX264*$^{-/-}$ which was included in 2 repeats. Statistical analysis by one-way ANOVA compared to WT.

As TEX264 has dual functions as both a SAR and p97 co-factor (Fielden et al., 2022), I also explored if its p97-related functions are involved in trapped PARP1 processing by autophagy through mutation of its SHP box. In a similar manner to TEX264^{LIR*}, TEX264^{SHP*} was unable to rescue lysosomal PARP1 levels (Fig 22B, C). This

demonstrates the importance of this domain, and therefore the p97 co-factor function of TEX264, for autophagosomal processing of trapped PARP1.

4.5 Autophagic processing of trapped PARP1 is distinct from previous p97-dependent pathways

As I have demonstrated, trapped PARP1 is processed by selective autophagy which depends upon TEX264 acting as a SAR and p97 co-factor. Our group has previously demonstrated a pathway for the p97-mediated extraction of trapped PARP1 from chromatin. Briefly, trapped PARP1 is SUMOylated by PIAS4 followed by ubiquitination by the STUbL RNF4. This ubiquitination recruits p97-cofactor UFD1 which in turn recruits p97 to the trapped PARP1 lesion (Krastev et al., 2022). To test if components of this pathway are linked to autophagosomal processing of trapped PARP1, I began by validating the importance of p97 in this process. Cells treated with CB-5083, a specific and clinically relevant inhibitor of the AAA+-ATPase activity of p97 (Anderson et al., 2015; Kilgas & Ramadan, 2023), combined with trapping conditions displayed reduced lysosomal PARP1 accumulation (Fig 23A), in accordance with TEX264^{SHP*} expression. p97 is also involved in autophagy both at the stage of initiation, through beclin-1 stabilisation and assembly of PI3K complex for autophagophore formation (Hill et al., 2021; Z. Wang et al., 2024), and at a later stage of autophagosome-lysosome fusion (Ju et al., 2009; Tresse et al., 2010). In line with this, CB-5083 treatment is known to impair formation of LC3 puncta upon starvation, implying impaired autophagy function (Hill et al., 2021), whilst p97 knockdown results in accumulation of immature autophagosomes (Ju et al., 2009; Tresse et al., 2010). However, in Figure 23A, the presence of LC3 in the lysosome with CB-5083 treatment confirmed that the decrease in lysosomal PARP1 isn't due to inhibition of autophagy by CB-5083 but as part of a more specific PARP1-associated role of p97. To test

whether ubiquitination and SUMOylation are important in this process, cells were treated with E1 inhibitors MLN-7243 and ML-792, respectively. Strikingly, both inhibitors prevented PARPi-induced lysosomal accumulation of PARP1 (Fig 23B), implying that, alongside p97, both ubiquitination and SUMOylation are key for this process.

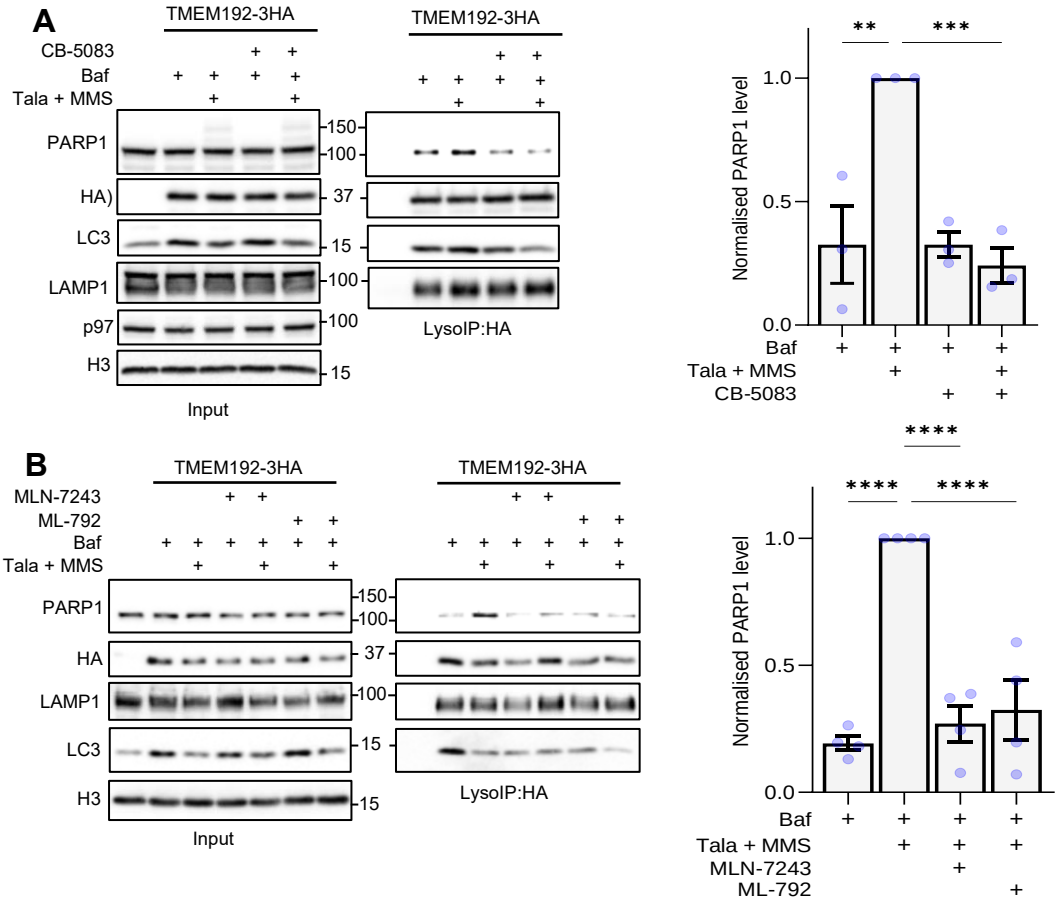

Figure 23: Autophagosomal processing of trapped PARP1 is p97 and ubiquitin/SUMO-dependent. (**A**) LysoIP in HeLa cells treated with talazoparib and MMS combined with p97i CB-5083 (10 μM). Right panel shows quantification from 3 repeats with statistical analysis by one-way ANOVA. (**B**) LysoIP in HeLa cells treated with either ubiquitination inhibitor MLN-7243 (5 μM) or SUMOylation inhibitor ML-792 (1 μM). Quantification in right panel from 4 repeats with analysis by one-way ANOVA

Having established the importance of p97 and PTMs ubiquitination and SUMOylation, for trapped PARP1 clearance by selective autophagy, I next tested whether known instigators of these modifications and interactions are also important. Either RNF4^{WT} or a dominant negative E2 binding mutant of RNF4 which carries M136A and R177A mutations (RNF4^{DN}) were overexpressed. Neither overexpression of RNF4^{WT} or

RNF4^{DN} affected PARP1 localisation to the lysosome (Fig 24A). This implies that RNF4 is not involved in autophagy-mediated trapped PARP1 clearance but must be acting in an alternate pathway. Similarly, depletion of UFD1 using two distinct siRNA had no effect on lysosomal PARP1 levels (Fig 24B). Therefore, although p97 activity, as well as ubiquitylation and SUMOylation are important for trapped PARP1 clearance via autophagy, this is not mediated or recognised by RNF4 or UFD1.

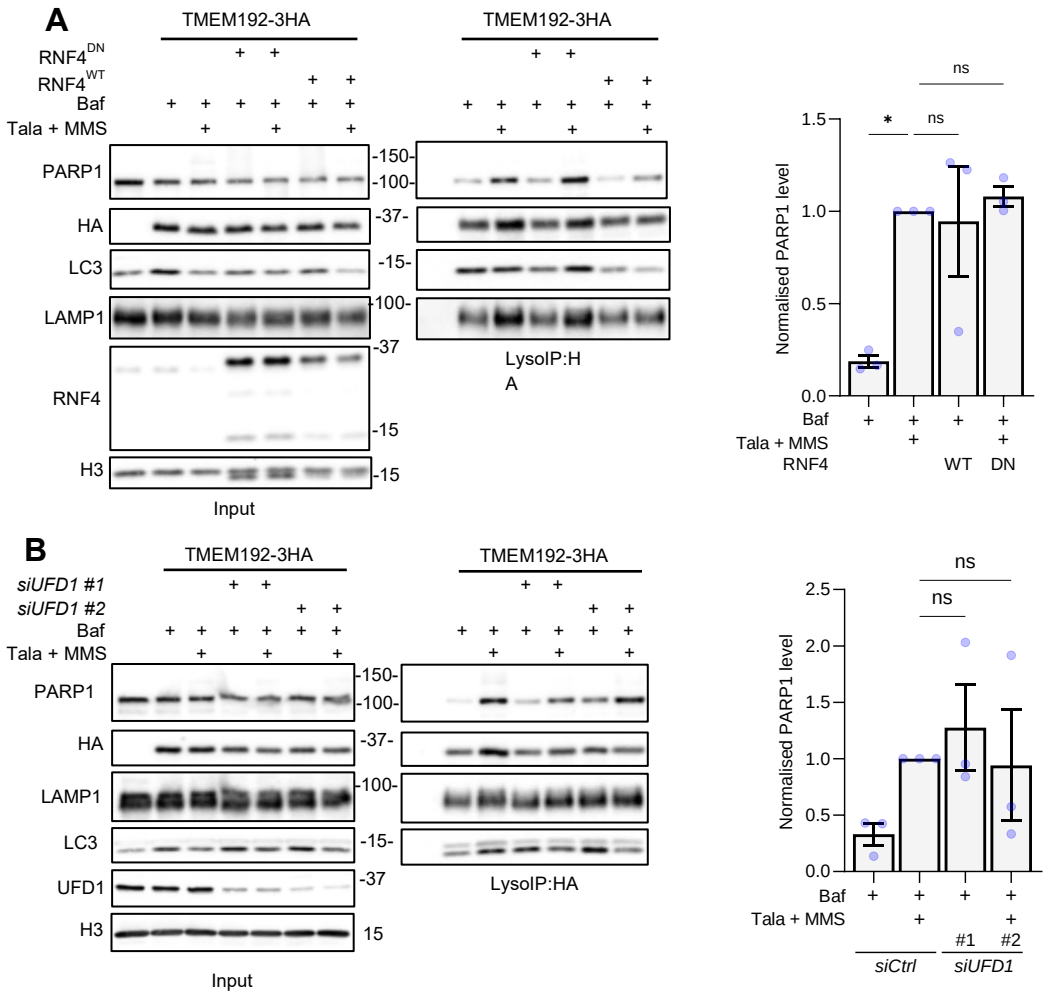

Figure 24: Autophagosomal processing of trapped PARP1 is independent of RNF4 and UFD1. (**A**) LysoIP in HeLa cells with overexpression of either RNF4 wild-type (RNF4^{WT}) or RNF4 dominant negative M136A+R177A mutant (RNF4^{DN}). (**B**) LysoIP in HeLa cells depleted of UFD1 using two different siRNA sequences. Graphs in right panels show quantification from 3 biological repeats with statistical analysis by one-way ANOVA.

4.6 Concluding remarks

I have demonstrated that trapped PARP1 is processed from chromatin by selective autophagy, whereby TEX264 acts as a SAR for PARP1. This process depends upon p97 through the role of TEX264 as a p97 co-factor and is also ubiquitin- and SUMO-dependent. Despite this, the autophagosomal processing of trapped PARP1 differs from a previously described pathway (Krastev et al., 2022) in that RNF4 and UFD1 are not involved. The PIAS4/RNF4 axis is well-established for SUMO-targeted ubiquitination of substrates to drive their proteasomal degradation (Sriramachandran & Dohmen, 2014). RNF4 was first shown to drive proteasomal degradation of promyelocytic leukaemia protein (PML) to disrupt PML-bodies (Lallemand-Breitenbach et al., 2008; Tatham et al., 2008; Weisshaar et al., 2008), with many substrates identified since, including PARP1 in response to heat shock (Martin et al., 2009). UFD1, commonly working as a complex with NPL4, is one of the best characterised p97 co-factors and has been shown in yeast to function downstream of STUbL-mediated ubiquitination to promote p97-mediated unfolding and proteasomal degradation of substrates (Køhler et al., 2015; H. G. Lee, Lemmon, & Lima, 2023). Taking this into account, it is likely that RNF4 and UFD1 are involved in an undescribed proteasomal processing of trapped PARP1 whilst autophagosomal processing relies upon TEX264 and as yet unidentified ubiquitin and SUMO ligases to work alongside p97.

5. Results: Disruption to the TEX264-p97-autophagy axis causes increased replication-associated damage and overcomes PARPi resistance

N.B. Some work in this chapter was generated in collaboration with two students who were under my supervision for 3-month research placements: Junyi Li and Cynthia Hou. They contributed to figures 26, 27B and 28.

PARPi is known to cause excessive replication-associated DNA damage, likely due to collision between trapped PARP1 and the replisome, leading to replication fork collapse into DSBs (Helleday, 2011; Pommier, O'Connor, & de Bono, 2016; Wicks et al., 2022). As a result of this, PARP1 trapping orchestrates increases in DDR markers such as γH2AX and 53BP1 (Murai et al., 2012). These serve primarily as markers for DSBs when H2AX is phosphorylated by ATM at Ser139 in the early stage of DSB recognition (Burma, Chen, Murphy, Kurimasa, & Chen, 2001), enabling a signalling cascade to recruit downstream repair factors, one being 53BP1 which restrains DNA end processing to promote NHEJ (Bunting et al., 2010; Panier & Boulton, 2014). PARPi are also associated with the accumulation of chromatin-bound RPA, an indicator of replication stress and ssDNA gaps (Belan et al., 2022; Cong et al., 2021; Paes Dias et al., 2021) where RPA binds to exposed ssDNA to protect it from aberrant degradation and to promote downstream repair (Oakley & Patrick, 2010). PARPi-induced DNA damage forms in a replication-associated manner (Michelena et al., 2018), consistent with increased replication stress, shown by heightened ATR signalling (Gralewska et al., 2020), and changes in fork dynamics (Maya-Mendoza et al., 2018). I aimed to observe how disruption to TEX264/p97-mediated selective autophagy of trapped PARP1 affects DNA damage levels in response to PARPi, with a focus on these well-established markers.

5.1 PARPi-induced DNA damage response signalling is altered in *TEX264*$^{-/-}$ cells

To determine how TEX264/p97-mediated selective autophagy affects PARPi-induced DDR, I carried out RNA-sequencing in *TEX264*$^{-/-}$ cells which are deficient in this pathway, as shown by impaired PARP1 transport to the lysosome, accumulation of trapped PARP1 and increased sensitivity to talazoparib. I compared gene expression between WT and *TEX264*$^{-/-}$ HeLa and CAL51 cells after 24 hrs treatment with 100 nM talazoparib, a dose at which *TEX264*$^{-/-}$ cells were ~3-fold (HeLa) or ~4-fold (CAL51) more sensitive than their WT counterparts. I probed RNA-seq data with a DDR gene set (GO:0006974) and observed significant differential expression of 60 and 37 genes related to DNA damage repair in HeLa and CAL51 cells, respectively (Fig 25). 34 (HeLa) and 20 (CAL51) of these genes encode proteins involved in DSB repair, indicating this pathway is altered in *TEX264*$^{-/-}$ cells. NER and BER were also altered, with 10 (HeLa) and 3 (CAL51) genes affected that are involved in one of these pathways. PARP1 becomes trapped on these lesions as PARP1 signalling is key in NER and BER for scaffolding recruitment of repair machinery (Pines et al., 2012; Reynolds et al., 2015; Robu et al., 2013). 29 (HeLa) and 24 (CAL51) genes related to cell cycle checkpoint signalling and apoptosis were also differentially expressed in *TEX264*$^{-/-}$ cells exposed to talazoparib, consistent with TEX264 loss disrupting cell cycle progression and promoting apoptosis in response to dysregulation of DDR (Fig 25). Altogether, this indicates that TEX264-deficient cells experience altered DDR signalling under PARPi treatment.

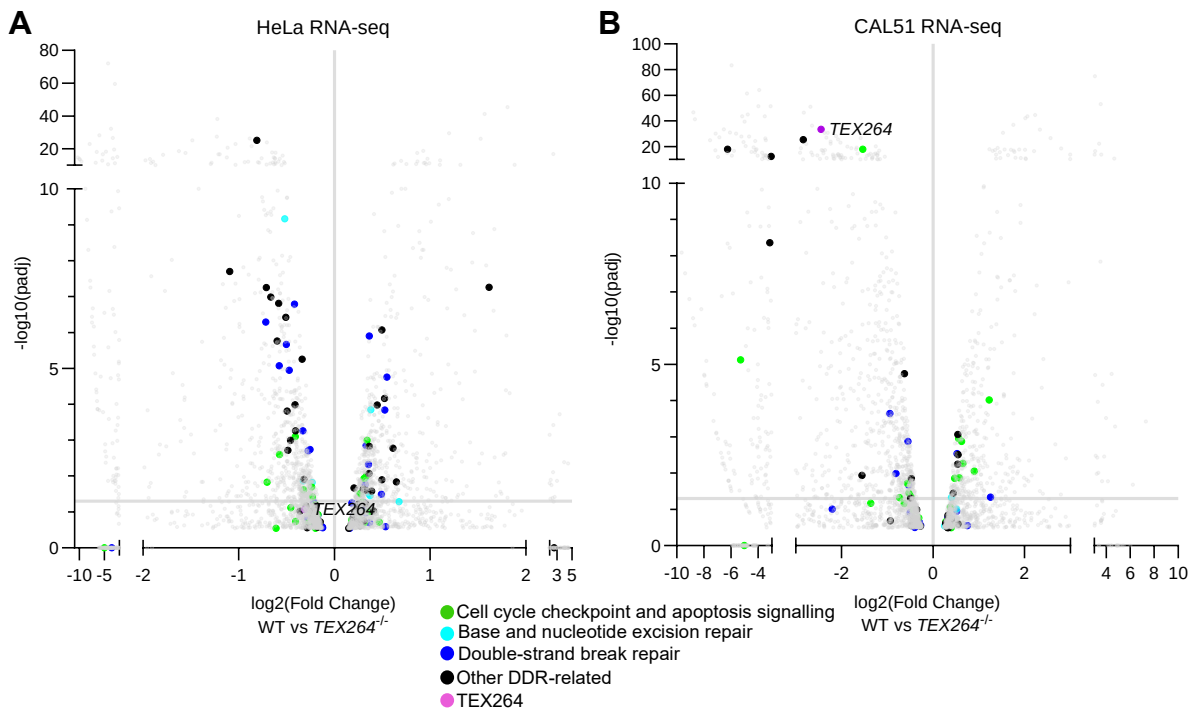

Figure 25: DDR genes are differentially expressed in *TEX264*$^{-/-}$ cells in response to talazoparib. (**A and B**) Volcano plot showing differential gene expression in HeLa (**A**) or CAL51 (**B**) by RNA-seq. Comparison is between *TEX264*$^{-/-}$ and wild-type cells after treatment with talazoparib (100 nM, 24 hrs). Genes relating to DNA damage response are coloured as shown. *TEX264* is labelled. Grey line showing adjusted p value of 0.05.

5.2 Trapped PARP1 accumulation induces DNA damage and replication stress in *TEX264*$^{-/-}$ cells

TEX264, through its role in mediating selective autophagic processing of trapped PARP1, seems to be involved in the PARPi-induced DNA damage response. To further explore this, I used immunofluorescence with detergent pre-extraction to compare PARPi-induced γH2AX, RPA and 53BP1 foci in WT and *TEX264*$^{-/-}$ HeLa cells. As expected, these DDR markers were activated by talazoparib treatment. Strikingly, a 1.4-, 2.1- and 1.8-fold increase in γH2AX, RPA and 53BP1 foci, respectively, was observed in HeLa *TEX264*$^{-/-}$ cells compared to WT (Fig 26A, B). An increase was also observed in CAL51 cells (Fig 26D, E). As well as DNA damage, PARPi induce replication stress, as seen by increased levels of pRPA2 (S33) and pCHK1 (S345),

phosphorylation markers induced by ATR signalling. These markers were further increased in *TEX264*$^{-/-}$ cells in response to PARPi (Fig 26C), suggesting an increase in ATR signalling associated with replication stress. Importantly, *TEX264*$^{-/-}$ alone did not result in changes to either DDR or replication stress markers, confirming that the increase observed is not simply due to the previously described PARPi-independent role of TEX264 in the removal of TOP1cc at the replication fork (Fielden et al., 2022; Fielden et al., 2020; Lascaux et al., 2024).

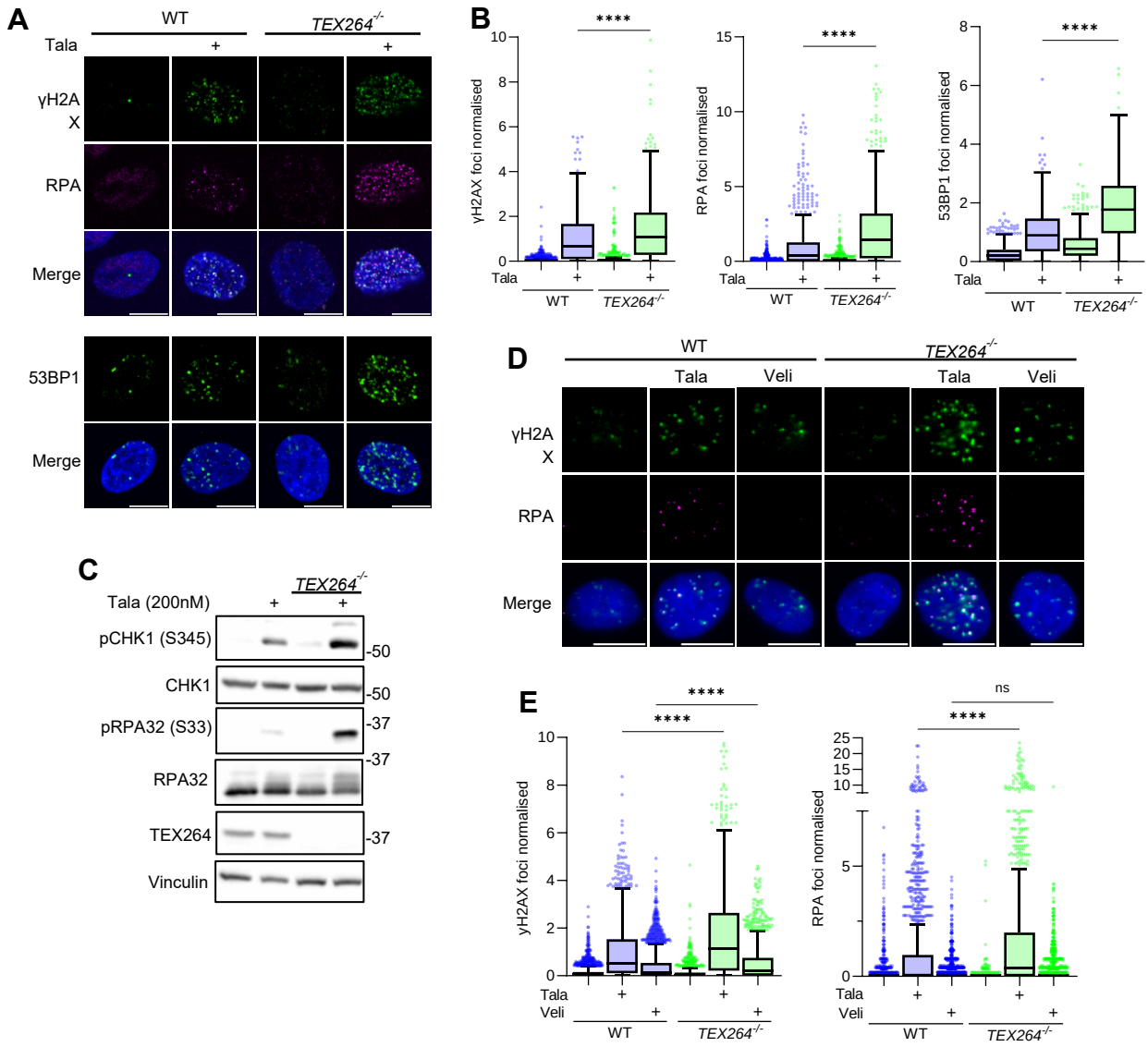

Figure 26: TEX264 loss causes PARPi-induced genome instability. (**A**) Images and (**B**) quantification of RPA, 53BP1 and γH2AX foci in HeLa WT and *TEX264*$^{-/-}$ cells after 24 hrs talazoparib treatment. Quantification from >700 cells across 3 biological repeats, shown as Tukey box plot with statistical

analysis by one-way ANOVA. (**C**) Immunoblotting of replication stress markers in HeLa WT and *TEX264*$^{-/-}$ cells treated with talazoparib for 24 hrs. Images (**D**) and quantification (**E**) of γH2AX and RPA foci in CAL51 WT and *TEX264*$^{-/-}$ cells treated with either talazoparib (200 nM) or veliparib (10 μM) for 24 hours. Quantification shows >900 cells from 3 biological repeats as Tukey box plot with statistical analysis by one-way ANOVA.

I have demonstrated that TEX264/p97-mediated selective autophagy acts specifically on trapped PARP1, as disruption to this pathway caused sensitivity specifically to trapping PARPi (talazoparib) but not non-trapping catalytic PARPi (veliparib). Accordingly, RPA foci were significantly increased in *TEX264*$^{-/-}$ cells only in response to talazoparib and not veliparib (Fig 26D, E). Whilst γH2AX foci were increased in *TEX264*$^{-/-}$ cells in response to both PARPi, levels of this DDR marker were far lower upon veliparib than talazoparib treatment, showing the dependence on trapping for inducing DNA damage. Overall, this indicates that the PARPi-induced damage accumulation observed in *TEX264*$^{-/-}$ cells is due to the accumulation of trapped PARP1.

5.3 Inhibition of p97 or autophagy causes increased PARPi-induced DNA damage

The role of TEX264 in repairing trapped PARP1 is essential for restraining DNA damage and replication stress levels in response to PARPi. This role in repairing trapped PARP1 relies on its interaction with p97 and the selective autophagy machinery LC3 through its SHP and LIR domains, respectively, as the mutation of either of these domains prevented the shuttling of PARP1 to the lysosome. To explore if this wider pathway regulates PARPi-induced DNA damage, I generated cell lines where WT, SHP* or LIR* variants of TEX264 were expressed in a *TEX264*-null background, then observed talazoparib-induced γH2AX and RPA levels by immunofluorescence and cellular sensitivity by colony formation assay. Notably, the expression of TEX264^{WT} rescued both γH2AX and RPA foci levels and cellular

sensitivity to be in line with WT cells (Fig 27). However, DNA damage levels remained high in cells expressing either TEX264^{SHP*} or TEX264^{LIR*} mutants, with these mutants also conferring hypersensitivity to talazoparib (Fig 27). This demonstrates, as with lysoIP experiments, that TEX264 interaction with p97 and LC3 is essential in clearing trapped PARP1 to restrain genomic instability and talazoparib sensitivity.

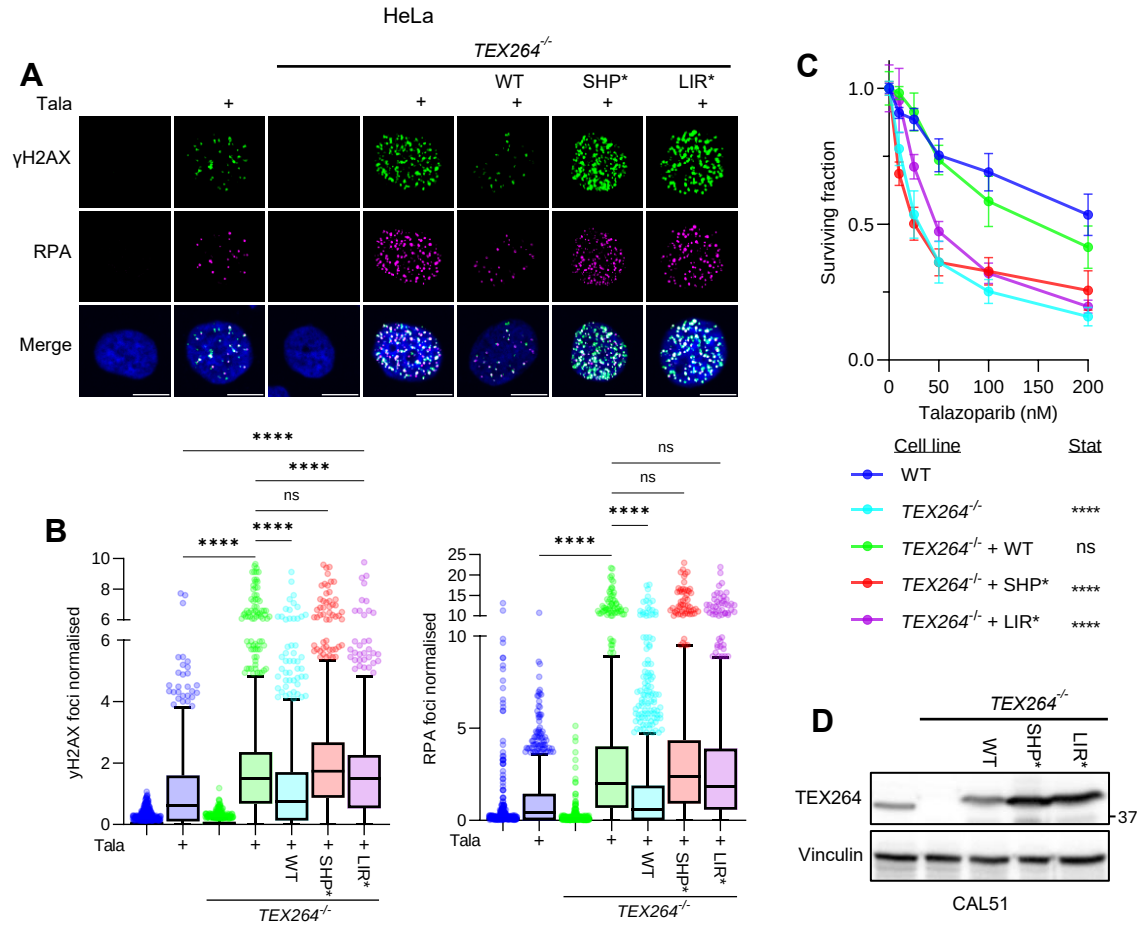

Figure 27: TEX264 SHP and LIR domains are essential for genome stability and sensitivity in response to PARPi. (**A**) Images and (**B**) quantification of RPA and γH2AX foci in HeLa WT, *TEX264*$^{-/-}$ or *TEX264*$^{-/-}$ cells stably expressing indicated TEX264 variants, treated with talazoparib. Quantification is from >600 cells over 4 biological repeats with statistical analysis by one-way ANOVA. (**C**) Colony formation assay in CAL51 WT, *TEX264*$^{-/-}$ or *TEX264*$^{-/-}$ cells stably expressing indicated TEX264 variants, treated with talazoparib for 24 hrs. 6 technical replicates from 2 biological repeats with statistical analysis by two-way ANOVA. (**D**) Immunoblotting of TEX264 in CAL51 either wild-type, *TEX264*$^{-/-}$ or *TEX264*$^{-/-}$ with TEX264-V5 variants stably introduced.

Alongside mutation of SHP to interrupt TEX264-p97 interaction, p97 can be inhibited chemically using CB-5083 which I earlier showed to inhibit PARP1 shuttling to the

lysosome. In accordance with this and with TEX264^{SHP*} expression, CB-5083 combined with talazoparib increased RPA levels compared with talazoparib alone. However, the opposite effect was observed for γH2AX foci under p97i conditions (Fig 28A, B). This is to be expected as p97 inhibition is known to impair ATM kinase activity (Blandine Roux et al., 2021), the central kinase for phosphorylation of H2AX (γH2AX) in response to DNA damage (Burma et al., 2001). In previous work, CB-5083 treatment hypersensitised cells to PARPi (Krastev et al., 2022). Altogether, this validates observations seen with the TEX264^{SHP*} mutant and confirms that disruption of trapped PARP1 clearance by TEX264-p97 hypersensitises cells to PARPi through heightened genomic instability.

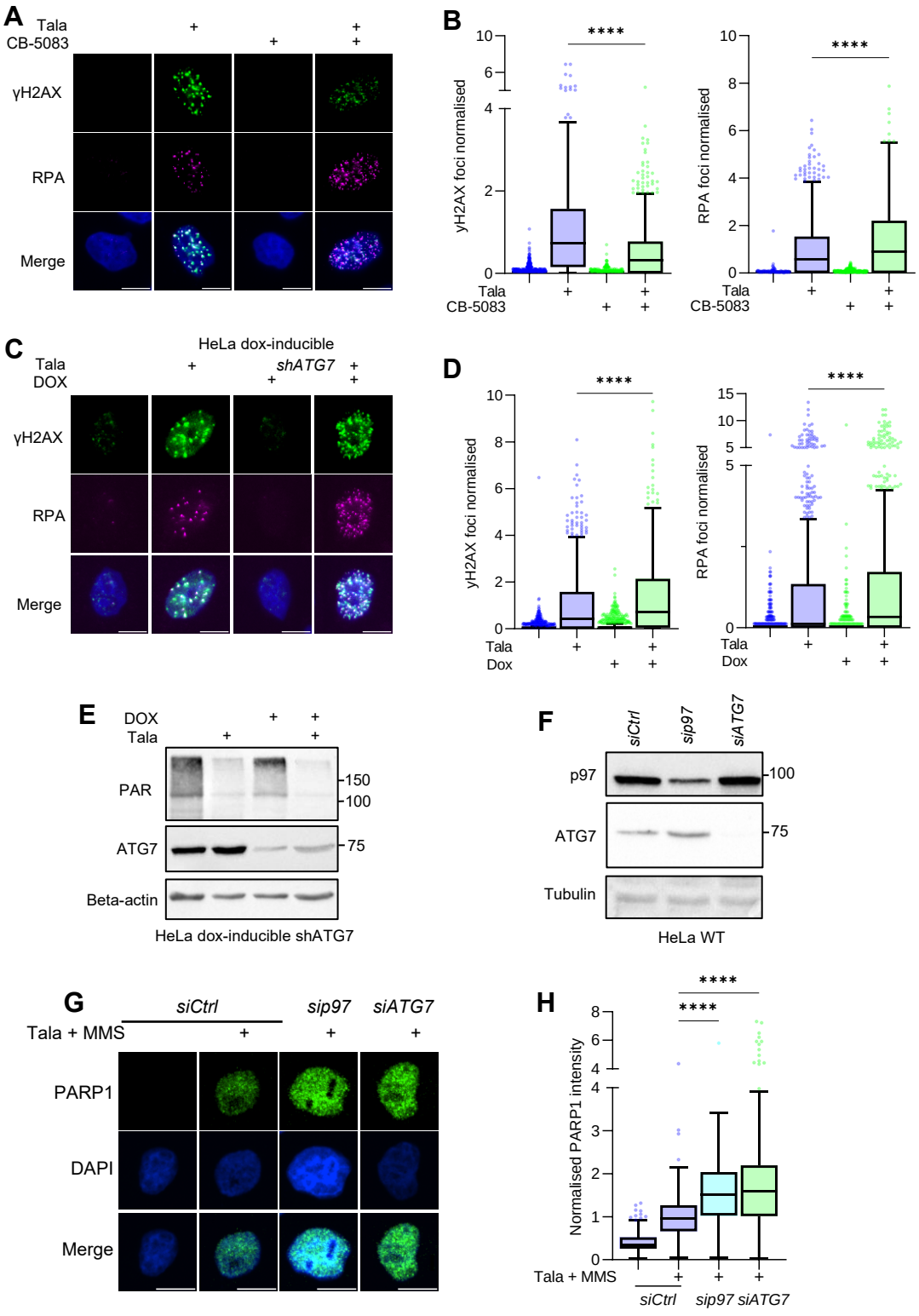

Figure 28: p97 or autophagy inhibition increases PARPi-induced DNA damage. (**A and B**) Images (**A**) and quantification (**B**) of γH2AX and RPA foci in HeLa WT cells treated with talazoparib for 24 hrs with or without CB-5083 (10 μM) for last 4 hrs. Quantification shows >900 cells from 3 biological repeats as Tukey box plot with statistical analysis by one-way ANOVA. (**C and D**) Images (**C**) and quantification (**D**) of γH2AX and RPA foci in HeLa doxycycline-inducible *shATG7* cells treated with talazoparib for 24 hrs with or without doxycycline. Quantification shows >900 cells from 3 biological repeats as Tukey box

plot with statistical analysis by one-way ANOVA. (**E**) Immunoblot control showing successful ATG7 depletion for (C) and (D). (**F**) Immunoblot showing successful depletion of either p97 or ATG7 for experiments in (G) and (H). (**G and H**) Immunofluorescence with detergent pre-extraction to detect trapped PARP1 foci in cells depleted for the indicated proteins using siRNA and treated with talazoparib and MMS. Images have 10 μM scale bar. Quantification is from >300 cells across 2 biological repeats shown as a Tukey box plot with statistical analysis by one-way ANOVA.

Disruption of the role of TEX264 as a SAR by TEX264^{LIR*} expression also led to increased PARPi-induced genomic instability and hypersensitivity. To further validate this, I used cells expressing short hairpin RNA (shRNA) against ATG7 under a doxycycline-inducible promoter. This allowed the targeted knockdown of ATG7 to disrupt LC3 conjugation to the autophagophore, thereby inhibiting selective autophagy (Slobodkin & Elazar, 2013). As with TEX264^{LIR*}, *shATG7* caused an accumulation of γH2AX and RPA foci in response to talazoparib (Fig 28C-E). Autophagy has been shown to maintain genomic stability (Rodriguez-Rocha, Garcia-Garcia, Panayiotidis, & Franco, 2011) by regulating nucleotide availability (Vanzo et al., 2020), restricting levels of damaging ROS (Karantza-Wadsworth et al., 2007; Mortensen et al., 2011) and by controlling the levels of DNA repair factors accessible to lesions (Cahuzac et al., 2022; J. H. Chen et al., 2015; Muciño-Hernández et al., 2023; Robert et al., 2011; Santiago-O'Farrill et al., 2020). However, I observed no effect of *shATG7* alone on γH2AX and RPA foci when compared to WT. Further to this, ATG7 depletion caused an increase in trapped PARP1 levels under trapping conditions to a similar extent as p97 depletion (Fig 28F-H), validating its role in the removal of trapped PARP1. Altogether, this supports that the increased genomic stability observed when autophagy is inhibited in combination with PARPi is due to accumulated, unrepaired trapped PARP1, rather than PARP-independent roles of autophagy in regulating genome stability.

5.4 Autophagy modulation affects cellular survival in response to PARPi

To maintain genome stability, TEX264-orchestrated p97-mediated selective autophagy clears trapped PARP1 from chromatin. Due to this, disruption of either TEX264 or p97 hypersensitised cells to treatment with trapping PARPi, talazoparib. Combination therapies are being explored to improve use of PARPi in the clinical setting, with a handful of studies pointing to autophagy as a potential target (Elshazly et al., 2022). To explore this, I modulated autophagy both chemically and genetically and assessed sensitivity to PARPi. Inhibition of autophagy through depletion of either ATG7, involved in the early stages of autophagy, or syntaxin-17, a regulator of autophagosome-lysosome fusion later in autophagy (Itakura et al., 2012), caused increased sensitivity to talazoparib (Fig 29A, B). Similarly, Bafilomycin A1, an inhibitor of lysosome acidification and substrate degradation, hypersensitized cells to talazoparib (Fig 29C). To assess the effect of boosting autophagy flux, talazoparib treatment was combined with Torin-1, an inhibitor of mTOR signalling to cause increased autophagy flux (Thoreen et al., 2009). Strikingly, Torin-1 caused a stark resistance to talazoparib (Fig 29C). Autophagy is important for maintaining cell fitness, especially under stress. However, modulation of autophagy with bafilomycin or torin-1 had no effect on cellular sensitivity to non-trapping PARPi veliparib, even at high, cytotoxic micromolar doses (Fig 29D). Altogether, this demonstrates that modulation of the autophagy pathway affects sensitivity to PARPi and could be further explored as a combination therapy.

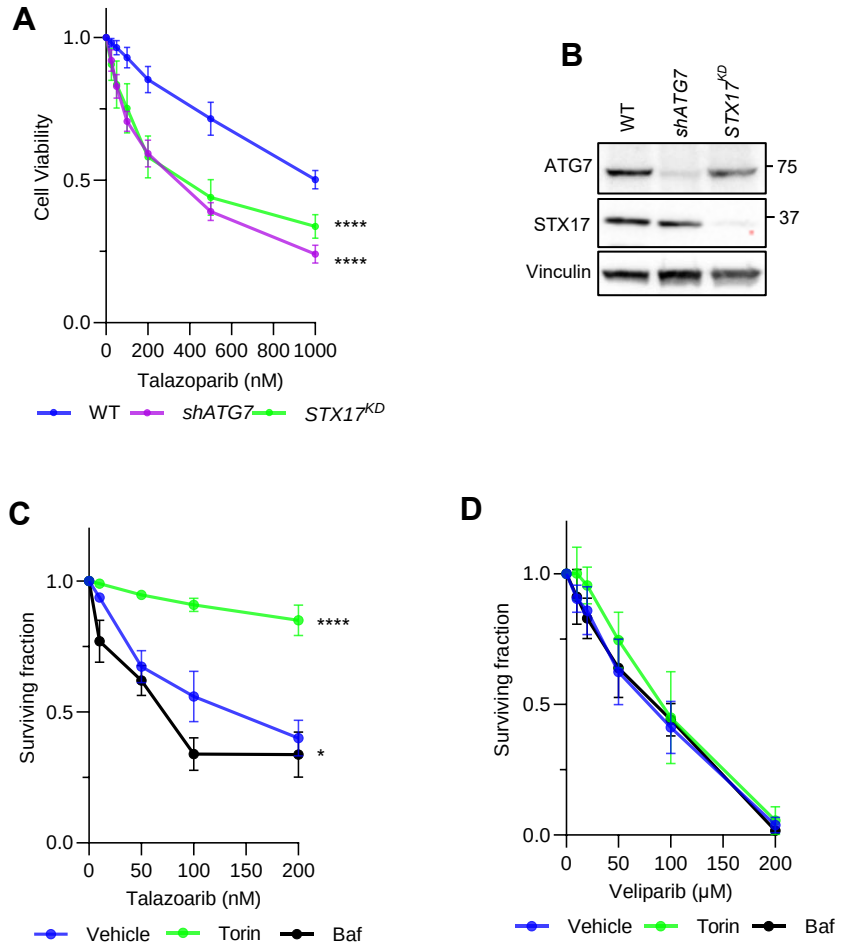

Figure 29: Autophagy modulation affects sensitivity to trapping PARPi. (**A**) Cell viability measured by resazurin assay in HeLa cells, either WT, dox-inducible *shATG7*, or syntaxin-17 knockdown (*STX17^{KD}*), treated with talazoparib for 24 hrs, then allowed to recover for 48 hrs. (**B**) Immunoblotting validating depletion of indicated proteins in (A). (**C and D**) Colony formation assay in HeLa cells treated with talazoparib (**C**) or veliparib (**D**) and Bafilomycin A1 (25 nM) or Torin-1 (150 nM) for 24 hrs. Data from at least 3 biological repeats with statistical analysis by 2-way ANOVA.

5.5 Impairing TEX264-orchestrated nucleophagy re-sensitises resistant cells to PARPi

Many patients treated with PARPi show *de novo* resistance or acquire resistance during the course of treatment, with limited treatment options available to overcome this. As inhibition of TEX264-orchestrated nucleophagy, either chemically or genetically, appeared to hypersensitise cells to talazoparib, I wanted to explore how resistant cells would respond if this pathway was impaired. RPE *hTERT TP53$^{-/-}$*

BRCA1$^{-/-}$ cells were hypersensitive to Olaparib and talazoparib, due to loss of BRCA1 activity, but had acquired resistance by long-term treatment with escalating doses of Olaparib (cells generated by collaborators in the laboratory of Madalena Tarsounas). Resistance to both Olaparib and talazoparib was confirmed by measuring cell viability (Fig 30A, B). To assess the effect of impaired trapped PARP1 nucleophagy, TEX264 or ATG7 were depleted by RNAi in resistant cells (Fig 30C). Strikingly, depletion of either protein resulted in a strong re-sensitisation of resistant cells to both Olaparib and talazoparib (Fig 30A, B). Interestingly, the strongest effect was observed with talazoparib, the stronger trapper of the two PARPi, supporting that cytotoxicity caused by impaired TEX264-orchestrated nucleophagy is reliant on PARP1 trapping.

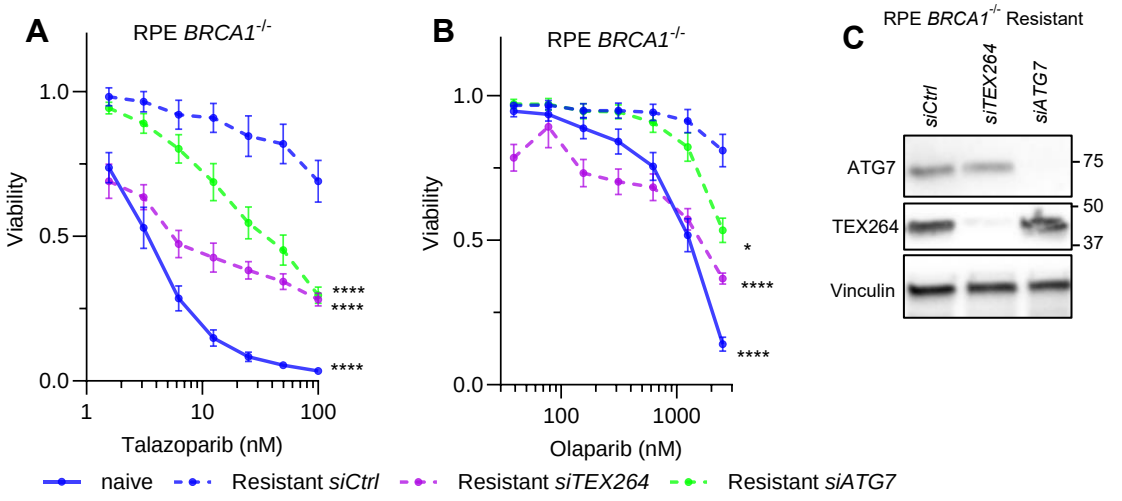

Figure 30: Inhibition of TEX264-mediated autophagy reverses acquired PARPi resistance. (**A and B**) Cell viability measured by resazurin assay in RPE *TP53*$^{-/-}$ *hTERT BRCA1*$^{-/-}$ cells, either naïve or resistant to Olaparib. Resistant cells are depleted of TEX264, ATG7 or a luciferase control. Treatment is with talazoparib (**A**) or Olaparib (**B**) for 6 days. 12 technical replicates across 4 biological repeats with statistical analysis by two-way ANOVA. (**C**) Immunoblotting validating depletion of TEX264 and ATG7 for (A) and (B).

5.6 Concluding remarks

PARPi induce cytotoxicity through PARP1 trapping leading to genome instability. I have shown that blocking the TEX264- and p97-mediated clearance of trapped PARP1

by selective autophagy causes increased PARPi-induced genome instability which is responsible for hypersensitising cells to trapping PARPi. This was observed both chemically, with p97 inhibition, and genetically, through mutation of TEX264 or RNAi-mediated depletion of autophagy factors ATG7 and syntaxin-17. Whilst the individual functions of p97, TEX264 and autophagy in maintaining genome stability have been previously explored, albeit with varying clarity, this study demonstrates the first instance where selective autophagy, in this case mediated by TEX264 and p97, modulates genome stability in response to PARPi by directly clearing trapped PARP1 from DNA lesions. Beyond elucidation of a new mechanism of trapped PARP1 clearance, understanding the importance of this pathway for maintaining genome stability and cell survival has promising clinical implications in relation to PARPi resistance as impairing trapped PARP1 clearance by TEX264 or ATG7 depletion resensitised resistant cells to two clinically available PARPi.

6. Discussion

6.1 Summary and model

The use of PARPi for treatment of HR-defective breast, ovarian, prostate and pancreatic cancer has been a major breakthrough in terms of applying a synthetic lethal approach to the clinic. However, as with many therapies, both acquired, and *de novo* resistance threaten the efficacy of PARPi therapy. By investigating the cellular response to trapped PARP1, the cytotoxic lesion caused by PARPi, it may be possible to exploit this response to uncover better predictive biomarkers for resistance or develop therapies that reduce or overcome resistance. In pursuit of this, I explored the processing of trapped PARP1 lesions by the p97 system which relies on its co-factors. I uncovered a novel role of p97 co-factor TEX264 in regulating trapped PARP1, as modelled in Figure 31, thereby promoting tolerance specifically to clinically relevant trapping PARPi. Mechanistic studies uncovered that TEX264 directly interacts with trapped PARP1 and acts as a SAR, promoting the processing of trapped PARP1 by selective nucleophagy. This pathway is not only TEX264-mediated, but also relies on p97 activity and the ubiquitin and SUMO conjugation pathways. Impairment of this process, either through TEX264 mutation or by chemical or genetic inhibition of autophagy or p97, results in heightened DNA damage and replication stress in multiple cell lines, underlying PARPi hypersensitivity induced by TEX264 loss. In line with this, autophagy modulation by chemical inhibition or upregulation caused PARPi hypersensitivity or resistance, respectively. Strikingly, PARPi-resistant cells could be re-sensitised to both talazoparib and Olaparib by inhibiting TEX264-mediated selective autophagy, implying clinical relevance in relation to overcoming PARPi resistance.

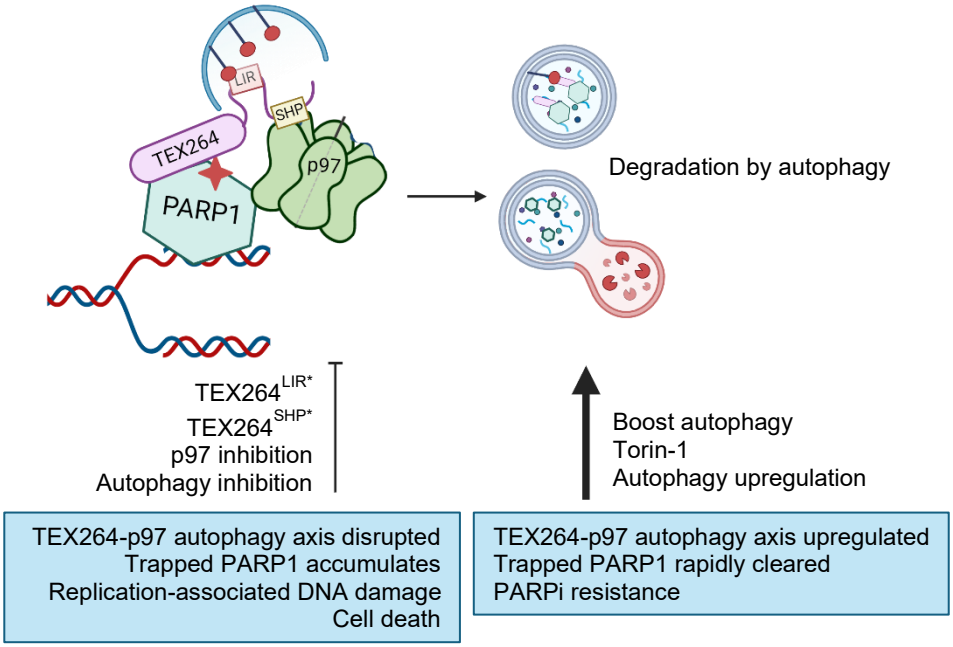

Figure 31: Model. TEX264-orchestrated p97-mediated selective nucleophagy of trapped PARP1 in response to PARPi.

6.2 A novel TEX264 substrate

In this study, I have uncovered a novel p97-co-factor functional complex, whereby TEX264 orchestrates p97-dependent selective nucleophagy of trapped PARP1, reliant upon both its p97- and LC3-interacting regions. Both p97 and autophagy-related functions of TEX264 have been previously identified in relation to TOP1cc repair (Fielden et al., 2020; Lascaux et al., 2024) and reticulophagy (An et al., 2019; Chino et al., 2019). However, this study bridges these two roles and identifies a new substrate of TEX264. Whilst I conclusively demonstrated that TEX264 interacts with trapped PARP1, with a strong PLA signal implying a proximity of less than 40 nm, the nature of this interaction is still unclear. During TOP1cc repair, TEX264 binds TOP1 through a bona fide TOP1 binding surface close to the GyrI-like domain, which is disrupted through mutation of the Glu194 residue and other nearby residues (Fielden et al., 2020). Whilst it has not been explored, TEX264-PARP1 interaction could occur directly through a similar binding surface. The GyrI-like domain of TEX264 is a promising candidate for substrate binding as the crystal structure of other GyrI proteins shows it

forms a solvent-exposed surface (Romanowski, Gibney, & Burley, 2002), and it contains an SHS2 fold, highly conserved across all TEX264 orthologs (Fielden et al., 2022) and shown to mediate protein-protein interactions in a diverse array of protein superfamilies (Anantharaman & Aravind, 2004). This region of TEX264 is lesser explored so mutational profiling could improve understanding of its relevance for trapped PARP1 processing.

The activity of TEX264 in reticulophagy also depends upon direct interaction with its substrate, whereby an N-terminal transmembrane domain directly links it to the damaged ER membrane (An et al., 2019; Chino et al., 2019; Fielden et al., 2020). This makes TEX264 a ubiquitin-independent SAR, in contrast to ubiquitin-dependent SARs such as p62 and OPTN (Vargas et al., 2023). Interestingly, I found both ubiquitination and SUMOylation to be essential for selective nucleophagy of trapped PARP1, raising the possibility that these PTMs regulate the interaction between TEX264 and PARP1. Analysis of TEX264 structure previously uncovered two SIMs, but an absence of ubiquitin-binding regions (Fielden et al., 2020). Through these motifs, TEX264 readily binds SUMO1, with SIM2 shown to be the most relevant for binding to SUMOylated TOP1 (Fielden et al., 2020). PARP1 is also modified by SUMO1, with its PARPi-induced enrichment in the PARP1 interactome suggesting this modification occurs preferentially on trapped PARP1 (Krastev et al., 2022). Interestingly, SUMO1 has been implicated in the recognition of a handful of other selective autophagy substrates, including Ataxin-3 aggregates (Hwang & Lee, 2017), and Lamin A/C (Y. Li et al., 2019). In the case of nucleophagy of the nuclear lamina, DNA damage-induced modification of Lamin A/C by SUMO1 promotes its interaction with LC3 for clearance by nucleophagy (Y. Li et al., 2019). Whilst these processes don't implicate a receptor for mediating the autophagic processing of the SUMOylated substrates, SARs have been

shown to act through ubiquitin-like modifications, such as HYPK which serves as a SAR during proteotoxic stress-induced aggrephagy by binding to aggregates modified by the ubiquitin-like modifier NEDD8 (Ghosh & Ranjan, 2022). Whether TEX264 relies on SUMOylation for PARP1 binding remains to be shown, but research may focus on SUMO E3 ligases that target trapped PARP1. Whilst not essential for SUMOylation to occur, various SUMO E3 ligases have been characterised that give substrate selectivity (W. Wang & Matunis, 2023). PIAS4 has already been shown to modify trapped PARP1. However, as it is highly linked to proteasomal degradation, residual SUMOylation remains in its absence (Krastev et al., 2022) so other ligases may regulate this modification.

6.3 Mechanisms of Nucleophagy

As described in the introduction, a handful of nucleophagy substrates have previously been described including the nuclear lamina during senescence (Dou et al., 2015; Lenain et al., 2015; Y. Li et al., 2019) and, more recently, TOP2cc which co-localise with autophagic machinery in nuclear buds in response to TOP2 poisons (Muciño-Hernández et al., 2023). However, unlike for trapped PARP1, these studies do not implicate a SAR in nucleophagy. Interestingly, parallel work undertaken by our group identified a similar pathway of p97-mediated TEX264-orchestrated selective nucleophagy in the processing of TOP1cc (Lascaux et al., 2024). One outstanding question in relation to selective nucleophagy is the way in which substrates exit the nucleus and how autophagy is initiated here. In the case of nuclear lamina, extraction of Lamin A/C (Y. Li et al., 2019) and B1 (Dou et al., 2015) from the nuclear envelope relies on their direct interaction with LC3, so autophagy machinery appears to be directly recruited. Some SARs, such as p62 and OPTN, not only bridge substrates to the growing autophagophore but also aid in its formation through recruitment of

machinery such as the ULK1 complex, ATG9A vesicles and ATG5-ATG12-ATG16L1 complex (Vargas et al., 2023), as was described in the introduction. However, this has not been explored for TEX264. Trapped PARP1, which occurs directly on chromatin, must first be localised to the nuclear periphery, and then exit the nucleus to associate with an autophagophore. PARP1-TEX264 interaction was concentrated around the nuclear periphery by PLA, supporting that trapped PARP1 localises here. Localisation of lesions to the nuclear periphery is best described for DSBs (Oza, Jaspersen, Miele, Dekker, & Peterson, 2009; Ryu et al., 2015) and stressed replication forks (N. Lamm et al., 2020) as nuclear pore complexes and other nuclear envelope components can aid in homology-directed repair (Noa Lamm, Rogers, & Cesare, 2021; Lemaître et al., 2012). Localisation of lesions to the nuclear periphery is an active process which relies upon the nuclear cytoskeleton (Caridi et al., 2018; N. Lamm et al., 2020; Shokrollahi et al., 2024). Interestingly, this process is promoted by ATR and mTORC1 kinase signalling (N. Lamm et al., 2020), which are both known and shown in this study to be increased by PARPi, as well as SUMOylation (Horigome et al., 2016; Kramarz et al., 2020; Nagai et al., 2008; Ryu et al., 2015), a PTM I found to be essential for trapped PARP1 nucleophagy. As trapped PARP1 is highly associated with DSBs and stressed replication forks, these lesions could localise to the nuclear periphery in a similar manner. A recent study uncovered interaction between DSBs and nuclear envelope repair factors linked to lamin B1 tubules that infiltrate the nucleus (Shokrollahi et al., 2024). Strikingly, these tubules were observed in BRCA1-defective TNBC cells upon Olaparib treatment (Shokrollahi et al., 2024), supporting that PARPi-induced lesions can contact nuclear envelope structures.

In relation to nuclear exit, microscopy experiments showed trapped PARP1, as well as other targets of selective nucleophagy, TOP1cc (Lascaux et al., 2024) and TOP2cc

(Muciño-Hernández et al., 2023), localise with autophagic machinery in the cytosol without severe defects in nuclear architecture or cell death occurring, implying the nuclear envelope remains intact. In the case of selective nucleophagy of TOP1cc, the nuclear pore complex is not involved in mediating substrate exit. However, high resolution imaging of the nuclear envelope by electron microscopy showed blister structures form where TOP1 was found to localise, implying TOP1cc could exit the nucleus by local disruption of the nuclear envelope (Lascaux et al., 2024). It would be interesting to observe whether the same occurs for trapped PARP1. Interestingly, replication stress and associated ATR signalling were recently shown to cause local rupture of the nuclear envelope through phosphorylation of lamin A/C (Kovacs et al., 2023) so it is possible that PARPi-induced ATR signalling aids in nuclear exit of trapped PARP1 by driving nuclear envelope rupture. Local rupture caused by this phosphorylation event was driven by connections between the nuclear lamina, cytoskeleton and chromatin (Kovacs et al., 2023), supporting that movement of lesions to the nuclear periphery is concurrent with their nuclear exit. Interestingly, HR-deficient cancer cells had higher incidence of nuclear envelope rupture (Kovacs et al., 2023), so nucleophagy-mediated lesion repair could be of significant relevance for these cancers.

6.4 Relevance of trapped PARP1 nucleophagy

As TOP1cc and trapped PARP1 are cleared by a similar pathway of TEX264-orchestrated nucleophagy, it follows that TEX264 may serve a more general purpose as a SAR for DPC and DPC-like lesions. In accordance with this, TOP1, along with accompanying DNA fragments which make up the TOP1cc lesion, were identified in the lysosome in a way which depended upon the SHP and LIR domains of TEX264 (Lascaux et al., 2024), similar to trapped PARP1. Similar to trapped PARP1

nucleophagy, this was relevant for maintaining genome stability and prevention of TOP1cc-induced mutations. To further understand this, it would be interesting to investigate if trapped PARP1-associated DNA is also shuttled to the lysosome by TEX264-orchestrated nucleophagy, in a similar way to TOP1cc DNA fragments. Studies in mouse models (Chabanon et al., 2019; Ding et al., 2018; Pantelidou et al., 2019), and through in-depth analysis of clinical trial data (Chopra et al., 2020) have found that PARPi induce accumulation of cytosolic DNA which is recognised by the DNA sensor cGAS and activates STING signalling, inducing a pro-inflammatory response and immune cell infiltration. This has been proposed to drive PARPi cytotoxicity (Wicks et al., 2022) and is tightly linked to trapping as immune cell infiltration is suppressed in *PARP1*-null cells (Chabanon et al., 2019). It would therefore be interesting to investigate whether PARPi-induced cytosolic DNA is associated with TEX264-orchestrated nucleophagy of trapped PARP1 and how modulation of this pathway effects the immune response. In the case of TOP1cc clearance, accumulation of aggregates containing TOP1 seemed to underly cytotoxicity when TEX264-mediated nucleophagy was impaired (Lascaux et al., 2024), as autophagy has long been associated with clearance of aggregates (Ravikumar, Duden, & Rubinsztein, 2002). It is unclear whether the same is true for trapped PARP1 clearance but as p97 is known to be involved in aggregate formation by unfolding and extracting proteins (Kobayashi, Manno, & Kakizuka, 2007; Mukkavalli, Klickstein, Ortiz, Juo, & Raman, 2021), it is a possibility that PARP1 aggregates form as a result of p97-mediated extraction from chromatin and that TEX264-orchestrated autophagy is required to resolve this.

6.5 Targeting TEX264-orchestrated nucleophagy in the clinic

In this study, I observed that inhibition of autophagy had detrimental effects on cancer cell survival in response to PARPi, whilst boosting autophagy caused resistance to PARPi. This effect has been observed by numerous other studies in multiple cancers and with all clinically available PARPi (Cahuzac et al., 2022; Elshazly et al., 2022; Y. Liu et al., 2019; Pai Bellare et al., 2021; Pai Bellare & Sankar Patro, 2022; Ren et al., 2020; Santiago-O'Farrill et al., 2020; Uddin et al., 2022), suggesting autophagy inhibition in combination with PARPi therapy could be a promising target. However, as described in the introduction, CQ and its derivatives, already approved for treatment of malaria, show mixed responses when used in combination with other cancer therapies (Amaravadi, Kimmelman, & Debnath, 2019), and there is some evidence suggesting their autophagy inhibitory effect are weak (Rosenfeld et al., 2014). By better understanding how autophagy regulates PARPi response, it may be possible to specifically target the underlying pathway. I demonstrated that depletion of TEX264 or ATG7 to inhibit TEX264-orchestrated selective nucleophagy of trapped PARP1 could re-sensitise resistant cells to PARPi, a promising result due to the lack of therapies available to overcome PARPi resistance in the clinic. The association of autophagy with resistance is validated in the literature, where autophagy upregulation has been linked to Olaparib resistance in breast (Uddin et al., 2022) and pancreatic cancer cells, with the latter shown both *in vivo* and *in vitro* (Xiao et al., 2024), although it remains to be seen if the same is true in patients.

Inhibition of p97 with CB-5083 was previously shown to hypersensitise mouse and patient-derived BRCA1-mutant breast cancer organoids to PARPi (Krastev et al., 2022). However, this inhibitor failed in clinical trials for advanced solid tumours and multiple myeloma due to off-target effects. Targeting the p97 co-factor TEX264 may

allow specific inhibition of p97-mediated trapped PARP1 repair without affecting other p97 functions. However, targeting TEX264 is complicated as it appears to act as a scaffolding factor with no catalytic domain to exploit. One strategy may be to develop a proteolysis-targeting chimera (PROTAC) molecule against TEX264. This technology utilises the UPS, bridging ubiquitination machinery to a specific substrate to allow the targeted degradation of previously undruggable targets. PROTACs against androgen and oestrogen receptors in prostate and breast cancer, respectively, have proven to be safe and effective in clinical trials (Békés, Langley, & Crews, 2022; Petrylak et al., 2020; Snyder et al., 2021), supporting the exploration of PROTACs as an approach to targeting substrates such as TEX264.

TEX264 could also be targeted by inhibiting its interaction with p97 and autophagy machinery. Other p97 inhibitors have been developed that target specific co-factors, such as CuET which acts against NPL4. It binds to the zinc-finger domain of NPL4, causing the co-factor to form nuclear aggregates which impairs p97 function by immobilising it at these aggregates and leads to cell death by triggering a heat shock response (Skrott et al., 2017). In this way, CuET demonstrates how inhibitors can have tumour anti-proliferative effects (Skrott et al., 2017) by indirectly inhibiting p97 function through immobilisation of one of its co-factors. In a similar manner, inhibition of selective autophagy could be achieved by targeting the interaction between LC3 and specific SARs. This has been explored for p62, with the discovery that the antibiotic novobiocin and its derivatives impair p62-LC3 interaction by binding the LIR-docking site of LC3 (Hartmann et al., 2021). Their initial approach used an assay to detect the interaction between LC3 and a polypeptide that included the p62-LIR sequence *in vitro* when exposed to a library of approved drugs (Hartmann et al., 2021). If this strategy was applied for other co-factors, such as TEX264, further inhibitors could be

uncovered that impair specific pathways of autophagy for improved therapeutic targeting.

Overall, I have uncovered a novel pathway of trapped PARP1 clearance by p97-mediated TEX264-orchestrated nucleophagy which is critical in the PARPi response and promotes resistance to PARPi. Uncovering biomarkers of PARPi resistance and developing therapies to overcome it is of major clinical need so further work may focus on whether this pathway could be exploited in patients.

Publications

I currently have a first author paper under review in Nature Cell Biology, which contains much of the work presented in this thesis. I have also contributed to several publications during my DPhil, which are listed below.

Original Scientific Articles

1. Krastev, D. B., Li, S., Sun, Y., Wicks, A. J., **Hoslett, G**., Weekes, D., . . . Ramadan, K. & Lord, C. J. (2022). The ubiquitin-dependent ATPase p97 removes cytotoxic trapped PARP1 from chromatin. *Nat Cell Biol, 24*(1), 62-73. doi:10.1038/s41556-021-00807-6
2. Lascaux, P., **Hoslett, G**., Tribble, S., Trugenberger, C., Antičević, I., Otten, C., . . . & Ramadan, K. (2024). TEX264 drives selective autophagy of DNA lesions to promote DNA repair and cell survival. *Cell, 187*, 1-21. doi:http://doi.org/10.1016/j.cell.2024.08.020

Review Articles

Torrecilla, I., Ruggiano, A., Kiianitsa, K., Aljarbou, F., Lascaux, P., **Hoslett, G**., . . . & Ramadan, K. (2024). Isolation and detection of DNA-protein crosslinks in mammalian cells. *Nucleic Acids Res, 52*(2), 525-547. doi:10.1093/nar/gkad1178

References

Abu-Remaileh, M., Wyant, G. A., Kim, C., Laqtom, N. N., Abbasi, M., Chan, S. H., . . . Sabatini, D. M. (2017). Lysosomal metabolomics reveals V-ATPase- and mTOR-dependent regulation of amino acid efflux from lysosomes. *Science, 358*(6364), 807-813. doi:10.1126/science.aan6298

Acs, K., Luijsterburg, M. S., Ackermann, L., Salomons, F. A., Hoppe, T., & Dantuma, N. P. (2011). The AAA-ATPase VCP/p97 promotes 53BP1 recruitment by removing L3MBTL1 from DNA double-strand breaks. *Nat Struct Mol Biol, 18*(12), 1345-1350. doi:10.1038/nsmb.2188

Agarwal, N., Azad, A. A., Carles, J., Fay, A. P., Matsubara, N., Heinrich, D., . . . Fizazi, K. (2023). Talazoparib plus enzalutamide in men with first-line metastatic castration-resistant prostate cancer (TALAPRO-2): a randomised, placebo-controlled, phase 3 trial. *Lancet, 402*(10398), 291-303. doi:10.1016/s0140-6736(23)01055-3

Agarwal, S., Bell, C. M., Taylor, S. M., & Moran, R. G. (2016). p53 Deletion or Hotspot Mutations Enhance mTORC1 Activity by Altering Lysosomal Dynamics of TSC2 and Rheb. *Mol Cancer Res, 14*(1), 66-77. doi:10.1158/1541-7786.Mcr-15-0159

Aguilar-Quesada, R., Muñoz-Gámez, J. A., Martín-Oliva, D., Peralta, A., Valenzuela, M. T., Matínez-Romero, R., . . . Oliver, F. J. (2007). Interaction between ATM and PARP-1 in response to DNA damage and sensitization of ATM deficient cells through PARP inhibition. *BMC Mol Biol, 8*, 29. doi:10.1186/1471-2199-8-29

Alam, M. S. (2022). Proximity Ligation Assay (PLA)Proximity ligation assay (PLA). In L. Del Valle (Ed.), *Immunohistochemistry and Immunocytochemistry: Methods and Protocols* (pp. 191-201). New York, NY: Springer US.

Alexander, A., Cai, S. L., Kim, J., Nanez, A., Sahin, M., MacLean, K. H., . . . Walker, C. L. (2010). ATM signals to TSC2 in the cytoplasm to regulate mTORC1 in response to ROS. *Proc Natl Acad Sci U S A, 107*(9), 4153-4158. doi:10.1073/pnas.0913860107

Ali, A. A. E., Timinszky, G., Arribas-Bosacoma, R., Kozlowski, M., Hassa, P. O., Hassler, M., . . . Oliver, A. W. (2012). The zinc-finger domains of PARP1 cooperate to recognize DNA strand breaks. *Nat Struct Mol Biol, 19*(7), 685-692. doi:10.1038/nsmb.2335

Amaravadi, R. K., Kimmelman, A. C., & Debnath, J. (2019). Targeting Autophagy in Cancer: Recent Advances and Future Directions. *Cancer Discov, 9*(9), 1167-1181. doi:10.1158/2159-8290.Cd-19-0292

Ambrosio, S., & Majello, B. (2020). Autophagy Roles in Genome Maintenance. *Cancers (Basel), 12*(7). doi:10.3390/cancers12071793

Amé, J.-C., Rolli, V., Schreiber, V., Niedergang, C., Apiou, F., Decker, P., . . . de Murcia, G. (1999). PARP-2, A novel mammalian DNA damage-dependent poly (ADP-ribose) polymerase. *Journal of Biological Chemistry, 274*(25), 17860-17868.

Amé, J. C., Spenlehauer, C., & De Murcia, G. (2004). The PARP superfamily. *Bioessays, 26*(8), 882-893.

An, H., Ordureau, A., Paulo, J. A., Shoemaker, C. J., Denic, V., & Harper, J. W. (2019). TEX264 Is an Endoplasmic Reticulum-Resident ATG8-Interacting Protein Critical for ER Remodeling during Nutrient Stress. *Mol Cell, 74*(5), 891-908 e810. doi:10.1016/j.molcel.2019.03.034

Anantharaman, V., & Aravind, L. (2004). The SHS2 module is a common structural theme in functionally diverse protein groups, like Rpb7p, FtsA, GyrI, and MTH1598/TM1083 superfamilies. *Proteins, 56*(4), 795-807. doi:10.1002/prot.20140

Anderson, D. J., Le Moigne, R., Djakovic, S., Kumar, B., Rice, J., Wong, S., . . . Rolfe, M. (2015). Targeting the AAA ATPase p97 as an Approach to Treat Cancer through Disruption of Protein Homeostasis. *Cancer Cell, 28*(5), 653-665. doi:10.1016/j.ccell.2015.10.002

Arora, S. P., Moseley, J. L., Tenner, L. L., Arellano, L., Salazar, M., Liu, Q., . . . Mahalingam, D. (2021). Phase II study of modulation of sorafenib (SOR)-induced autophagy using hydroxychloroquine (HCQ) in advanced hepatocellular cancer (HCC): Planned interim efficacy and safety analysis. *Journal of Clinical Oncology, 39*(3_suppl), 305-305. doi:10.1200/JCO.2021.39.3_suppl.305

Arun, B., Akar, U., Gutierrez-Barrera, A. M., Hortobagyi, G. N., & Ozpolat, B. (2015). The PARP inhibitor AZD2281 (Olaparib) induces autophagy/mitophagy in BRCA1 and BRCA2 mutant breast cancer cells. *Int J Oncol, 47*(1), 262-268. doi:10.3892/ijo.2015.3003

Audeh, M. W., Carmichael, J., Penson, R. T., Friedlander, M., Powell, B., Bell-McGuinn, K. M., . . . Tutt, A. (2010). Oral poly(ADP-ribose) polymerase inhibitor olaparib in patients with BRCA1 or BRCA2 mutations and recurrent ovarian cancer: a proof-of-concept trial. *Lancet, 376*(9737), 245-251. doi:10.1016/S0140-6736(10)60893-8

Axe, E. L., Walker, S. A., Manifava, M., Chandra, P., Roderick, H. L., Habermann, A., . . . Ktistakis, N. T. (2008). Autophagosome formation from membrane compartments enriched in phosphatidylinositol 3-phosphate and dynamically connected to the endoplasmic reticulum. *J Cell Biol, 182*(4), 685-701. doi:10.1083/jcb.200803137

Banerjee, S., Bartesaghi, A., Merk, A., Rao, P., Bulfer, S. L., Yan, Y., . . . Subramaniam, S. (2016). 2.3 Å resolution cryo-EM structure of human p97 and mechanism of allosteric inhibition. *Science, 351*(6275), 871-875. doi:10.1126/science.aad7974

Bansal, M., Moharir, S. C., Sailasree, S. P., Sirohi, K., Sudhakar, C., Sarathi, D. P., . . . Swarup, G. (2018). Optineurin promotes autophagosome formation by recruiting the autophagy-related Atg12-5-16L1 complex to phagophores containing the Wipi2 protein. *J Biol Chem, 293*(1), 132-147. doi:10.1074/jbc.M117.801944

Békés, M., Langley, D. R., & Crews, C. M. (2022). PROTAC targeted protein degraders: the past is prologue. *Nature Reviews Drug Discovery, 21*(3), 181-200. doi:10.1038/s41573-021-00371-6

Belan, O., Sebald, M., Adamowicz, M., Anand, R., Vancevska, A., Neves, J., . . . Boulton, S. J. (2022). POLQ seals post-replicative ssDNA gaps to maintain genome stability in BRCA-deficient cancer cells. *Mol Cell, 82*(24), 4664-4680 e4669. doi:10.1016/j.molcel.2022.11.008

Berti, M., Ray Chaudhuri, A., Thangavel, S., Gomathinayagam, S., Kenig, S., Vujanovic, M., . . . Vindigni, A. (2013). Human RECQ1 promotes restart of replication forks reversed by DNA topoisomerase I inhibition. *Nat Struct Mol Biol, 20*(3), 347-354. doi:10.1038/nsmb.2501

Blueggel, M., Kroening, A., Kracht, M., van den Boom, J., Dabisch, M., Goehring, A., . . . Beuck, C. (2023). The UBX domain in UBXD1 organizes ubiquitin binding

at the C-terminus of the VCP/p97 AAA-ATPase. *Nat Commun, 14*(1), 3258. doi:10.1038/s41467-023-38604-4
Bodnar, N. O., & Rapoport, T. A. (2017). Molecular Mechanism of Substrate Processing by the Cdc48 ATPase Complex. *Cell, 169*(4), 722-735.e729. doi:10.1016/j.cell.2017.04.020
Bonfiglio, J. J., Fontana, P., Zhang, Q., Colby, T., Gibbs-Seymour, I., Atanassov, I., . . . Matic, I. (2017). Serine ADP-Ribosylation Depends on HPF1. *Mol Cell, 65*(5), 932-940.e936. doi:10.1016/j.molcel.2017.01.003
Bordi, M., De Cegli, R., Testa, B., Nixon, R. A., Ballabio, A., & Cecconi, F. (2021). A gene toolbox for monitoring autophagy transcription. *Cell Death Dis, 12*(11), 1044. doi:10.1038/s41419-021-04121-9
Bouwman, P., Aly, A., Escandell, J. M., Pieterse, M., Bartkova, J., van der Gulden, H., . . . Jonkers, J. (2010). 53BP1 loss rescues BRCA1 deficiency and is associated with triple-negative and BRCA-mutated breast cancers. *Nat Struct Mol Biol, 17*(6), 688-695. doi:10.1038/nsmb.1831
Brandman, O., Stewart-Ornstein, J., Wong, D., Larson, A., Williams, C. C., Li, G. W., . . . Weissman, J. S. (2012). A ribosome-bound quality control complex triggers degradation of nascent peptides and signals translation stress. *Cell, 151*(5), 1042-1054. doi:10.1016/j.cell.2012.10.044
Bryant, H. E., Petermann, E., Schultz, N., Jemth, A. S., Loseva, O., Issaeva, N., . . . Helleday, T. (2009). PARP is activated at stalled forks to mediate Mre11-dependent replication restart and recombination. *EMBO J, 28*(17), 2601-2615. doi:10.1038/emboj.2009.206
Bryant, H. E., Schultz, N., Thomas, H. D., Parker, K. M., Flower, D., Lopez, E., . . . Helleday, T. (2005). Specific killing of BRCA2-deficient tumours with inhibitors of poly(ADP-ribose) polymerase. *Nature, 434*(7035), 913-917. doi:10.1038/nature03443
Buchberger, A., Schindelin, H., & Hanzelmann, P. (2015). Control of p97 function by cofactor binding. *FEBS Lett, 589*(19 Pt A), 2578-2589. doi:10.1016/j.febslet.2015.08.028
Budanov, A. V., & Karin, M. (2008). p53 target genes sestrin1 and sestrin2 connect genotoxic stress and mTOR signaling. *Cell, 134*(3), 451-460. doi:10.1016/j.cell.2008.06.028
Bunting, S. F., Callén, E., Wong, N., Chen, H. T., Polato, F., Gunn, A., . . . Nussenzweig, A. (2010). 53BP1 inhibits homologous recombination in Brca1-deficient cells by blocking resection of DNA breaks. *Cell, 141*(2), 243-254. doi:10.1016/j.cell.2010.03.012
Burma, S., Chen, B. P., Murphy, M., Kurimasa, A., & Chen, D. J. (2001). ATM phosphorylates histone H2AX in response to DNA double-strand breaks. *J Biol Chem, 276*(45), 42462-42467. doi:10.1074/jbc.C100466200
Cahuzac, M., Langlois, P., Peant, B., Fleury, H., Mes-Masson, A. M., & Saad, F. (2022). Pre-activation of autophagy impacts response to olaparib in prostate cancer cells. *Commun Biol, 5*(1), 251. doi:10.1038/s42003-022-03210-5
Caldecott, K. W. (2019). XRCC1 protein; Form and function. *DNA repair, 81*, 102664.
Caldecott, K. W., Aoufouchi, S., Johnson, P., & Shall, S. (1996). XRCC1 polypeptide interacts with DNA polymerase β and possibly poly (ADP-ribose) polymerase, and DNA ligase III is a novel molecular 'nick-sensor' in vitro. *Nucleic Acids Research, 24*(22), 4387-4394. doi:10.1093/nar/24.22.4387

Capranico, G., Ferri, F., Fogli, M. V., Russo, A., Lotito, L., & Baranello, L. (2007). The effects of camptothecin on RNA polymerase II transcription: roles of DNA topoisomerase I. *Biochimie, 89*(4), 482-489. doi:10.1016/j.biochi.2007.01.001

Caridi, C. P., D'Agostino, C., Ryu, T., Zapotoczny, G., Delabaere, L., Li, X., . . . Chiolo, I. (2018). Nuclear F-actin and myosins drive relocalization of heterochromatic breaks. *Nature, 559*(7712), 54-60. doi:10.1038/s41586-018-0242-8

Castroviejo-Bermejo, M., Cruz, C., Llop-Guevara, A., Gutiérrez-Enríquez, S., Ducy, M., Ibrahim, Y. H., . . . Serra, V. (2018). A RAD51 assay feasible in routine tumor samples calls PARP inhibitor response beyond BRCA mutation. *EMBO Mol Med, 10*(12). doi:10.15252/emmm.201809172

Chabanon, R. M., Muirhead, G., Krastev, D. B., Adam, J., Morel, D., Garrido, M., . . . Postel-Vinay, S. (2019). PARP inhibition enhances tumor cell-intrinsic immunity in ERCC1-deficient non-small cell lung cancer. *J Clin Invest, 129*(3), 1211-1228. doi:10.1172/jci123319

Chang, B. D., Swift, M. E., Shen, M., Fang, J., Broude, E. V., & Roninson, I. B. (2002). Molecular determinants of terminal growth arrest induced in tumor cells by a chemotherapeutic agent. *Proc Natl Acad Sci U S A, 99*(1), 389-394. doi:10.1073/pnas.012602599

Chapman, J. R., Barral, P., Vannier, J. B., Borel, V., Steger, M., Tomas-Loba, A., . . . Boulton, S. J. (2013). RIF1 is essential for 53BP1-dependent nonhomologous end joining and suppression of DNA double-strand break resection. *Mol Cell, 49*(5), 858-871. doi:10.1016/j.molcel.2013.01.002

Chappidi, N., Quail, T., Doll, S., Vogel, L. T., Aleksandrov, R., Felekyan, S., . . . Alberti, S. (2024). PARP1-DNA co-condensation drives DNA repair site assembly to prevent disjunction of broken DNA ends. *Cell*. doi:10.1016/j.cell.2024.01.015

Chen, J. H., Zhang, P., Chen, W. D., Li, D. D., Wu, X. Q., Deng, R., . . . Zhu, X. F. (2015). ATM-mediated PTEN phosphorylation promotes PTEN nuclear translocation and autophagy in response to DNA-damaging agents in cancer cells. *Autophagy, 11*(2), 239-252. doi:10.1080/15548627.2015.1009767

Chen, W., Zhang, L., Zhang, K., Zhou, B., Kuo, M. L., Hu, S., . . . Yen, Y. (2014). Reciprocal regulation of autophagy and dNTP pools in human cancer cells. *Autophagy, 10*(7), 1272-1284. doi:10.4161/auto.28954

Chino, H., Hatta, T., Natsume, T., & Mizushima, N. (2019). Intrinsically Disordered Protein TEX264 Mediates ER-phagy. *Mol Cell, 74*(5), 909-921 e906. doi:10.1016/j.molcel.2019.03.033

Chino, H., Yamasaki, A., Ode, K. L., Ueda, H. R., Noda, N. N., & Mizushima, N. (2022). Phosphorylation by casein kinase 2 enhances the interaction between ER-phagy receptor TEX264 and ATG8 proteins. *EMBO Rep*, e54801. doi:10.15252/embr.202254801

Choi, J., Topouza, D. G., Tarnouskaya, A., Nesdoly, S., Koti, M., & Duan, Q. L. (2020). Gene networks and expression quantitative trait loci associated with adjuvant chemotherapy response in high-grade serous ovarian cancer. *BMC Cancer, 20*(1), 413. doi:10.1186/s12885-020-06922-1

Chopra, N., Tovey, H., Pearson, A., Cutts, R., Toms, C., Proszek, P., . . . Turner, N. C. (2020). Homologous recombination DNA repair deficiency and PARP inhibition activity in primary triple negative breast cancer. *Nat Commun, 11*(1), 2662. doi:10.1038/s41467-020-16142-7

Chou, T. F., Brown, S. J., Minond, D., Nordin, B. E., Li, K., Jones, A. C., . . . Deshaies, R. J. (2011). Reversible inhibitor of p97, DBeQ, impairs both ubiquitin-dependent and autophagic protein clearance pathways. *Proc Natl Acad Sci U S A, 108*(12), 4834-4839. doi:10.1073/pnas.1015312108

Christie, E. L., Pattnaik, S., Beach, J., Copeland, A., Rashoo, N., Fereday, S., . . . Bowtell, D. D. L. (2019). Multiple ABCB1 transcriptional fusions in drug resistant high-grade serous ovarian and breast cancer. *Nat Commun, 10*(1), 1295. doi:10.1038/s41467-019-09312-9

Cong, K., Peng, M., Kousholt, A. N., Lee, W. T. C., Lee, S., Nayak, S., . . . Cantor, S. B. (2021). Replication gaps are a key determinant of PARP inhibitor synthetic lethality with BRCA deficiency. *Mol Cell, 81*(15), 3128-3144 e3127. doi:10.1016/j.molcel.2021.06.011

Cortesi, L., Rugo, H. S., & Jackisch, C. (2021). An Overview of PARP Inhibitors for the Treatment of Breast Cancer. *Target Oncol, 16*(3), 255-282. doi:10.1007/s11523-021-00796-4

Costantini, S., Capone, F., Polo, A., Bagnara, P., & Budillon, A. (2021). Valosin-Containing Protein (VCP)/p97: A Prognostic Biomarker and Therapeutic Target in Cancer. *Int J Mol Sci, 22*(18). doi:10.3390/ijms221810177

Crighton, D., Wilkinson, S., O'Prey, J., Syed, N., Smith, P., Harrison, P. R., . . . Ryan, K. M. (2006). DRAM, a p53-induced modulator of autophagy, is critical for apoptosis. *Cell, 126*(1), 121-134. doi:10.1016/j.cell.2006.05.034

Cristini, A., Park, J. H., Capranico, G., Legube, G., Favre, G., & Sordet, O. (2016). DNA-PK triggers histone ubiquitination and signaling in response to DNA double-strand breaks produced during the repair of transcription-blocking topoisomerase I lesions. *Nucleic Acids Res, 44*(3), 1161-1178. doi:10.1093/nar/gkv1196

Cruz-García, A., López-Saavedra, A., & Huertas, P. (2014). BRCA1 accelerates CtIP-mediated DNA-end resection. *Cell Rep, 9*(2), 451-459. doi:10.1016/j.celrep.2014.08.076

Cruz, C., Castroviejo-Bermejo, M., Gutiérrez-Enríquez, S., Llop-Guevara, A., Ibrahim, Y. H., Gris-Oliver, A., . . . Serra, V. (2018). RAD51 foci as a functional biomarker of homologous recombination repair and PARP inhibitor resistance in germline BRCA-mutated breast cancer. *Ann Oncol, 29*(5), 1203-1210. doi:10.1093/annonc/mdy099

Cui, J., Ogasawara, Y., Kurata, I., Matoba, K., Fujioka, Y., Noda, N. N., . . . Watanabe, T. (2022). Targeting the ATG5-ATG16L1 Protein-Protein Interaction with a Hydrocarbon-Stapled Peptide Derived from ATG16L1 for Autophagy Inhibition. *J Am Chem Soc, 144*(38), 17671-17679. doi:10.1021/jacs.2c07648

Cui, Y., Niu, M., Zhang, X., Zhong, Z., Wang, J., & Pang, D. (2015). High expression of valosin-containing protein predicts poor prognosis in patients with breast carcinoma. *Tumour Biol, 36*(12), 9919-9927. doi:10.1007/s13277-015-3748-9

Das, B. B., Huang, S. Y., Murai, J., Rehman, I., Ame, J. C., Sengupta, S., . . . Pommier, Y. (2014). PARP1-TDP1 coupling for the repair of topoisomerase I-induced DNA damage. *Nucleic Acids Res, 42*(7), 4435-4449. doi:10.1093/nar/gku088

Davies, J. M., Brunger, A. T., & Weis, W. I. (2008). Improved structures of full-length p97, an AAA ATPase: implications for mechanisms of nucleotide-dependent conformational change. *Structure, 16*(5), 715-726. doi:10.1016/j.str.2008.02.010

Davis, E. J., Lachaud, C., Appleton, P., Macartney, T. J., Näthke, I., & Rouse, J. (2012). DVC1 (C1orf124) recruits the p97 protein segregase to sites of DNA damage. *Nat Struct Mol Biol, 19*(11), 1093-1100. doi:10.1038/nsmb.2394
Dawicki-McKenna, J. M., Langelier, M.-F., DeNizio, J. E., Riccio, A. A., Cao, C. D., Karch, K. R., . . . Pascal, J. M. (2015). PARP-1 activation requires local unfolding of an autoinhibitory domain. *Molecular cell, 60*(5), 755-768.
Deeks, E. D. (2015). Olaparib: first global approval. *Drugs, 75*(2), 231-240. doi:10.1007/s40265-015-0345-6
Dev, H., Chiang, T. W., Lescale, C., de Krijger, I., Martin, A. G., Pilger, D., . . . Jackson, S. P. (2018). Shieldin complex promotes DNA end-joining and counters homologous recombination in BRCA1-null cells. *Nat Cell Biol, 20*(8), 954-965. doi:10.1038/s41556-018-0140-1
Dibitetto, D., Widmer, C. A., & Rottenberg, S. (2024). PARPi, BRCA, and gaps: controversies and future research. *Trends Cancer*. doi:10.1016/j.trecan.2024.06.008
Ding, L., Kim, H. J., Wang, Q., Kearns, M., Jiang, T., Ohlson, C. E., . . . Zhao, J. J. (2018). PARP Inhibition Elicits STING-Dependent Antitumor Immunity in Brca1-Deficient Ovarian Cancer. *Cell Rep, 25*(11), 2972-2980.e2975. doi:10.1016/j.celrep.2018.11.054
Domchek, S. M., & Weber, B. L. (2006). Clinical management of BRCA1 and BRCA2 mutation carriers. *Oncogene, 25*(43), 5825-5831. doi:10.1038/sj.onc.1209881
Dou, Z., Xu, C., Donahue, G., Shimi, T., Pan, J. A., Zhu, J., . . . Berger, S. L. (2015). Autophagy mediates degradation of nuclear lamina. *Nature, 527*(7576), 105-109. doi:10.1038/nature15548
Drané, P., Brault, M. E., Cui, G., Meghani, K., Chaubey, S., Detappe, A., . . . Chowdhury, D. (2017). TIRR regulates 53BP1 by masking its histone methyl-lysine binding function. *Nature, 543*(7644), 211-216. doi:10.1038/nature21358
Durkacz, B. W., Omidiji, O., Gray, D. A., & Shall, S. (1980). (ADP-ribose)n participates in DNA excision repair. *Nature, 283*(5747), 593-596. doi:10.1038/283593a0
Duscharla, D., Reddy Kami Reddy, K., Dasari, C., Bhukya, S., & Ummanni, R. (2018). Interleukin-6 induced overexpression of valosin-containing protein (VCP)/p97 is associated with androgen-independent prostate cancer (AIPC) progression. *J Cell Physiol, 233*(10), 7148-7164. doi:10.1002/jcp.26639
Edwards, S. L., Brough, R., Lord, C. J., Natrajan, R., Vatcheva, R., Levine, D. A., . . . Ashworth, A. (2008). Resistance to therapy caused by intragenic deletion in BRCA2. *Nature, 451*(7182), 1111-1115. doi:10.1038/nature06548
Egan, D. F., Chun, M. G., Vamos, M., Zou, H., Rong, J., Miller, C. J., . . . Shaw, R. J. (2015). Small Molecule Inhibition of the Autophagy Kinase ULK1 and Identification of ULK1 Substrates. *Mol Cell, 59*(2), 285-297. doi:10.1016/j.molcel.2015.05.031
Elshazly, A. M., Nguyen, T. V. V., & Gewirtz, D. A. (2022). Is autophagy induction by PARP inhibitors a target for therapeutic benefit? *Oncol Res, 30*(1), 1-12. doi:10.32604/or.2022.026459
Escribano-Díaz, C., Orthwein, A., Fradet-Turcotte, A., Xing, M., Young, J. T., Tkáč, J., . . . Durocher, D. (2013). A cell cycle-dependent regulatory circuit composed of 53BP1-RIF1 and BRCA1-CtIP controls DNA repair pathway choice. *Mol Cell, 49*(5), 872-883. doi:10.1016/j.molcel.2013.01.001
Farmer, H., McCabe, N., Lord, C. J., Tutt, A. N., Johnson, D. A., Richardson, T. B., . . . Ashworth, A. (2005). Targeting the DNA repair defect in BRCA mutant cells

as a therapeutic strategy. *Nature, 434*(7035), 917-921. doi:10.1038/nature03445
Fielden, J., Popovic, M., & Ramadan, K. (2022). TEX264 at the intersection of autophagy and DNA repair. *Autophagy, 18*(1), 40-49. doi:10.1080/15548627.2021.1894059
Fielden, J., Wiseman, K., Torrecilla, I., Li, S., Hume, S., Chiang, S. C., . . . Ramadan, K. (2020). TEX264 coordinates p97- and SPRTN-mediated resolution of topoisomerase 1-DNA adducts. *Nat Commun, 11*(1), 1274. doi:10.1038/s41467-020-15000-w
Fong, P. C., Yap, T. A., Boss, D. S., Carden, C. P., Mergui-Roelvink, M., Gourley, C., . . . Kaye, S. B. (2010). Poly(ADP)-ribose polymerase inhibition: frequent durable responses in BRCA carrier ovarian cancer correlating with platinum-free interval. *J Clin Oncol, 28*(15), 2512-2519. doi:10.1200/JCO.2009.26.9589
Franz, A., Ackermann, L., & Hoppe, T. (2016). Ring of Change: CDC48/p97 Drives Protein Dynamics at Chromatin. *Front Genet, 7*, 73. doi:10.3389/fgene.2016.00073
Franz, A., Orth, M., Pirson, P. A., Sonneville, R., Blow, J. J., Gartner, A., . . . Hoppe, T. (2011). CDC-48/p97 coordinates CDT-1 degradation with GINS chromatin dissociation to ensure faithful DNA replication. *Mol Cell, 44*(1), 85-96. doi:10.1016/j.molcel.2011.08.028
Franz, A., Pirson, P. A., Pilger, D., Halder, S., Achuthankutty, D., Kashkar, H., . . . Hoppe, T. (2016). Chromatin-associated degradation is defined by UBXN-3/FAF1 to safeguard DNA replication fork progression. *Nat Commun, 7*, 10612. doi:10.1038/ncomms10612
Franz, A., Valledor, P., Ubieto-Capella, P., Pilger, D., Galarreta, A., Lafarga, V., . . . Lecona, E. (2021). USP7 and VCP(FAF1) define the SUMO/Ubiquitin landscape at the DNA replication fork. *Cell Rep, 37*(2), 109819. doi:10.1016/j.celrep.2021.109819
Fu, M.-m., Nirschl, J. J., & Holzbaur, E. L. (2014). LC3 binding to the scaffolding protein JIP1 regulates processive dynein-driven transport of autophagosomes. *Developmental cell, 29*(5), 577-590.
Gammoh, N. (2020). The multifaceted functions of ATG16L1 in autophagy and related processes. *Journal of Cell Science, 133*(20). doi:10.1242/jcs.249227
George, M. A., Mayer, T. M., Moore, D., Chen, C., White, E., DiPaola, R. S., . . . Stein, M. N. (2017). Autophagic cell death with hydroxychloroquine in patients with hormone-dependent prostate-specific antigen progression after local therapy for prostate cancer. *Journal of Clinical Oncology, 35*(6_suppl), 102-102. doi:10.1200/JCO.2017.35.6_suppl.102
Ghosh, D. K., & Ranjan, A. (2022). HYPK coordinates degradation of polyneddylated proteins by autophagy. *Autophagy, 18*(8), 1763-1784. doi:10.1080/15548627.2021.1997053
Gibbs-Seymour, I., Fontana, P., Rack, J. G. M., & Ahel, I. (2016). HPF1/C4orf27 Is a PARP-1-Interacting Protein that Regulates PARP-1 ADP-Ribosylation Activity. *Mol Cell, 62*(3), 432-442. doi:10.1016/j.molcel.2016.03.008
Gogola, E., Duarte, A. A., de Ruiter, J. R., Wiegant, W. W., Schmid, J. A., de Bruijn, R., . . . Rottenberg, S. (2018). Selective Loss of PARG Restores PARylation and Counteracts PARP Inhibitor-Mediated Synthetic Lethality. *Cancer Cell, 33*(6), 1078-1093 e1012. doi:10.1016/j.ccell.2018.05.008
Goodall, J., Mateo, J., Yuan, W., Mossop, H., Porta, N., Miranda, S., . . . de Bono, J. S. (2017). Circulating Cell-Free DNA to Guide Prostate Cancer Treatment

with PARP Inhibition. *Cancer Discov, 7*(9), 1006-1017. doi:10.1158/2159-8290.Cd-17-0261
Gopal, A. A., Fernandez, B., Delano, J., Weissleder, R., & Dubach, J. M. (2024). PARP trapping is governed by the PARP inhibitor dissociation rate constant. *Cell Chem Biol*. doi:10.1016/j.chembiol.2023.12.019
Gralewska, P., Gajek, A., Marczak, A., Mikuła, M., Ostrowski, J., Śliwińska, A., & Rogalska, A. (2020). PARP Inhibition Increases the Reliance on ATR/CHK1 Checkpoint Signaling Leading to Synthetic Lethality—An Alternative Treatment Strategy for Epithelial Ovarian Cancer Cells Independent from HR Effectiveness. *International Journal of Molecular Sciences, 21*(24), 9715. Retrieved from https://www.mdpi.com/1422-0067/21/24/9715
Groelly, F. J., Fawkes, M., Dagg, R. A., Blackford, A. N., & Tarsounas, M. (2023). Targeting DNA damage response pathways in cancer. *Nat Rev Cancer, 23*(2), 78-94. doi:10.1038/s41568-022-00535-5
Guillemette, S., Serra, R. W., Peng, M., Hayes, J. A., Konstantinopoulos, P. A., Green, M. R., & Cantor, S. B. (2015). Resistance to therapy in BRCA2 mutant cells due to loss of the nucleosome remodeling factor CHD4. *Genes Dev, 29*(5), 489-494. doi:10.1101/gad.256214.114
Gullberg, M., Gústafsdóttir, S. M., Schallmeiner, E., Jarvius, J., Bjarnegård, M., Betsholtz, C., . . . Fredriksson, S. (2004). Cytokine detection by antibody-based proximity ligation. *Proc Natl Acad Sci U S A, 101*(22), 8420-8424. doi:10.1073/pnas.0400552101
Guo, J. Y., Chen, H. Y., Mathew, R., Fan, J., Strohecker, A. M., Karsli-Uzunbas, G., . . . White, E. (2011). Activated Ras requires autophagy to maintain oxidative metabolism and tumorigenesis. *Genes Dev, 25*(5), 460-470. doi:10.1101/gad.2016311
Guo, J. Y., Xia, B., & White, E. (2013). Autophagy-mediated tumor promotion. *Cell, 155*(6), 1216-1219. doi:10.1016/j.cell.2013.11.019
Gupta, R., Somyajit, K., Narita, T., Maskey, E., Stanlie, A., Kremer, M., . . . Choudhary, C. (2018). DNA Repair Network Analysis Reveals Shieldin as a Key Regulator of NHEJ and PARP Inhibitor Sensitivity. *Cell, 173*(4), 972-988.e923. doi:10.1016/j.cell.2018.03.050
Haince, J. F., Kozlov, S., Dawson, V. L., Dawson, T. M., Hendzel, M. J., Lavin, M. F., & Poirier, G. G. (2007). Ataxia telangiectasia mutated (ATM) signaling network is modulated by a novel poly(ADP-ribose)-dependent pathway in the early response to DNA-damaging agents. *J Biol Chem, 282*(22), 16441-16453. doi:10.1074/jbc.M608406200
Haince, J. F., McDonald, D., Rodrigue, A., Dery, U., Masson, J. Y., Hendzel, M. J., & Poirier, G. G. (2008). PARP1-dependent kinetics of recruitment of MRE11 and NBS1 proteins to multiple DNA damage sites. *J Biol Chem, 283*(2), 1197-1208. doi:10.1074/jbc.M706734200
Haince, J. F., McDonald, D., Rodrigue, A., Déry, U., Masson, J. Y., Hendzel, M. J., & Poirier, G. G. (2008). PARP1-dependent kinetics of recruitment of MRE11 and NBS1 proteins to multiple DNA damage sites. *J Biol Chem, 283*(2), 1197-1208. doi:10.1074/jbc.M706734200
Hama, Y., Ogasawara, Y., & Noda, N. N. (2023). Autophagy and cancer: Basic mechanisms and inhibitor development. *Cancer Sci, 114*(7), 2699-2708. doi:10.1111/cas.15803

Hamasaki, M., Furuta, N., Matsuda, A., Nezu, A., Yamamoto, A., Fujita, N., . . . Yoshimori, T. (2013). Autophagosomes form at ER-mitochondria contact sites. *Nature, 495*(7441), 389-393. doi:10.1038/nature11910

Hanahan, D., & Weinberg, R. A. (2011). Hallmarks of cancer: the next generation. *Cell, 144*(5), 646-674. doi:10.1016/j.cell.2011.02.013

Hanzlikova, H., Gittens, W., Krejcikova, K., Zeng, Z., & Caldecott, K. W. (2017). Overlapping roles for PARP1 and PARP2 in the recruitment of endogenous XRCC1 and PNKP into oxidized chromatin. *Nucleic Acids Res, 45*(5), 2546-2557. doi:10.1093/nar/gkw1246

Hanzlikova, H., Kalasova, I., Demin, A. A., Pennicott, L. E., Cihlarova, Z., & Caldecott, K. W. (2018). The Importance of Poly(ADP-Ribose) Polymerase as a Sensor of Unligated Okazaki Fragments during DNA Replication. *Mol Cell, 71*(2), 319-331 e313. doi:10.1016/j.molcel.2018.06.004

Hartmann, M., Huber, J., Kramer, J. S., Heering, J., Pietsch, L., Stark, H., . . . Proschak, E. (2021). Demonstrating Ligandability of the LC3A and LC3B Adapter Interface. *J Med Chem, 64*(7), 3720-3746. doi:10.1021/acs.jmedchem.0c01564

Harvey-Jones, E., Raghunandan, M., Robbez-Masson, L., Magraner-Pardo, L., Alaguthurai, T., Yablonovitch, A., . . . Tutt, A. N. J. (2024). Longitudinal profiling identifies co-occurring BRCA1/2 reversions, TP53BP1, RIF1 and PAXIP1 mutations in PARP inhibitor-resistant advanced breast cancer. *Ann Oncol, 35*(4), 364-380. doi:10.1016/j.annonc.2024.01.003

Helleday, T. (2011). The underlying mechanism for the PARP and BRCA synthetic lethality: clearing up the misunderstandings. *Mol Oncol, 5*(4), 387-393. doi:10.1016/j.molonc.2011.07.001

Hewitt, G., Carroll, B., Sarallah, R., Correia-Melo, C., Ogrodnik, M., Nelson, G., . . . Korolchuk, V. I. (2016). SQSTM1/p62 mediates crosstalk between autophagy and the UPS in DNA repair. *Autophagy, 12*(10), 1917-1930. doi:10.1080/15548627.2016.1210368

Hill, S. M., Wrobel, L., Ashkenazi, A., Fernandez-Estevez, M., Tan, K., Burli, R. W., & Rubinsztein, D. C. (2021). VCP/p97 regulates Beclin-1-dependent autophagy initiation. *Nat Chem Biol, 17*(4), 448-455. doi:10.1038/s41589-020-00726-x

Ho, Y. C., Ku, C. S., Tsai, S. S., Shiu, J. L., Jiang, Y. Z., Miriam, H. E., . . . Liaw, H. (2022). PARP1 recruits DNA translocases to restrain DNA replication and facilitate DNA repair. *PLoS Genet, 18*(12), e1010545. doi:10.1371/journal.pgen.1010545

Horigome, C., Bustard, D. E., Marcomini, I., Delgoshaie, N., Tsai-Pflugfelder, M., Cobb, J. A., & Gasser, S. M. (2016). PolySUMOylation by Siz2 and Mms21 triggers relocation of DNA breaks to nuclear pores through the Slx5/Slx8 STUbL. *Genes Dev, 30*(8), 931-945. doi:10.1101/gad.277665.116

Hoy, S. M. (2018). Talazoparib: First Global Approval. *Drugs, 78*(18), 1939-1946. doi:10.1007/s40265-018-1026-z

Hrychova, K., Burdova, K., Polackova, Z., Giamaki, D., Valtorta, B., Brazina, J., . . . Hanzlikova, H. (2024). Dispensability of HPF1 for cellular removal of DNA single-strand breaks. *Nucleic Acids Research, 52*(18), 10986-10998. doi:10.1093/nar/gkae708

Hu, Y., Petit, S. A., Ficarro, S. B., Toomire, K. J., Xie, A., Lim, E., . . . Livingston, D. M. (2014). PARP1-driven poly-ADP-ribosylation regulates BRCA1 function in homologous recombination-mediated DNA repair. *Cancer Discov, 4*(12), 1430-1447. doi:10.1158/2159-8290.Cd-13-0891

Huang, S. C., Adhikari, S., Brownell, J. E., Calderwood, E. F., Chouitar, J., D'Amore, N. R., . . . Gould, A. E. (2020). Discovery and optimization of pyrazolopyrimidine sulfamates as ATG7 inhibitors. *Bioorg Med Chem, 28*(19), 115681. doi:10.1016/j.bmc.2020.115681

Hurley, R. M., McGehee, C. D., Nesic, K., Correia, C., Weiskittel, Taylor M., Kelly, Rebecca L., . . . Kaufmann, Scott H. (2021). Characterization of a RAD51C-silenced high-grade serous ovarian cancer model during development of PARP inhibitor resistance. *NAR Cancer, 3*(3). doi:10.1093/narcan/zcab028

Hwang, S. P., & Lee, D. H. (2017). Autophagy mediates SUMO-induced degradation of a polyglutamine protein ataxin-3. *Anim Cells Syst (Seoul), 21*(3), 169-176. doi:10.1080/19768354.2017.1330765

Inami, Y., Waguri, S., Sakamoto, A., Kouno, T., Nakada, K., Hino, O., . . . Komatsu, M. (2011). Persistent activation of Nrf2 through p62 in hepatocellular carcinoma cells. *J Cell Biol, 193*(2), 275-284. doi:10.1083/jcb.201102031

Itakura, E., Kishi-Itakura, C., & Mizushima, N. (2012). The hairpin-type tail-anchored SNARE syntaxin 17 targets to autophagosomes for fusion with endosomes/lysosomes. *Cell, 151*(6), 1256-1269. doi:10.1016/j.cell.2012.11.001

Jaspers, J. E., Kersbergen, A., Boon, U., Sol, W., van Deemter, L., Zander, S. A., . . . Rottenberg, S. (2013). Loss of 53BP1 causes PARP inhibitor resistance in Brca1-mutated mouse mammary tumors. *Cancer Discov, 3*(1), 68-81. doi:10.1158/2159-8290.CD-12-0049

Ji, Z., Li, H., Peterle, D., Paulo, J. A., Ficarro, S. B., Wales, T. E., . . . Rapoport, T. A. (2022). Translocation of polyubiquitinated protein substrates by the hexameric Cdc48 ATPase. *Mol Cell, 82*(3), 570-584.e578. doi:10.1016/j.molcel.2021.11.033

Johansen, T., & Lamark, T. (2020). Selective Autophagy: ATG8 Family Proteins, LIR Motifs and Cargo Receptors. *J Mol Biol, 432*(1), 80-103. doi:10.1016/j.jmb.2019.07.016

Jones, P., Wilcoxen, K., Rowley, M., & Toniatti, C. (2015). Niraparib: A Poly(ADP-ribose) Polymerase (PARP) Inhibitor for the Treatment of Tumors with Defective Homologous Recombination. *Journal of Medicinal Chemistry, 58*(8), 3302-3314. doi:10.1021/jm5018237

Ju, J.-S., Fuentealba, R. A., Miller, S. E., Jackson, E., Piwnica-Worms, D., Baloh, R. H., & Weihl, C. C. (2009). Valosin-containing protein (VCP) is required for autophagy and is disrupted in VCP disease. *Journal of Cell Biology, 187*(6), 875-888. doi:10.1083/jcb.200908115

Jung, C. H., Jun, C. B., Ro, S. H., Kim, Y. M., Otto, N. M., Cao, J., . . . Kim, D. H. (2009). ULK-Atg13-FIP200 complexes mediate mTOR signaling to the autophagy machinery. *Mol Biol Cell, 20*(7), 1992-2003. doi:10.1091/mbc.e08-12-1249

Kabeya, Y., Mizushima, N., Ueno, T., Yamamoto, A., Kirisako, T., Noda, T., . . . Yoshimori, T. (2000). LC3, a mammalian homologue of yeast Apg8p, is localized in autophagosome membranes after processing. *EMBO J, 19*(21), 5720-5728. doi:10.1093/emboj/19.21.5720

Kane, L. A., Lazarou, M., Fogel, A. I., Li, Y., Yamano, K., Sarraf, S. A., . . . Youle, R. J. (2014). PINK1 phosphorylates ubiquitin to activate Parkin E3 ubiquitin ligase activity. *J Cell Biol, 205*(2), 143-153. doi:10.1083/jcb.201402104

Kanev, P.-B., Atemin, A., Stoynov, S., & Aleksandrov, R. (2024). PARP1 roles in DNA repair and DNA replication: The basi(c)s of PARP inhibitor efficacy and

resistance. *Seminars in Oncology, 51*(1), 2-18. doi:https://doi.org/10.1053/j.seminoncol.2023.08.001
Karantza-Wadsworth, V., Patel, S., Kravchuk, O., Chen, G., Mathew, R., Jin, S., & White, E. (2007). Autophagy mitigates metabolic stress and genome damage in mammary tumorigenesis. *Genes Dev, 21*(13), 1621-1635. doi:10.1101/gad.1565707
Karasic, T. B., O'Hara, M. H., Loaiza-Bonilla, A., Reiss, K. A., Teitelbaum, U. R., Borazanci, E., . . . O'Dwyer, P. J. (2019). Effect of Gemcitabine and nab-Paclitaxel With or Without Hydroxychloroquine on Patients With Advanced Pancreatic Cancer: A Phase 2 Randomized Clinical Trial. *JAMA Oncol, 5*(7), 993-998. doi:10.1001/jamaoncol.2019.0684
Kenzelmann Broz, D., Spano Mello, S., Bieging, K. T., Jiang, D., Dusek, R. L., Brady, C. A., . . . Attardi, L. D. (2013). Global genomic profiling reveals an extensive p53-regulated autophagy program contributing to key p53 responses. *Genes Dev, 27*(9), 1016-1031. doi:10.1101/gad.212282.112
Ketley, Ruth F., & Gullerova, M. (2020). Jack of all trades? The versatility of RNA in DNA double-strand break repair. *Essays in Biochemistry, 64*(5), 721-735. doi:10.1042/ebc20200008
Khaminets, A., Behl, C., & Dikic, I. (2016). Ubiquitin-Dependent And Independent Signals In Selective Autophagy. *Trends Cell Biol, 26*(1), 6-16. doi:10.1016/j.tcb.2015.08.010
Kilgas, S., & Ramadan, K. (2023). Inhibitors of the ATPase p97/VCP: From basic research to clinical applications. *Cell Chem Biol, 30*(1), 3-21. doi:10.1016/j.chembiol.2022.12.007
Kilgas, S., Singh, A. N., Paillas, S., Then, C. K., Torrecilla, I., Nicholson, J., . . . Ramadan, K. (2021). p97/VCP inhibition causes excessive MRE11-dependent DNA end resection promoting cell killing after ionizing radiation. *Cell Rep, 35*(8), 109153. doi:10.1016/j.celrep.2021.109153
Kim, D. S., Camacho, C. V., Nagari, A., Malladi, V. S., Challa, S., & Kraus, W. L. (2019). Activation of PARP-1 by snoRNAs Controls Ribosome Biogenesis and Cell Growth via the RNA Helicase DDX21. *Mol Cell, 75*(6), 1270-1285.e1214. doi:10.1016/j.molcel.2019.06.020
Kim, I., Rodriguez-Enriquez, S., & Lemasters, J. J. (2007). Selective degradation of mitochondria by mitophagy. *Archives of biochemistry and biophysics, 462*(2), 245-253.
Kimura, S., Noda, T., & Yoshimori, T. (2007). Dissection of the autophagosome maturation process by a novel reporter protein, tandem fluorescent-tagged LC3. *Autophagy, 3*(5), 452-460. doi:10.4161/auto.4451
Kirkin, V., McEwan, D. G., Novak, I., & Dikic, I. (2009). A Role for Ubiquitin in Selective Autophagy. *Molecular cell, 34*(3), 259-269. doi:10.1016/j.molcel.2009.04.026
Kitada, T., Asakawa, S., Hattori, N., Matsumine, H., Yamamura, Y., Minoshima, S., . . . Shimizu, N. (1998). Mutations in the parkin gene cause autosomal recessive juvenile parkinsonism. *Nature, 392*(6676), 605-608. doi:10.1038/33416
Kloppsteck, P., Ewens, C. A., Förster, A., Zhang, X., & Freemont, P. S. (2012). Regulation of p97 in the ubiquitin-proteasome system by the UBX protein-family. *Biochim Biophys Acta, 1823*(1), 125-129. doi:10.1016/j.bbamcr.2011.09.006

Kobayashi, T., Manno, A., & Kakizuka, A. (2007). Involvement of valosin-containing protein (VCP)/p97 in the formation and clearance of abnormal protein aggregates. *Genes Cells, 12*(7), 889-901. doi:10.1111/j.1365-2443.2007.01099.x
Koegl, M., Hoppe, T., Schlenker, S., Ulrich, H. D., Mayer, T. U., & Jentsch, S. (1999). A Novel Ubiquitination Factor, E4, Is Involved in Multiubiquitin Chain Assembly. *Cell, 96*(5), 635-644. doi:10.1016/S0092-8674(00)80574-7
Køhler, J. B., Tammsalu, T., Jørgensen, M. M., Steen, N., Hay, R. T., & Thon, G. (2015). Targeting of SUMO substrates to a Cdc48-Ufd1-Npl4 segregase and STUbL pathway in fission yeast. *Nat Commun, 6*, 8827. doi:10.1038/ncomms9827
Kojima, Y., Machida, Y., Palani, S., Caulfield, T. R., Radisky, E. S., Kaufmann, S. H., & Machida, Y. J. (2020). FAM111A protects replication forks from protein obstacles via its trypsin-like domain. *Nat Commun, 11*(1), 1318. doi:10.1038/s41467-020-15170-7
Kondrashova, O., Nguyen, M., Shield-Artin, K., Tinker, A. V., Teng, N. N. H., Harrell, M. I., . . . Scott, C. L. (2017). Secondary Somatic Mutations Restoring RAD51C and RAD51D Associated with Acquired Resistance to the PARP Inhibitor Rucaparib in High-Grade Ovarian Carcinoma. *Cancer Discov, 7*(9), 984-998. doi:10.1158/2159-8290.Cd-17-0419
Kondrashova, O., Topp, M., Nesic, K., Lieschke, E., Ho, G.-Y., Harrell, M. I., . . . Australian Ovarian Cancer, S. (2018). Methylation of all BRCA1 copies predicts response to the PARP inhibitor rucaparib in ovarian carcinoma. *Nature Communications, 9*(1), 3970. doi:10.1038/s41467-018-05564-z
Kovacs, M. T., Vallette, M., Wiertsema, P., Dingli, F., Loew, D., Nader, G. P. F., . . . Ceccaldi, R. (2023). DNA damage induces nuclear envelope rupture through ATR-mediated phosphorylation of lamin A/C. *Mol Cell*. doi:10.1016/j.molcel.2023.09.023
Koyano, F., Okatsu, K., Kosako, H., Tamura, Y., Go, E., Kimura, M., . . . Matsuda, N. (2014). Ubiquitin is phosphorylated by PINK1 to activate parkin. *Nature, 510*(7503), 162-166. doi:10.1038/nature13392
Kraft, C., Kijanska, M., Kalie, E., Siergiejuk, E., Lee, S. S., Semplicio, G., . . . Peter, M. (2012). Binding of the Atg1/ULK1 kinase to the ubiquitin-like protein Atg8 regulates autophagy. *EMBO J, 31*(18), 3691-3703. doi:10.1038/emboj.2012.225
Kramarz, K., Schirmeisen, K., Boucherit, V., Ait Saada, A., Lovo, C., Palancade, B., . . . Lambert, S. A. E. (2020). The nuclear pore primes recombination-dependent DNA synthesis at arrested forks by promoting SUMO removal. *Nat Commun, 11*(1), 5643. doi:10.1038/s41467-020-19516-z
Krastev, D. B., Li, S., Sun, Y., Wicks, A. J., Hoslett, G., Weekes, D., . . . Lord, C. J. (2022). The ubiquitin-dependent ATPase p97 removes cytotoxic trapped PARP1 from chromatin. *Nat Cell Biol, 24*(1), 62-73. doi:10.1038/s41556-021-00807-6
Kristeleit, R., Lisyanskaya, A., Fedenko, A., Dvorkin, M., de Melo, A. C., Shparyk, Y., . . . Oza, A. M. (2022). Rucaparib versus standard-of-care chemotherapy in patients with relapsed ovarian cancer and a deleterious BRCA1 or BRCA2 mutation (ARIEL4): an international, open-label, randomised, phase 3 trial. *Lancet Oncol, 23*(4), 465-478. doi:10.1016/s1470-2045(22)00122-x
Kröning, A., van den Boom, J., Kracht, M., Kueck, A. F., & Meyer, H. (2022). Ubiquitin-directed AAA+ ATPase p97/VCP unfolds stable proteins crosslinked

to DNA for proteolysis by SPRTN. *J Biol Chem, 298*(6), 101976. doi:10.1016/j.jbc.2022.101976
Krshnan, L., van de Weijer, M. L., & Carvalho, P. (2022). Endoplasmic Reticulum-Associated Protein Degradation. *Cold Spring Harb Perspect Biol, 14*(12). doi:10.1101/cshperspect.a041247
Kuhlbrodt, K., Janiesch, P. C., Kevei, É., Segref, A., Barikbin, R., & Hoppe, T. (2011). The Machado-Joseph disease deubiquitylase ATX-3 couples longevity and proteostasis. *Nat Cell Biol, 13*(3), 273-281. doi:10.1038/ncb2200
Kumar, S., Chauhan, S., Jain, A., Ponpuak, M., Choi, S. W., Mudd, M., . . . Deretic, V. (2017). Galectins and TRIMs directly interact and orchestrate autophagic response to endomembrane damage. *Autophagy, 13*(6), 1086-1087. doi:10.1080/15548627.2017.1307487
Kumar, S., Jain, A., Farzam, F., Jia, J., Gu, Y., Choi, S. W., . . . Deretic, V. (2018). Mechanism of Stx17 recruitment to autophagosomes via IRGM and mammalian Atg8 proteins. *J Cell Biol, 217*(3), 997-1013. doi:10.1083/jcb.201708039
Kutuzov, M. M., Belousova, E. A., Kurgina, T. A., Ukraintsev, A. A., Vasil'eva, I. A., Khodyreva, S. N., & Lavrik, O. I. (2021). The contribution of PARP1, PARP2 and poly(ADP-ribosyl)ation to base excision repair in the nucleosomal context. *Sci Rep, 11*(1), 4849. doi:10.1038/s41598-021-84351-1
Lai, Y., Yu, R., Hartwell, H. J., Moeller, B. C., Bodnar, W. M., & Swenberg, J. A. (2016). Measurement of Endogenous versus Exogenous Formaldehyde–Induced DNA–Protein Crosslinks in Animal Tissues by Stable Isotope Labeling and Ultrasensitive Mass Spectrometry. *Cancer Research, 76*(9), 2652-2661. doi:10.1158/0008-5472.Can-15-2527
Lallemand-Breitenbach, V., Jeanne, M., Benhenda, S., Nasr, R., Lei, M., Peres, L., . . . de Thé, H. (2008). Arsenic degrades PML or PML–RARα through a SUMO-triggered RNF4/ubiquitin-mediated pathway. *Nature Cell Biology, 10*(5), 547-555. doi:10.1038/ncb1717
Lamm, N., Read, M. N., Nobis, M., Van Ly, D., Page, S. G., Masamsetti, V. P., . . . Cesare, A. J. (2020). Nuclear F-actin counteracts nuclear deformation and promotes fork repair during replication stress. *Nat Cell Biol, 22*(12), 1460-1470. doi:10.1038/s41556-020-00605-6
Lamm, N., Rogers, S., & Cesare, A. J. (2021). Chromatin mobility and relocation in DNA repair. *Trends in Cell Biology, 31*(10), 843-855. doi:10.1016/j.tcb.2021.06.002
Langelier, M.-F., Planck, J. L., Roy, S., & Pascal, J. M. (2012). Structural Basis for DNA Damage–Dependent Poly(ADP-ribosyl)ation by Human PARP-1. *Science, 336*(6082), 728-732. doi:doi:10.1126/science.1216338
Langelier, M.-F., Ruhl, D. D., Planck, J. L., Kraus, W. L., & Pascal, J. M. (2010). The Zn3 Domain of Human Poly(ADP-ribose) Polymerase-1 (PARP-1) Functions in Both DNA-dependent Poly(ADP-ribose) Synthesis Activity and Chromatin Compaction*. *Journal of Biological Chemistry, 285*(24), 18877-18887. doi:https://doi.org/10.1074/jbc.M110.105668
Lascaux, P., Hoslett, G., Tribble, S., Trugenberger, C., Antičević, I., Otten, C., . . . Ramadan, K. (2024). TEX264 drives selective autophagy of DNA lesions to promote DNA repair and cell survival. *Cell*. doi:10.1016/j.cell.2024.08.020
Laspata, N., Muoio, D., & Fouquerel, E. (2024). Multifaceted Role of PARP1 in Maintaining Genome Stability Through Its Binding to Alternative DNA

Structures. *Journal of Molecular Biology, 436*(1), 168207. doi:https://doi.org/10.1016/j.jmb.2023.168207
Lazarou, M., Sliter, D. A., Kane, L. A., Sarraf, S. A., Wang, C., Burman, J. L., . . . Youle, R. J. (2015). The ubiquitin kinase PINK1 recruits autophagy receptors to induce mitophagy. *Nature, 524*(7565), 309-314. doi:10.1038/nature14893
Ledermann, J., Harter, P., Gourley, C., Friedlander, M., Vergote, I., Rustin, G., . . . Matulonis, U. (2012). Olaparib Maintenance Therapy in Platinum-Sensitive Relapsed Ovarian Cancer. *New England Journal of Medicine, 366*(15), 1382-1392. doi:doi:10.1056/NEJMoa1105535
Lee, A. (2021). Fuzuloparib: First Approval. *Drugs, 81*(10), 1221-1226. doi:10.1007/s40265-021-01541-x
Lee, H. G., Lemmon, A. A., & Lima, C. D. (2023). SUMO enhances unfolding of SUMO-polyubiquitin-modified substrates by the Ufd1/Npl4/Cdc48 complex. *Proc Natl Acad Sci U S A, 120*(1), e2213703120. doi:10.1073/pnas.2213703120
Lee, J. Y., Lee, Y. Y., Park, J. Y., Shim, S. H., Kim, S. I., Kong, T. W., . . . Suh, D. H. (2023). Major clinical research advances in gynecologic cancer in 2022: highlight on late-line PARP inhibitor withdrawal in ovarian cancer, the impact of ARIEL-4, and SOLO-3. *J Gynecol Oncol, 34*(2), e51. doi:10.3802/jgo.2023.34.e51
Lee, Y., Chou, T. F., Pittman, S. K., Keith, A. L., Razani, B., & Weihl, C. C. (2017). Keap1/Cullin3 Modulates p62/SQSTM1 Activity via UBA Domain Ubiquitination. *Cell Rep, 19*(1), 188-202. doi:10.1016/j.celrep.2017.03.030
Leinonen, H., Cheng, C., Pitkänen, M., Sander, C. L., Zhang, J., Saeid, S., . . . Palczewski, K. (2021). A p97/Valosin-Containing Protein Inhibitor Drug CB-5083 Has a Potent but Reversible Off-Target Effect on Phosphodiesterase-6. *J Pharmacol Exp Ther, 378*(1), 31-41. doi:10.1124/jpet.120.000486
Lemaître, C., Fischer, B., Kalousi, A., Hoffbeck, A. S., Guirouilh-Barbat, J., Shahar, O. D., . . . Soutoglou, E. (2012). The nucleoporin 153, a novel factor in double-strand break repair and DNA damage response. *Oncogene, 31*(45), 4803-4809. doi:10.1038/onc.2011.638
Lenain, C., Gusyatiner, O., Douma, S., van den Broek, B., & Peeper, D. S. (2015). Autophagy-mediated degradation of nuclear envelope proteins during oncogene-induced senescence. *Carcinogenesis, 36*(11), 1263-1274. doi:10.1093/carcin/bgv124
Lessel, D., Vaz, B., Halder, S., Lockhart, P. J., Marinovic-Terzic, I., Lopez-Mosqueda, J., . . . Kubisch, C. (2014). Mutations in SPRTN cause early onset hepatocellular carcinoma, genomic instability and progeroid features. *Nat Genet, 46*(11), 1239-1244. doi:10.1038/ng.3103
Leung, A. K. L. (2020). Poly(ADP-ribose): A Dynamic Trigger for Biomolecular Condensate Formation. *Trends Cell Biol, 30*(5), 370-383. doi:10.1016/j.tcb.2020.02.002
Li, C., Huang, Y., Fan, Q., Quan, H., Dong, Y., Nie, M., . . . Wang, L. (2021). p97/VCP is highly expressed in the stem-like cells of breast cancer and controls cancer stemness partly through the unfolded protein response. *Cell Death Dis, 12*(4), 286. doi:10.1038/s41419-021-03555-5
Li, H., Liu, Z. Y., Wu, N., Chen, Y. C., Cheng, Q., & Wang, J. (2020). PARP inhibitor resistance: the underlying mechanisms and clinical implications. *Mol Cancer, 19*(1), 107. doi:10.1186/s12943-020-01227-0

Li, M., & Yu, X. (2013). Function of BRCA1 in the DNA damage response is mediated by ADP-ribosylation. *Cancer Cell, 23*(5), 693-704. doi:10.1016/j.ccr.2013.03.025

Li, X., He, S., & Ma, B. (2020). Autophagy and autophagy-related proteins in cancer. *Mol Cancer, 19*(1), 12. doi:10.1186/s12943-020-1138-4

Li, Y., Jiang, X., Zhang, Y., Gao, Z., Liu, Y., Hu, J., . . . Gao, N. (2019). Nuclear accumulation of UBC9 contributes to SUMOylation of lamin A/C and nucleophagy in response to DNA damage. *J Exp Clin Cancer Res, 38*(1), 67. doi:10.1186/s13046-019-1048-8

Liang, X. H., Jackson, S., Seaman, M., Brown, K., Kempkes, B., Hibshoosh, H., & Levine, B. (1999). Induction of autophagy and inhibition of tumorigenesis by beclin 1. *Nature, 402*(6762), 672-676. doi:10.1038/45257

Lilyestrom, W., van der Woerd, M. J., Clark, N., & Luger, K. (2010). Structural and Biophysical Studies of Human PARP-1 in Complex with Damaged DNA. *Journal of Molecular Biology, 395*(5), 983-994. doi:https://doi.org/10.1016/j.jmb.2009.11.062

Lin, C.-P., Ban, Y., Lyu, Y. L., Desai, S. D., & Liu, L. F. (2008). A Ubiquitin-Proteasome Pathway for the Repair of Topoisomerase I-DNA Covalent Complexes *. *Journal of Biological Chemistry, 283*(30), 21074-21083. doi:10.1074/jbc.M803493200

Lin, K. K., Harrell, M. I., Oza, A. M., Oaknin, A., Ray-Coquard, I., Tinker, A. V., . . . Swisher, E. M. (2019). BRCA Reversion Mutations in Circulating Tumor DNA Predict Primary and Acquired Resistance to the PARP Inhibitor Rucaparib in High-Grade Ovarian Carcinoma. *Cancer Discov, 9*(2), 210-219. doi:10.1158/2159-8290.Cd-18-0715

Litton, J. K., Hurvitz, S. A., Mina, L. A., Rugo, H. S., Lee, K. H., Gonçalves, A., . . . Ettl, J. (2020). Talazoparib versus chemotherapy in patients with germline BRCA1/2-mutated HER2-negative advanced breast cancer: final overall survival results from the EMBRACA trial. *Ann Oncol, 31*(11), 1526-1535. doi:10.1016/j.annonc.2020.08.2098

Litton, J. K., Rugo, H. S., Ettl, J., Hurvitz, S. A., Gonçalves, A., Lee, K.-H., . . . Blum, J. L. (2018). Talazoparib in Patients with Advanced Breast Cancer and a Germline BRCA Mutation. *New England Journal of Medicine, 379*(8), 753-763. doi:doi:10.1056/NEJMoa1802905

Liu, J. C. Y., Kuhbacher, U., Larsen, N. B., Borgermann, N., Garvanska, D. H., Hendriks, I. A., . . . Mailand, N. (2021). Mechanism and function of DNA replication-independent DNA-protein crosslink repair via the SUMO-RNF4 pathway. *EMBO J*, e107413. doi:10.15252/embj.2020107413

Liu, S., Yao, S., Yang, H., Liu, S., & Wang, Y. (2023). Autophagy: Regulator of cell death. *Cell Death Dis, 14*(10), 648. doi:10.1038/s41419-023-06154-8

Liu, Y., Song, H., Song, H., Feng, X., Zhou, C., & Huo, Z. (2019). Targeting autophagy potentiates the anti-tumor effect of PARP inhibitor in pediatric chronic myeloid leukemia. *AMB Express, 9*(1), 108. doi:10.1186/s13568-019-0836-z

Liu, Y., Zou, W., Yang, P., Wang, L., Ma, Y., Zhang, H., & Wang, X. (2018). Autophagy-dependent ribosomal RNA degradation is essential for maintaining nucleotide homeostasis during C. elegans development. *Elife, 7*. doi:10.7554/eLife.36588

Livingstone, M., Ruan, H., Weiner, J., Clauser, K. R., Strack, P., Jin, S., . . . Halazonetis, T. D. (2005). Valosin-containing protein phosphorylation at

Ser784 in response to DNA damage. *Cancer Res, 65*(17), 7533-7540. doi:10.1158/0008-5472.Can-04-3729
Lopez-Mosqueda, J., Maddi, K., Prgomet, S., Kalayil, S., Marinovic-Terzic, I., Terzic, J., & Dikic, I. (2016). SPRTN is a mammalian DNA-binding metalloprotease that resolves DNA-protein crosslinks. *Elife, 5*, e21491.
LP, A. P. (2022). Lynparza (olaparib) v. 10/22 [package insert].
Maede, Y., Shimizu, H., Fukushima, T., Kogame, T., Nakamura, T., Miki, T., . . . Murai, J. (2014). Differential and common DNA repair pathways for topoisomerase I- and II-targeted drugs in a genetic DT40 repair cell screen panel. *Mol Cancer Ther, 13*(1), 214-220. doi:10.1158/1535-7163.Mct-13-0551
Magnaghi, P., D'Alessio, R., Valsasina, B., Avanzi, N., Rizzi, S., Asa, D., . . . Isacchi, A. (2013). Covalent and allosteric inhibitors of the ATPase VCP/p97 induce cancer cell death. *Nat Chem Biol, 9*(9), 548-556. doi:10.1038/nchembio.1313
Mansour, W. Y., Rhein, T., & Dahm-Daphi, J. (2010). The alternative end-joining pathway for repair of DNA double-strand breaks requires PARP1 but is not dependent upon microhomologies. *Nucleic Acids Res, 38*(18), 6065-6077. doi:10.1093/nar/gkq387
Maric, M., Maculins, T., De Piccoli, G., & Labib, K. (2014). Cdc48 and a ubiquitin ligase drive disassembly of the CMG helicase at the end of DNA replication. *Science, 346*(6208), 1253596. doi:10.1126/science.1253596
Marin-Muller, C., Li, D., Bharadwaj, U., Li, M., Chen, C., Hodges, S. E., . . . Yao, Q. (2013). A tumorigenic factor interactome connected through tumor suppressor microRNA-198 in human pancreatic cancer. *Clin Cancer Res, 19*(21), 5901-5913. doi:10.1158/1078-0432.Ccr-12-3776
Markham, A. (2021). Pamiparib: First Approval. *Drugs, 81*(11), 1343-1348. doi:10.1007/s40265-021-01552-8
Martin, N., Schwamborn, K., Schreiber, V., Werner, A., Guillier, C., Zhang, X. D., . . . Dejean, A. (2009). PARP-1 transcriptional activity is regulated by sumoylation upon heat shock. *The EMBO Journal, 28*(22), 3534-3548. doi:https://doi.org/10.1038/emboj.2009.279
Maskey, R. S., Flatten, K. S., Sieben, C. J., Peterson, K. L., Baker, D. J., Nam, H. J., . . . Machida, Y. J. (2017). Spartan deficiency causes accumulation of Topoisomerase 1 cleavage complexes and tumorigenesis. *Nucleic Acids Res, 45*(8), 4564-4576. doi:10.1093/nar/gkx107
Maskey, R. S., Kim, M. S., Baker, D. J., Childs, B., Malureanu, L. A., Jeganathan, K. B., . . . Machida, Y. J. (2014). Spartan deficiency causes genomic instability and progeroid phenotypes. *Nat Commun, 5*, 5744. doi:10.1038/ncomms6744
Maya-Mendoza, A., Moudry, P., Merchut-Maya, J. M., Lee, M., Strauss, R., & Bartek, J. (2018). High speed of fork progression induces DNA replication stress and genomic instability. *Nature, 559*(7713), 279-284. doi:10.1038/s41586-018-0261-5
Meerang, M., Ritz, D., Paliwal, S., Garajova, Z., Bosshard, M., Mailand, N., . . . Ramadan, K. (2011). The ubiquitin-selective segregase VCP/p97 orchestrates the response to DNA double-strand breaks. *Nat Cell Biol, 13*(11), 1376-1382. doi:10.1038/ncb2367
Menear, K. A., Adcock, C., Boulter, R., Cockcroft, X. L., Copsey, L., Cranston, A., . . . Martin, N. M. (2008). 4-[3-(4-cyclopropanecarbonylpiperazine-1-carbonyl)-4-fluorobenzyl]-2H-phthalazin-1-one: a novel bioavailable inhibitor of poly(ADP-ribose) polymerase-1. *J Med Chem, 51*(20), 6581-6591. doi:10.1021/jm8001263

Messner, S., Altmeyer, M., Zhao, H., Pozivil, A., Roschitzki, B., Gehrig, P., . . . Hottiger, M. O. (2010). PARP1 ADP-ribosylates lysine residues of the core histone tails. *Nucleic Acids Research, 38*(19), 6350-6362. doi:10.1093/nar/gkq463

Meyer, H., Bug, M., & Bremer, S. (2012). Emerging functions of the VCP/p97 AAA-ATPase in the ubiquitin system. *Nat Cell Biol, 14*(2), 117-123. doi:10.1038/ncb2407

Michelena, J., Lezaja, A., Teloni, F., Schmid, T., Imhof, R., & Altmeyer, M. (2018). Analysis of PARP inhibitor toxicity by multidimensional fluorescence microscopy reveals mechanisms of sensitivity and resistance. *Nat Commun, 9*(1), 2678. doi:10.1038/s41467-018-05031-9

Mirman, Z., Lottersberger, F., Takai, H., Kibe, T., Gong, Y., Takai, K., . . . de Lange, T. (2018). 53BP1-RIF1-shieldin counteracts DSB resection through CST- and Polα-dependent fill-in. *Nature, 560*(7716), 112-116. doi:10.1038/s41586-018-0324-7

Mirsanaye, A. S., Hoffmann, S., Weisser, M., Mund, A., Lopez Mendez, B., Typas, D., . . . Mailand, N. (2024). VCF1 is a p97/VCP cofactor promoting recognition of ubiquitylated p97-UFD1-NPL4 substrates. *Nat Commun, 15*(1), 2459. doi:10.1038/s41467-024-46760-4

Mizushima, N. (2020). The ATG conjugation systems in autophagy. *Curr Opin Cell Biol, 63*, 1-10. doi:10.1016/j.ceb.2019.12.001

Mizushima, N., Noda, T., Yoshimori, T., Tanaka, Y., Ishii, T., George, M. D., . . . Ohsumi, Y. (1998). A protein conjugation system essential for autophagy. *Nature, 395*(6700), 395-398. doi:10.1038/26506

Mizushima, N., Sugita, H., Yoshimori, T., & Ohsumi, Y. (1998). A new protein conjugation system in human. The counterpart of the yeast Apg12p conjugation system essential for autophagy. *J Biol Chem, 273*(51), 33889-33892. doi:10.1074/jbc.273.51.33889

Moir, D., Stewart, S. E., Osmond, B. C., & Botstein, D. (1982). Cold-sensitive cell-division-cycle mutants of yeast: isolation, properties, and pseudoreversion studies. *Genetics, 100*(4), 547-563. doi:10.1093/genetics/100.4.547

Moreno, S. P., Bailey, R., Campion, N., Herron, S., & Gambus, A. (2014). Polyubiquitylation drives replisome disassembly at the termination of DNA replication. *Science, 346*(6208), 477-481. doi:10.1126/science.1253585

Morishita, H., & Mizushima, N. (2019). Diverse Cellular Roles of Autophagy. *Annu Rev Cell Dev Biol, 35*, 453-475. doi:10.1146/annurev-cellbio-100818-125300

Morselli, E., Tasdemir, E., Maiuri, M. C., Galluzzi, L., Kepp, O., Criollo, A., . . . Kroemer, G. (2008). Mutant p53 protein localized in the cytoplasm inhibits autophagy. *Cell Cycle, 7*(19), 3056-3061. doi:10.4161/cc.7.19.6751

Mortensen, M., Soilleux, E. J., Djordjevic, G., Tripp, R., Lutteropp, M., Sadighi-Akha, E., . . . Simon, A. K. (2011). The autophagy protein Atg7 is essential for hematopoietic stem cell maintenance. *J Exp Med, 208*(3), 455-467. doi:10.1084/jem.20101145

Mosbech, A., Gibbs-Seymour, I., Kagias, K., Thorslund, T., Beli, P., Povlsen, L., . . . Mailand, N. (2012). DVC1 (C1orf124) is a DNA damage-targeting p97 adaptor that promotes ubiquitin-dependent responses to replication blocks. *Nat Struct Mol Biol, 19*(11), 1084-1092. doi:10.1038/nsmb.2395

Muciño-Hernández, G., Acevo-Rodríguez, P. S., Cabrera-Benitez, S., Guerrero, A. O., Merchant-Larios, H., & Castro-Obregón, S. (2023). Nucleophagy contributes to genome stability through degradation of type II topoisomerases

A and B and nucleolar components. *J Cell Sci, 136*(1). doi:10.1242/jcs.260563
Mukkavalli, S., Klickstein, J. A., Ortiz, B., Juo, P., & Raman, M. (2021). The p97-UBXN1 complex regulates aggresome formation. *J Cell Sci, 134*(7). doi:10.1242/jcs.254201
Murai, J., Huang, S. Y., Das, B. B., Renaud, A., Zhang, Y., Doroshow, J. H., . . . Pommier, Y. (2012). Trapping of PARP1 and PARP2 by Clinical PARP Inhibitors. *Cancer Res, 72*(21), 5588-5599. doi:10.1158/0008-5472.CAN-12-2753
Murai, J., Huang, S. Y., Renaud, A., Zhang, Y., Ji, J., Takeda, S., . . . Pommier, Y. (2014). Stereospecific PARP trapping by BMN 673 and comparison with olaparib and rucaparib. *Mol Cancer Ther, 13*(2), 433-443. doi:10.1158/1535-7163.Mct-13-0803
Nag, S., Qin, J., Srivenugopal, K. S., Wang, M., & Zhang, R. (2013). The MDM2-p53 pathway revisited. *J Biomed Res, 27*(4), 254-271. doi:10.7555/jbr.27.20130030
Nagai, S., Dubrana, K., Tsai-Pflugfelder, M., Davidson, M. B., Roberts, T. M., Brown, G. W., . . . Krogan, N. J. (2008). Functional targeting of DNA damage to a nuclear pore-associated SUMO-dependent ubiquitin ligase. *Science, 322*(5901), 597-602. doi:10.1126/science.1162790
Nakano, T., Miyamoto-Matsubara, M., Shoulkamy, M. I., Salem, A. M., Pack, S. P., Ishimi, Y., & Ide, H. (2013). Translocation and stability of replicative DNA helicases upon encountering DNA-protein cross-links. *J Biol Chem, 288*(7), 4649-4658. doi:10.1074/jbc.M112.419358
Nakano, T., Ouchi, R., Kawazoe, J., Pack, S. P., Makino, K., & Ide, H. (2012). T7 RNA polymerases backed up by covalently trapped proteins catalyze highly error prone transcription. *J Biol Chem, 287*(9), 6562-6572. doi:10.1074/jbc.M111.318410
Nakatogawa, H. (2020). Mechanisms governing autophagosome biogenesis. *Nat Rev Mol Cell Biol, 21*(8), 439-458. doi:10.1038/s41580-020-0241-0
Nakatogawa, H., Ohbayashi, S., Sakoh-Nakatogawa, M., Kakuta, S., Suzuki, S. W., Kirisako, H., . . . Ohsumi, Y. (2012). The autophagy-related protein kinase Atg1 interacts with the ubiquitin-like protein Atg8 via the Atg8 family interacting motif to facilitate autophagosome formation. *J Biol Chem, 287*(34), 28503-28507. doi:10.1074/jbc.C112.387514
Narendra, D., Tanaka, A., Suen, D. F., & Youle, R. J. (2008). Parkin is recruited selectively to impaired mitochondria and promotes their autophagy. *J Cell Biol, 183*(5), 795-803. doi:10.1083/jcb.200809125
Nesic, K., Kondrashova, O., Hurley, R. M., McGehee, C. D., Vandenberg, C. J., Ho, G. Y., . . . Scott, C. L. (2021). Acquired RAD51C Promoter Methylation Loss Causes PARP Inhibitor Resistance in High-Grade Serous Ovarian Carcinoma. *Cancer Res, 81*(18), 4709-4722. doi:10.1158/0008-5472.CAN-21-0774
Nie, P., Cao, Z., Yu, R., Dong, C., Zhang, W., Meng, Y., . . . Zhou, Z. (2024). Targeting p97–Npl4 interaction inhibits tumor Treg cell development to enhance tumor immunity. *Nature Immunology*. doi:10.1038/s41590-024-01912-y
Noda, N. N. (2021). Atg2 and Atg9: Intermembrane and interleaflet lipid transporters driving autophagy. *Biochim Biophys Acta Mol Cell Biol Lipids, 1866*(8), 158956. doi:10.1016/j.bbalip.2021.158956

Noireterre, A., & Stutz, F. (2024). Cdc48/p97 segregase: Spotlight on DNA-protein crosslinks. *DNA repair, 139*, 103691. doi:https://doi.org/10.1016/j.dnarep.2024.103691
Noordermeer, S. M., Adam, S., Setiaputra, D., Barazas, M., Pettitt, S. J., Ling, A. K., . . . Durocher, D. (2018). The shieldin complex mediates 53BP1-dependent DNA repair. *Nature, 560*(7716), 117-121. doi:10.1038/s41586-018-0340-7
Oakley, G. G., & Patrick, S. M. (2010). Replication protein A: directing traffic at the intersection of replication and repair. *Front Biosci (Landmark Ed), 15*(3), 883-900. doi:10.2741/3652
Oza, P., Jaspersen, S. L., Miele, A., Dekker, J., & Peterson, C. L. (2009). Mechanisms that regulate localization of a DNA double-strand break to the nuclear periphery. *Genes Dev, 23*(8), 912-927. doi:10.1101/gad.1782209
Paes Dias, M., Tripathi, V., van der Heijden, I., Cong, K., Manolika, E. M., Bhin, J., . . . Jonkers, J. (2021). Loss of nuclear DNA ligase III reverts PARP inhibitor resistance in BRCA1/53BP1 double-deficient cells by exposing ssDNA gaps. *Mol Cell*. doi:10.1016/j.molcel.2021.09.005
Pai Bellare, G., Saha, B., & Patro, B. S. (2021). Targeting autophagy reverses de novo resistance in homologous recombination repair proficient breast cancers to PARP inhibition. *Br J Cancer, 124*(7), 1260-1274. doi:10.1038/s41416-020-01238-0
Pai Bellare, G., & Sankar Patro, B. (2022). Resveratrol sensitizes breast cancer to PARP inhibitor, talazoparib through dual inhibition of AKT and autophagy flux. *Biochem Pharmacol, 199*, 115024. doi:10.1016/j.bcp.2022.115024
Palazzo, L., Leidecker, O., Prokhorova, E., Dauben, H., Matic, I., & Ahel, I. (2018). Serine is the major residue for ADP-ribosylation upon DNA damage. *Elife, 7*. doi:10.7554/eLife.34334
Pan, J. A., Sun, Y., Jiang, Y. P., Bott, A. J., Jaber, N., Dou, Z., . . . Zong, W. X. (2016). TRIM21 Ubiquitylates SQSTM1/p62 and Suppresses Protein Sequestration to Regulate Redox Homeostasis. *Mol Cell, 61*(5), 720-733. doi:10.1016/j.molcel.2016.02.007
Panier, S., & Boulton, S. J. (2014). Double-strand break repair: 53BP1 comes into focus. *Nature Reviews Molecular Cell Biology, 15*(1), 7-18. doi:10.1038/nrm3719
Pantelidou, C., Sonzogni, O., De Oliveria Taveira, M., Mehta, A. K., Kothari, A., Wang, D., . . . Shapiro, G. I. (2019). PARP Inhibitor Efficacy Depends on CD8(+) T-cell Recruitment via Intratumoral STING Pathway Activation in BRCA-Deficient Models of Triple-Negative Breast Cancer. *Cancer Discov, 9*(6), 722-737. doi:10.1158/2159-8290.Cd-18-1218
Papadopoulos, C., Kirchner, P., Bug, M., Grum, D., Koerver, L., Schulze, N., . . . Meyer, H. (2017). VCP/p97 cooperates with YOD1, UBXD1 and PLAA to drive clearance of ruptured lysosomes by autophagy. *EMBO J, 36*(2), 135-150. doi:10.15252/embj.201695148
Papadopoulos, C., Kravic, B., & Meyer, H. (2020). Repair or Lysophagy: Dealing with Damaged Lysosomes. *J Mol Biol, 432*(1), 231-239. doi:10.1016/j.jmb.2019.08.010
Pascal, J. M., & Ellenberger, T. (2015). The rise and fall of poly(ADP-ribose): An enzymatic perspective. *DNA Repair (Amst), 32*, 10-16. doi:10.1016/j.dnarep.2015.04.008
Patch, A.-M., Christie, E. L., Etemadmoghadam, D., Garsed, D. W., George, J., Fereday, S., . . . The Australian Ovarian Cancer Study, G. (2015). Whole–

genome characterization of chemoresistant ovarian cancer. *Nature, 521*(7553), 489-494. doi:10.1038/nature14410

Penson, R. T., Valencia, R. V., Cibula, D., Colombo, N., Leath, C. A., 3rd, Bidziński, M., . . . Scambia, G. (2020). Olaparib Versus Nonplatinum Chemotherapy in Patients With Platinum-Sensitive Relapsed Ovarian Cancer and a Germline BRCA1/2 Mutation (SOLO3): A Randomized Phase III Trial. *J Clin Oncol, 38*(11), 1164-1174. doi:10.1200/jco.19.02745

Petropoulos, M., Karamichali, A., Rossetti, G. G., Freudenmann, A., Iacovino, L. G., Dionellis, V. S., . . . Halazonetis, T. D. (2024). Transcription-replication conflicts underlie sensitivity to PARP inhibitors. *Nature, 628*(8007), 433-441. doi:10.1038/s41586-024-07217-2

Petrylak, D. P., Gao, X., Vogelzang, N. J., Garfield, M. H., Taylor, I., Dougan Moore, M., . . . Burris III, H. A. (2020). First-in-human phase I study of ARV-110, an androgen receptor (AR) PROTAC degrader in patients (pts) with metastatic castrate-resistant prostate cancer (mCRPC) following enzalutamide (ENZ) and/or abiraterone (ABI). In: American Society of Clinical Oncology.

Pettitt, S. J., Frankum, J. R., Punta, M., Lise, S., Alexander, J., Chen, Y., . . . Lord, C. J. (2020). Clinical BRCA1/2 Reversion Analysis Identifies Hotspot Mutations and Predicted Neoantigens Associated with Therapy Resistance. *Cancer Discov, 10*(10), 1475-1488. doi:10.1158/2159-8290.Cd-19-1485

Pettitt, S. J., Krastev, D. B., Brandsma, I., Drean, A., Song, F., Aleksandrov, R., . . . Lord, C. J. (2018). Genome-wide and high-density CRISPR-Cas9 screens identify point mutations in PARP1 causing PARP inhibitor resistance. *Nat Commun, 9*(1), 1849. doi:10.1038/s41467-018-03917-2

Pettitt, S. J., Rehman, F. L., Bajrami, I., Brough, R., Wallberg, F., Kozarewa, I., . . . Ashworth, A. (2013). A Genetic Screen Using the PiggyBac Transposon in Haploid Cells Identifies Parp1 as a Mediator of Olaparib Toxicity. *PLoS One, 8*(4), e61520. doi:10.1371/journal.pone.0061520

Pfeiffer, A., Herzog, L. K., Luijsterburg, M. S., Shah, R. G., Rother, M. B., Stoy, H., . . . Dantuma, N. P. (2021). Poly(ADP-ribosyl)ation temporally confines SUMO-dependent ataxin-3 recruitment to control DNA double-strand break repair. *J Cell Sci, 134*(3). doi:10.1242/jcs.247809

Pfeiffer, A., Luijsterburg, M. S., Acs, K., Wiegant, W. W., Helfricht, A., Herzog, L. K., . . . Dantuma, N. P. (2017). Ataxin-3 consolidates the MDC1-dependent DNA double-strand break response by counteracting the SUMO-targeted ubiquitin ligase RNF4. *EMBO J, 36*(8), 1066-1083. doi:10.15252/embj.201695151

Pines, A., Vrouwe, M. G., Marteijn, J. A., Typas, D., Luijsterburg, M. S., Cansoy, M., . . . Mullenders, L. (2012). PARP1 promotes nucleotide excision repair through DDB2 stabilization and recruitment of ALC1. *J Cell Biol, 199*(2), 235-249. doi:10.1083/jcb.201112132

Polo, L. M., Xu, Y., Hornyak, P., Garces, F., Zeng, Z., Hailstone, R., . . . Pearl, L. H. (2019). Efficient Single-Strand Break Repair Requires Binding to Both Poly(ADP-Ribose) and DNA by the Central BRCT Domain of XRCC1. *Cell Rep, 26*(3), 573-581 e575. doi:10.1016/j.celrep.2018.12.082

Pommier, Y., Barcelo, J. M., Rao, V. A., Sordet, O., Jobson, A. G., Thibaut, L., . . . Redon, C. (2006). Repair of topoisomerase I-mediated DNA damage. *Prog Nucleic Acid Res Mol Biol, 81*, 179-229. doi:10.1016/s0079-6603(06)81005-6

Pommier, Y., Nussenzweig, A., Takeda, S., & Austin, C. (2022). Human topoisomerases and their roles in genome stability and organization. *Nat Rev Mol Cell Biol, 23*(6), 407-427. doi:10.1038/s41580-022-00452-3

Pommier, Y., O'Connor, M. J., & de Bono, J. (2016). Laying a trap to kill cancer cells: PARP inhibitors and their mechanisms of action. *Sci Transl Med, 8*(362), 362ps317. doi:10.1126/scitranslmed.aaf9246
Poveda, A., Floquet, A., Ledermann, J. A., Asher, R., Penson, R. T., Oza, A. M., . . . Pujade-Lauraine, E. (2020). Final overall survival (OS) results from SOLO2/ENGOT-ov21: A phase III trial assessing maintenance olaparib in patients (pts) with platinum-sensitive, relapsed ovarian cancer and a BRCA mutation. *Journal of Clinical Oncology, 38*(15_suppl), 6002-6002. doi:10.1200/JCO.2020.38.15_suppl.6002
Prokhorova, E., Agnew, T., Wondisford, A. R., Tellier, M., Kaminski, N., Beijer, D., . . . Ahel, I. (2021). Unrestrained poly-ADP-ribosylation provides insights into chromatin regulation and human disease. *Mol Cell*. doi:10.1016/j.molcel.2021.04.028
Prokhorova, E., Zobel, F., Smith, R., Zentout, S., Gibbs-Seymour, I., Schutzenhofer, K., . . . Ahel, I. (2021). Serine-linked PARP1 auto-modification controls PARP inhibitor response. *Nat Commun, 12*(1), 4055. doi:10.1038/s41467-021-24361-9
Pujade-Lauraine, E., Ledermann, J. A., Selle, F., Gebski, V., Penson, R. T., Oza, A. M., . . . Pautier, P. (2017). Olaparib tablets as maintenance therapy in patients with platinum-sensitive, relapsed ovarian cancer and a BRCA1/2 mutation (SOLO2/ENGOT-Ov21): a double-blind, randomised, placebo-controlled, phase 3 trial. *Lancet Oncol, 18*(9), 1274-1284. doi:10.1016/s1470-2045(17)30469-2
Purnell, M. R., & Whish, W. J. (1980). Novel inhibitors of poly(ADP-ribose) synthetase. *Biochem J, 185*(3), 775-777. doi:10.1042/bj1850775
Ramadan, K., Bruderer, R., Spiga, F. M., Popp, O., Baur, T., Gotta, M., & Meyer, H. H. (2007). Cdc48/p97 promotes reformation of the nucleus by extracting the kinase Aurora B from chromatin. *Nature, 450*(7173), 1258-1262. doi:10.1038/nature06388
Ramadan, K., Halder, S., Wiseman, K., & Vaz, B. (2016). Strategic role of the ubiquitin-dependent segregase p97 (VCP or Cdc48) in DNA replication. *Chromosoma, 126*(1), 17-32. doi:10.1007/s00412-016-0587-4
Ravikumar, B., Duden, R., & Rubinsztein, D. C. (2002). Aggregate-prone proteins with polyglutamine and polyalanine expansions are degraded by autophagy. *Hum Mol Genet, 11*(9), 1107-1117. doi:10.1093/hmg/11.9.1107
Ray Chaudhuri, A., Callen, E., Ding, X., Gogola, E., Duarte, A. A., Lee, J. E., . . . Nussenzweig, A. (2016). Replication fork stability confers chemoresistance in BRCA-deficient cells. *Nature, 535*(7612), 382-387. doi:10.1038/nature18325
Ray Chaudhuri, A., & Nussenzweig, A. (2017). The multifaceted roles of PARP1 in DNA repair and chromatin remodelling. *Nat Rev Mol Cell Biol, 18*(10), 610-621. doi:10.1038/nrm.2017.53
Ren, H., Bakas, N. A., Vamos, M., Chaikuad, A., Limpert, A. S., Wimer, C. D., . . . Cosford, N. D. P. (2020). Design, Synthesis, and Characterization of an Orally Active Dual-Specific ULK1/2 Autophagy Inhibitor that Synergizes with the PARP Inhibitor Olaparib for the Treatment of Triple-Negative Breast Cancer. *J Med Chem, 63*(23), 14609-14625. doi:10.1021/acs.jmedchem.0c00873
Reynolds, P., Cooper, S., Lomax, M., & O'Neill, P. (2015). Disruption of PARP1 function inhibits base excision repair of a sub-set of DNA lesions. *Nucleic Acids Res, 43*(8), 4028-4038. doi:10.1093/nar/gkv250

Robert, T., Vanoli, F., Chiolo, I., Shubassi, G., Bernstein, K. A., Rothstein, R., . . . Foiani, M. (2011). HDACs link the DNA damage response, processing of double-strand breaks and autophagy. *Nature, 471*(7336), 74-79. doi:10.1038/nature09803

Robson, M., Im, S. A., Senkus, E., Xu, B., Domchek, S. M., Masuda, N., . . . Conte, P. (2017). Olaparib for Metastatic Breast Cancer in Patients with a Germline BRCA Mutation. *N Engl J Med, 377*(6), 523-533. doi:10.1056/NEJMoa1706450

Robu, M., Shah, R. G., Petitclerc, N., Brind'Amour, J., Kandan-Kulangara, F., & Shah, G. M. (2013). Role of poly(ADP-ribose) polymerase-1 in the removal of UV-induced DNA lesions by nucleotide excision repair. *Proc Natl Acad Sci U S A, 110*(5), 1658-1663. doi:10.1073/pnas.1209507110

Rodriguez-Rocha, H., Garcia-Garcia, A., Panayiotidis, M. I., & Franco, R. (2011). DNA damage and autophagy. *Mutat Res, 711*(1-2), 158-166. doi:10.1016/j.mrfmmm.2011.03.007

Rodríguez-Vargas, J. M., Ruiz-Magaña, M. J., Ruiz-Ruiz, C., Majuelos-Melguizo, J., Peralta-Leal, A., Rodríguez, M. I., . . . Oliver, F. J. (2012). ROS-induced DNA damage and PARP-1 are required for optimal induction of starvation-induced autophagy. *Cell Res, 22*(7), 1181-1198. doi:10.1038/cr.2012.70

Rojas-Fernandez, A., Plechanovová, A., Hattersley, N., Jaffray, E., Tatham, M. H., & Hay, R. T. (2014). SUMO chain-induced dimerization activates RNF4. *Mol Cell, 53*(6), 880-892. doi:10.1016/j.molcel.2014.02.031

Romanowski, M. J., Gibney, S. A., & Burley, S. K. (2002). Crystal structure of the Escherichia coli SbmC protein that protects cells from the DNA replication inhibitor microcin B17. *Proteins, 47*(3), 403-407. doi:10.1002/prot.10102

Rosenfeld, M. R., Ye, X., Supko, J. G., Desideri, S., Grossman, S. A., Brem, S., . . . Amaravadi, R. K. (2014). A phase I/II trial of hydroxychloroquine in conjunction with radiation therapy and concurrent and adjuvant temozolomide in patients with newly diagnosed glioblastoma multiforme. *Autophagy, 10*(8), 1359-1368. doi:10.4161/auto.28984

Rottenberg, S., Jaspers, J. E., Kersbergen, A., van der Burg, E., Nygren, A. O. H., Zander, S. A. L., . . . Jonkers, J. (2008). High sensitivity of BRCA1-deficient mammary tumors to the PARP inhibitor AZD2281 alone and in combination with platinum drugs. *Proceedings of the National Academy of Sciences, 105*(44), 17079-17084. doi:10.1073/pnas.0806092105

Roux, B., Vaganay, C., Vargas, J. D., Alexe, G., Benaksas, C., Pardieu, B., . . . Benajiba, L. (2021). Targeting acute myeloid leukemia dependency on VCP-mediated DNA repair through a selective second-generation small-molecule inhibitor. *Science Translational Medicine, 13*(587), eabg1168. doi:doi:10.1126/scitranslmed.abg1168

Roux, B., Vaganay, C., Vargas, J. D., Alexe, G., Benaksas, C., Pardieu, B., . . . Benajiba, L. (2021). Targeting acute myeloid leukemia dependency on VCP-mediated DNA repair through a selective second-generation small-molecule inhibitor. *Sci Transl Med, 13*(587). doi:10.1126/scitranslmed.abg1168

Rozenknop, A., Rogov, V. V., Rogova, N. Y., Löhr, F., Güntert, P., Dikic, I., & Dötsch, V. (2011). Characterization of the Interaction of GABARAPL-1 with the LIR Motif of NBR1. *Journal of Molecular Biology, 410*(3), 477-487. doi:https://doi.org/10.1016/j.jmb.2011.05.003

Ruggiano, A., Vaz, B., Kilgas, S., Popovic, M., Rodriguez-Berriguete, G., Singh, A. N., . . . Ramadan, K. (2021). The protease SPRTN and SUMOylation

coordinate DNA-protein crosslink repair to prevent genome instability. *Cell Rep, 37*(10), 110080. doi:10.1016/j.celrep.2021.110080

Ruscetti, T., Lehnert, B. E., Halbrook, J., Le Trong, H., Hoekstra, M. F., Chen, D. J., & Peterson, S. R. (1998). Stimulation of the DNA-dependent protein kinase by poly(ADP-ribose) polymerase. *J Biol Chem, 273*(23), 14461-14467. doi:10.1074/jbc.273.23.14461

Ryu, T., Spatola, B., Delabaere, L., Bowlin, K., Hopp, H., Kunitake, R., . . . Chiolo, I. (2015). Heterochromatic breaks move to the nuclear periphery to continue recombinational repair. *Nat Cell Biol, 17*(11), 1401-1411. doi:10.1038/ncb3258

Saha, L. K., Murai, Y., Saha, S., Jo, U., Tsuda, M., Takeda, S., & Pommier, Y. (2021). Replication-dependent cytotoxicity and Spartan-mediated repair of trapped PARP1-DNA complexes. *Nucleic Acids Res*. doi:10.1093/nar/gkab777

Sakai, W., Swisher, E. M., Karlan, B. Y., Agarwal, M. K., Higgins, J., Friedman, C., . . . Taniguchi, T. (2008). Secondary mutations as a mechanism of cisplatin resistance in BRCA2-mutated cancers. *Nature, 451*(7182), 1116-1120. doi:10.1038/nature06633

Sakasai, R., & Iwabuchi, K. (2016). The distinctive cellular responses to DNA strand breaks caused by a DNA topoisomerase I poison in conjunction with DNA replication and RNA transcription. *Genes Genet Syst, 90*(4), 187-194. doi:10.1266/ggs.15-00023

Santiago-O'Farrill, J. M., Weroha, S. J., Hou, X., Oberg, A. L., Heinzen, E. P., Maurer, M. J., . . . Bast, R. C., Jr. (2020). Poly(adenosine diphosphate ribose) polymerase inhibitors induce autophagy-mediated drug resistance in ovarian cancer cells, xenografts, and patient-derived xenograft models. *Cancer, 126*(4), 894-907. doi:10.1002/cncr.32600

Sarraf, S. A., Raman, M., Guarani-Pereira, V., Sowa, M. E., Huttlin, E. L., Gygi, S. P., & Harper, J. W. (2013). Landscape of the PARKIN-dependent ubiquitylome in response to mitochondrial depolarization. *Nature, 496*(7445), 372-376. doi:10.1038/nature12043

Schlacher, K., Christ, N., Siaud, N., Egashira, A., Wu, H., & Jasin, M. (2011). Double-strand break repair-independent role for BRCA2 in blocking stalled replication fork degradation by MRE11. *Cell, 145*(4), 529-542. doi:10.1016/j.cell.2011.03.041

Schlacher, K., Wu, H., & Jasin, M. (2012). A Distinct Replication Fork Protection Pathway Connects Fanconi Anemia Tumor Suppressors to RAD51-BRCA1/2. *Cancer Cell, 22*(1), 106-116. doi:https://doi.org/10.1016/j.ccr.2012.05.015

Schlegel, B. P., Jodelka, F. M., & Nunez, R. (2006). BRCA1 promotes induction of ssDNA by ionizing radiation. *Cancer Res, 66*(10), 5181-5189. doi:10.1158/0008-5472.Can-05-3209

Schröder, B., Wrocklage, C., Hasilik, A., & Saftig, P. (2010). Molecular characterisation of 'transmembrane protein 192' (TMEM192), a novel protein of the lysosomal membrane. *Biol Chem, 391*(6), 695-704. doi:10.1515/bc.2010.062

Sciarretta, S., Zhai, P., Shao, D., Maejima, Y., Robbins, J., Volpe, M., . . . Sadoshima, J. (2012). Rheb is a critical regulator of autophagy during myocardial ischemia: pathophysiological implications in obesity and metabolic syndrome. *Circulation, 125*(9), 1134-1146. doi:10.1161/circulationaha.111.078212

Scott, L. J. (2017). Niraparib: First Global Approval. *Drugs, 77*(9), 1029-1034. doi:10.1007/s40265-017-0752-y
Scully, R., Panday, A., Elango, R., & Willis, N. A. (2019). DNA double-strand break repair-pathway choice in somatic mammalian cells. *Nature Reviews Molecular Cell Biology, 20*(11), 698-714. doi:10.1038/s41580-019-0152-0
Sczepanski, J. T., Wong, R. S., McKnight, J. N., Bowman, G. D., & Greenberg, M. M. (2010). Rapid DNA-protein cross-linking and strand scission by an abasic site in a nucleosome core particle. *Proc Natl Acad Sci U S A, 107*(52), 22475-22480. doi:10.1073/pnas.1012860108
Shao, R. G., Cao, C. X., Zhang, H., Kohn, K. W., Wold, M. S., & Pommier, Y. (1999). Replication-mediated DNA damage by camptothecin induces phosphorylation of RPA by DNA-dependent protein kinase and dissociates RPA:DNA-PK complexes. *EMBO J, 18*(5), 1397-1406. doi:10.1093/emboj/18.5.1397
Shao, Z., Lee, B. J., Rouleau-Turcotte, E., Langelier, M. F., Lin, X., Estes, V. M., . . . Zha, S. (2020). Clinical PARP inhibitors do not abrogate PARP1 exchange at DNA damage sites in vivo. *Nucleic Acids Res, 48*(17), 9694-9709. doi:10.1093/nar/gkaa718
Shen, Y., Aoyagi-Scharber, M., & Wang, B. (2015). Trapping Poly(ADP-Ribose) Polymerase. *J Pharmacol Exp Ther, 353*(3), 446-457. doi:10.1124/jpet.114.222448
Shen, Y., Rehman, F. L., Feng, Y., Boshuizen, J., Bajrami, I., Elliott, R., . . . Ashworth, A. (2013). BMN 673, a novel and highly potent PARP1/2 inhibitor for the treatment of human cancers with DNA repair deficiency. *Clin Cancer Res, 19*(18), 5003-5015. doi:10.1158/1078-0432.Ccr-13-1391
Shokrollahi, M., Stanic, M., Hundal, A., Chan, J. N. Y., Urman, D., Jordan, C. A., . . . Mekhail, K. (2024). DNA double-strand break–capturing nuclear envelope tubules drive DNA repair. *Nature Structural & Molecular Biology*. doi:10.1038/s41594-024-01286-7
Singh, A. N., Oehler, J., Torrecilla, I., Kilgas, S., Li, S., Vaz, B., . . . Ramadan, K. (2019). The p97-Ataxin 3 complex regulates homeostasis of the DNA damage response E3 ubiquitin ligase RNF8. *EMBO J, 38*(21), e102361. doi:10.15252/embj.2019102361
Skrott, Z., Mistrik, M., Andersen, K. K., Friis, S., Majera, D., Gursky, J., . . . Bartek, J. (2017). Alcohol-abuse drug disulfiram targets cancer via p97 segregase adaptor NPL4. *Nature, 552*(7684), 194-199. doi:10.1038/nature25016
Slobodkin, M. R., & Elazar, Z. (2013). The Atg8 family: multifunctional ubiquitin-like key regulators of autophagy. *Essays Biochem, 55*, 51-64. doi:10.1042/bse0550051
Snyder, L. B., Flanagan, J. J., Qian, Y., Gough, S. M., Andreoli, M., Bookbinder, M., . . . Chandler, J. (2021). The discovery of ARV-471, an orally bioavailable estrogen receptor degrading PROTAC for the treatment of patients with breast cancer. *Cancer Res, 81*(13), 44.
Söderberg, O., Gullberg, M., Jarvius, M., Ridderstråle, K., Leuchowius, K.-J., Jarvius, J., . . . Landegren, U. (2006). Direct observation of individual endogenous protein complexes in situ by proximity ligation. *Nature Methods, 3*(12), 995-1000. doi:10.1038/nmeth947
Sordet, O., Redon, C. E., Guirouilh-Barbat, J., Smith, S., Solier, S., Douarre, C., . . . Pommier, Y. (2009). Ataxia telangiectasia mutated activation by transcription- and topoisomerase I-induced DNA double-strand breaks. *EMBO Rep, 10*(8), 887-893. doi:10.1038/embor.2009.97

Sriramachandran, A. M., & Dohmen, R. J. (2014). SUMO-targeted ubiquitin ligases. *Biochim Biophys Acta, 1843*(1), 75-85. doi:10.1016/j.bbamcr.2013.08.022
Stingele, J., Bellelli, R., Alte, F., Hewitt, G., Sarek, G., Maslen, S. L., . . . Boulton, S. J. (2016). Mechanism and Regulation of DNA-Protein Crosslink Repair by the DNA-Dependent Metalloprotease SPRTN. *Mol Cell, 64*(4), 688-703. doi:10.1016/j.molcel.2016.09.031
Stingele, J., Bellelli, R., & Boulton, S. J. (2017). Mechanisms of DNA–protein crosslink repair. *Nature Reviews Molecular Cell Biology, 18*(9), 563-573. doi:10.1038/nrm.2017.56
Stingele, J., Schwarz, M. S., Bloemeke, N., Wolf, P. G., & Jentsch, S. (2014). A DNA-dependent protease involved in DNA-protein crosslink repair. *Cell, 158*(2), 327-338. doi:10.1016/j.cell.2014.04.053
Stolz, A., Ernst, A., & Dikic, I. (2014). Cargo recognition and trafficking in selective autophagy. *Nat Cell Biol, 16*(6), 495-501. doi:10.1038/ncb2979
Sun, Y., Chen, J., Huang, S. N., Su, Y. P., Wang, W., Agama, K., . . . Pommier, Y. (2021). PARylation prevents the proteasomal degradation of topoisomerase I DNA-protein crosslinks and induces their deubiquitylation. *Nat Commun, 12*(1), 5010. doi:10.1038/s41467-021-25252-9
Sun, Y., Jenkins, L. M. M., Su, Y. P., Nitiss, K. C., Nitiss, J. L., & Pommier, Y. (2020). A conserved SUMO pathway repairs topoisomerase DNA-protein cross-links by engaging ubiquitin-mediated proteasomal degradation. *Science Advances, 6*(46), eaba6290. doi:doi:10.1126/sciadv.aba6290
Sun, Y., Soans, E., Mishina, M., Petricci, E., Pommier, Y., Nitiss, K. C., & Nitiss, J. L. (2022). Requirements for MRN endonuclease processing of topoisomerase II-mediated DNA damage in mammalian cells. *Front Mol Biosci, 9*, 1007064. doi:10.3389/fmolb.2022.1007064
Syed, Y. Y. (2017). Rucaparib: First Global Approval. *Drugs, 77*(5), 585-592. doi:10.1007/s40265-017-0716-2
Taglialatela, A., Alvarez, S., Leuzzi, G., Sannino, V., Ranjha, L., Huang, J.-W., . . . Ciccia, A. (2017). Restoration of Replication Fork Stability in BRCA1- and BRCA2-Deficient Cells by Inactivation of SNF2-Family Fork Remodelers. *Molecular cell, 68*(2), 414-430.e418. doi:https://doi.org/10.1016/j.molcel.2017.09.036
Tanaka, A., Cleland, M. M., Xu, S., Narendra, D. P., Suen, D. F., Karbowski, M., & Youle, R. J. (2010). Proteasome and p97 mediate mitophagy and degradation of mitofusins induced by Parkin. *J Cell Biol, 191*(7), 1367-1380. doi:10.1083/jcb.201007013
Tang, W. K., Odzorig, T., Jin, W., & Xia, D. (2019). Structural Basis of p97 Inhibition by the Site-Selective Anticancer Compound CB-5083. *Mol Pharmacol, 95*(3), 286-293. doi:10.1124/mol.118.114256
Tatham, M. H., Geoffroy, M.-C., Shen, L., Plechanovova, A., Hattersley, N., Jaffray, E. G., . . . Hay, R. T. (2008). RNF4 is a poly-SUMO-specific E3 ubiquitin ligase required for arsenic-induced PML degradation. *Nature Cell Biology, 10*(5), 538-546. doi:10.1038/ncb1716
Taylor, A. M. R., Rothblum-Oviatt, C., Ellis, N. A., Hickson, I. D., Meyer, S., Crawford, T. O., . . . Stewart, G. S. (2019). Chromosome instability syndromes. *Nat Rev Dis Primers, 5*(1), 64. doi:10.1038/s41572-019-0113-0
ter Brugge, P., Kristel, P., van der Burg, E., Boon, U., de Maaker, M., Lips, E., . . . Jonkers, J. (2016). Mechanisms of Therapy Resistance in Patient-Derived

Xenograft Models of BRCA1-Deficient Breast Cancer. *JNCI: Journal of the National Cancer Institute, 108*(11). doi:10.1093/jnci/djw148
Tew, W. P., Lacchetti, C., Kohn, E. C., & Panel, f. t. P. I. i. t. M. o. O. C. G. E. (2022). Poly(ADP-Ribose) Polymerase Inhibitors in the Management of Ovarian Cancer: ASCO Guideline Rapid Recommendation Update. *Journal of Clinical Oncology, 40*(33), 3878-3881. doi:10.1200/jco.22.01934
Thoreen, C. C., Kang, S. A., Chang, J. W., Liu, Q., Zhang, J., Gao, Y., . . . Gray, N. S. (2009). An ATP-competitive mammalian target of rapamycin inhibitor reveals rapamycin-resistant functions of mTORC1. *J Biol Chem, 284*(12), 8023-8032. doi:10.1074/jbc.M900301200
Thorslund, T., McIlwraith, M. J., Compton, S. A., Lekomtsev, S., Petronczki, M., Griffith, J. D., & West, S. C. (2010). The breast cancer tumor suppressor BRCA2 promotes the specific targeting of RAD51 to single-stranded DNA. *Nat Struct Mol Biol, 17*(10), 1263-1265. doi:10.1038/nsmb.1905
Tobalina, L., Armenia, J., Irving, E., O'Connor, M. J., & Forment, J. V. (2021). A meta-analysis of reversion mutations in BRCA genes identifies signatures of DNA end-joining repair mechanisms driving therapy resistance. *Ann Oncol, 32*(1), 103-112. doi:10.1016/j.annonc.2020.10.470
Torrecilla, I., Oehler, J., & Ramadan, K. (2017). The role of ubiquitin-dependent segregase p97 (VCP or Cdc48) in chromatin dynamics after DNA double strand breaks. *Philos Trans R Soc Lond B Biol Sci, 372*(1731). doi:10.1098/rstb.2016.0282
Tresse, E., Salomons, F. A., Vesa, J., Bott, L. C., Kimonis, V., Yao, T. P., . . . Taylor, J. P. (2010). VCP/p97 is essential for maturation of ubiquitin-containing autophagosomes and this function is impaired by mutations that cause IBMPFD. *Autophagy, 6*(2), 217-227. doi:10.4161/auto.6.2.11014
Trusch, F., Matena, A., Vuk, M., Koerver, L., Knævelsrud, H., Freemont, P. S., . . . Bayer, P. (2015). The N-terminal Region of the Ubiquitin Regulatory X (UBX) Domain-containing Protein 1 (UBXD1) Modulates Interdomain Communication within the Valosin-containing Protein p97. *J Biol Chem, 290*(49), 29414-29427. doi:10.1074/jbc.M115.680686
Tsuboyama, K., Koyama-Honda, I., Sakamaki, Y., Koike, M., Morishita, H., & Mizushima, N. (2016). The ATG conjugation systems are important for degradation of the inner autophagosomal membrane. *Science, 354*(6315), 1036-1041. doi:10.1126/science.aaf6136
Tsujimoto, Y., Tomita, Y., Hoshida, Y., Kono, T., Oka, T., Yamamoto, S., . . . Aozasa, K. (2004). Elevated expression of valosin-containing protein (p97) is associated with poor prognosis of prostate cancer. *Clin Cancer Res, 10*(9), 3007-3012. doi:10.1158/1078-0432.ccr-03-0191
Tsukada, M., & Ohsumi, Y. (1993). Isolation and characterization of autophagy-defective mutants of Saccharomyces cerevisiae. *FEBS Lett, 333*(1-2), 169-174. doi:10.1016/0014-5793(93)80398-e
Turner, N. C., Telli, M. L., Rugo, H. S., Mailliez, A., Ettl, J., Grischke, E. M., . . . Robson, M. E. (2019). A Phase II Study of Talazoparib after Platinum or Cytotoxic Nonplatinum Regimens in Patients with Advanced Breast Cancer and Germline BRCA1/2 Mutations (ABRAZO). *Clin Cancer Res, 25*(9), 2717-2724. doi:10.1158/1078-0432.Ccr-18-1891
Twomey, E. C., Ji, Z., Wales, T. E., Bodnar, N. O., Ficarro, S. B., Marto, J. A., . . . Rapoport, T. A. (2019). Substrate processing by the Cdc48 ATPase complex

is initiated by ubiquitin unfolding. *Science, 365*(6452). doi:10.1126/science.aax1033
Uddin, M. H., Zhou, J. Y., Pimentel, J., Patrick, S. M., Kim, S., Shekhar, M. P., & Wu, G. S. (2022). Proteomic Analysis Identifies p62/SQSTM1 as a Critical Player in PARP Inhibitor Resistance. *Front Oncol, 12*, 908603. doi:10.3389/fonc.2022.908603
Vaidyanathan, A., Sawers, L., Gannon, A.-L., Chakravarty, P., Scott, A. L., Bray, S. E., . . . Smith, G. (2016). ABCB1 (MDR1) induction defines a common resistance mechanism in paclitaxel- and olaparib-resistant ovarian cancer cells. *British Journal of Cancer, 115*(4), 431-441. doi:10.1038/bjc.2016.203
Vaitsiankova, A., Burdova, K., Sobol, M., Gautam, A., Benada, O., Hanzlikova, H., & Caldecott, K. W. (2022). PARP inhibition impedes the maturation of nascent DNA strands during DNA replication. *Nat Struct Mol Biol, 29*(4), 329-338. doi:10.1038/s41594-022-00747-1
Valente, E. M., Abou-Sleiman, P. M., Caputo, V., Muqit, M. M., Harvey, K., Gispert, S., . . . Wood, N. W. (2004). Hereditary early-onset Parkinson's disease caused by mutations in PINK1. *Science, 304*(5674), 1158-1160. doi:10.1126/science.1096284
van den Boom, J., & Meyer, H. (2018). VCP/p97-Mediated Unfolding as a Principle in Protein Homeostasis and Signaling. *Mol Cell, 69*(2), 182-194. doi:10.1016/j.molcel.2017.10.028
Vanzo, R., Bartkova, J., Merchut-Maya, J. M., Hall, A., Bouchal, J., Dyrskjot, L., . . . Bartek, J. (2020). Autophagy role(s) in response to oncogenes and DNA replication stress. *Cell Death Differ, 27*(3), 1134-1153. doi:10.1038/s41418-019-0403-9
Vargas, J. N. S., Hamasaki, M., Kawabata, T., Youle, R. J., & Yoshimori, T. (2023). The mechanisms and roles of selective autophagy in mammals. *Nat Rev Mol Cell Biol, 24*(3), 167-185. doi:10.1038/s41580-022-00542-2
Vargas, J. N. S., Wang, C., Bunker, E., Hao, L., Maric, D., Schiavo, G., . . . Youle, R. J. (2019). Spatiotemporal Control of ULK1 Activation by NDP52 and TBK1 during Selective Autophagy. *Mol Cell, 74*(2), 347-362.e346. doi:10.1016/j.molcel.2019.02.010
Vaz, B., Popovic, M., Newman, J. A., Fielden, J., Aitkenhead, H., Halder, S., . . . Ramadan, K. (2016). Metalloprotease SPRTN/DVC1 Orchestrates Replication-Coupled DNA-Protein Crosslink Repair. *Mol Cell, 64*(4), 704-719. doi:10.1016/j.molcel.2016.09.032
Vaz, B., Popovic, M., & Ramadan, K. (2017). DNA-Protein Crosslink Proteolysis Repair. *Trends Biochem Sci, 42*(6), 483-495. doi:10.1016/j.tibs.2017.03.005
Verma, R., Oania, R. S., Kolawa, N. J., & Deshaies, R. J. (2013). Cdc48/p97 promotes degradation of aberrant nascent polypeptides bound to the ribosome. *Elife, 2*, e00308. doi:10.7554/eLife.00308
Virág, L., Robaszkiewicz, A., Rodriguez-Vargas, J. M., & Oliver, F. J. (2013). Poly(ADP-ribose) signaling in cell death. *Mol Aspects Med, 34*(6), 1153-1167. doi:10.1016/j.mam.2013.01.007
Vyas, S., Chesarone-Cataldo, M., Todorova, T., Huang, Y. H., & Chang, P. (2013). A systematic analysis of the PARP protein family identifies new functions critical for cell physiology. *Nat Commun, 4*, 2240. doi:10.1038/ncomms3240
Wang, H., Ren, B., Liu, Y., Jiang, B., Guo, Y., Wei, M., . . . Zhou, C. (2020). Discovery of Pamiparib (BGB-290), a Potent and Selective Poly (ADP-ribose)

Polymerase (PARP) Inhibitor in Clinical Development. *Journal of Medicinal Chemistry, 63*(24), 15541-15563. doi:10.1021/acs.jmedchem.0c01346
Wang, M., Wu, W., Wu, W., Rosidi, B., Zhang, L., Wang, H., & Iliakis, G. (2006). PARP-1 and Ku compete for repair of DNA double strand breaks by distinct NHEJ pathways. *Nucleic Acids Res, 34*(21), 6170-6182. doi:10.1093/nar/gkl840
Wang, W., & Matunis, M. J. (2023). Paralogue-Specific Roles of SUMO1 and SUMO2/3 in Protein Quality Control and Associated Diseases. *Cells, 13*(1). doi:10.3390/cells13010008
Wang, Y., Zhang, N., Zhang, L., Li, R., Fu, W., Ma, K., . . . Zhao, Y. (2016). Autophagy Regulates Chromatin Ubiquitination in DNA Damage Response through Elimination of SQSTM1/p62. *Mol Cell, 63*(1), 34-48. doi:10.1016/j.molcel.2016.05.027
Wang, Z., Xiong, S., Wu, Z., Wang, X., Gong, Y., Zhu, W. G., & Xu, X. (2024). VCP/p97 UFMylation stabilizes BECN1 and facilitates the initiation of autophagy. *Autophagy*, 1-14. doi:10.1080/15548627.2024.2356488
Weidberg, H., Shpilka, T., Shvets, E., Abada, A., Shimron, F., & Elazar, Z. (2011). LC3 and GATE-16 N termini mediate membrane fusion processes required for autophagosome biogenesis. *Dev Cell, 20*(4), 444-454. doi:10.1016/j.devcel.2011.02.006
Weisshaar, S. R., Keusekotten, K., Krause, A., Horst, C., Springer, H. M., Göttsche, K., . . . Praefcke, G. J. (2008). Arsenic trioxide stimulates SUMO-2/3 modification leading to RNF4-dependent proteolytic targeting of PML. *FEBS letters, 582*(21-22), 3174-3178.
Wicks, A. J., Krastev, D. B., Pettitt, S. J., Tutt, A. N. J., & Lord, C. J. (2022). Opinion: PARP inhibitors in cancer-what do we still need to know? *Open Biol, 12*(7), 220118. doi:10.1098/rsob.220118
Williams, P. A., Parham, L. R., Acheampong, K. K., Danan, C. H., Ma, X., Simon, L. A., . . . Hamilton, K. E. (2022). IGF2BP1/IMP1 contributes to autophagy modulation directly via MAP1LC3B. *bioRxiv*, 2022.2002.2028.482365. doi:10.1101/2022.02.28.482365
Wrobel, L., Hill, S. M., Ashkenazi, A., & Rubinsztein, D. C. (2021). VCP/p97 modulates PtdIns3P production and autophagy initiation. *Autophagy, 17*(4), 1052-1053. doi:10.1080/15548627.2021.1898742
Xiao, M., Yang, J., Dong, M., Mao, X., Pan, H., Lei, Y., . . . Shi, S. (2024). NLRP4 renders pancreatic cancer resistant to olaparib through promotion of the DNA damage response and ROS-induced autophagy. *Cell Death & Disease, 15*(8), 620. doi:10.1038/s41419-024-06984-0
Xu, G., Chapman, J. R., Brandsma, I., Yuan, J., Mistrik, M., Bouwman, P., . . . Rottenberg, S. (2015). REV7 counteracts DNA double-strand break resection and affects PARP inhibition. *Nature, 521*(7553), 541-544. doi:10.1038/nature14328
Xu, S., Peng, G., Wang, Y., Fang, S., & Karbowski, M. (2011). The AAA-ATPase p97 is essential for outer mitochondrial membrane protein turnover. *Mol Biol Cell, 22*(3), 291-300. doi:10.1091/mbc.E10-09-0748
Xue, H., Bhardwaj, A., Yin, Y., Fijen, C., Ephstein, A., Zhang, L., . . . Rothenberg, E. (2022). A two-step mechanism governing PARP1-DNA retention by PARP inhibitors. *Science Advances, 8*(36), eabq0414. doi:doi:10.1126/sciadv.abq0414

Yamamoto, H., Kakuta, S., Watanabe, T. M., Kitamura, A., Sekito, T., Kondo-Kakuta, C., . . . Ohsumi, Y. (2012). Atg9 vesicles are an important membrane source during early steps of autophagosome formation. *J Cell Biol, 198*(2), 219-233. doi:10.1083/jcb.201202061

Yamamoto, S., Tomita, Y., Hoshida, Y., Sakon, M., Kameyama, M., Imaoka, S., . . . Aozasa, K. (2004). Expression of valosin-containing protein in colorectal carcinomas as a predictor for disease recurrence and prognosis. *Clin Cancer Res, 10*(2), 651-657. doi:10.1158/1078-0432.ccr-1576-03

Yamamoto, S., Tomita, Y., Hoshida, Y., Takiguchi, S., Fujiwara, Y., Yasuda, T., . . . Aozasa, K. (2003). Expression level of valosin-containing protein is strongly associated with progression and prognosis of gastric carcinoma. *J Clin Oncol, 21*(13), 2537-2544. doi:10.1200/jco.2003.12.102

Yamamoto, S., Tomita, Y., Nakamori, S., Hoshida, Y., Iizuka, N., Okami, J., . . . Monden, M. (2004). Valosin-containing protein (p97) and Ki-67 expression is a useful marker in detecting malignant behavior of pancreatic endocrine neoplasms. *Oncology, 66*(6), 468-475. doi:10.1159/000079501

Yamamoto, S., Tomita, Y., Nakamori, S., Hoshida, Y., Nagano, H., Dono, K., . . . Aozasa, K. (2003). Elevated expression of valosin-containing protein (p97) in hepatocellular carcinoma is correlated with increased incidence of tumor recurrence. *J Clin Oncol, 21*(3), 447-452. doi:10.1200/jco.2003.06.068

Yamano, K., Kikuchi, R., Kojima, W., Hayashida, R., Koyano, F., Kawawaki, J., . . . Matsuda, N. (2020). Critical role of mitochondrial ubiquitination and the OPTN-ATG9A axis in mitophagy. *J Cell Biol, 219*(9). doi:10.1083/jcb.201912144

Yang, H., Li, Q., Fan, J., Holloman, W. K., & Pavletich, N. P. (2005). The BRCA2 homologue Brh2 nucleates RAD51 filament formation at a dsDNA-ssDNA junction. *Nature, 433*(7026), 653-657. doi:10.1038/nature03234

Yang, S., Wang, X., Contino, G., Liesa, M., Sahin, E., Ying, H., . . . Kimmelman, A. C. (2011). Pancreatic cancers require autophagy for tumor growth. *Genes Dev, 25*(7), 717-729. doi:10.1101/gad.2016111

Ye, Y., Meyer, H. H., & Rapoport, T. A. (2003). Function of the p97-Ufd1-Npl4 complex in retrotranslocation from the ER to the cytosol: dual recognition of nonubiquitinated polypeptide segments and polyubiquitin chains. *J Cell Biol, 162*(1), 71-84. doi:10.1083/jcb.200302169

Ying, S., Hamdy, F. C., & Helleday, T. (2012). Mre11-dependent degradation of stalled DNA replication forks is prevented by BRCA2 and PARP1. *Cancer Res, 72*(11), 2814-2821. doi:10.1158/0008-5472.Can-11-3417

Yoshimori, T., Yamamoto, A., Moriyama, Y., Futai, M., & Tashiro, Y. (1991). Bafilomycin A1, a specific inhibitor of vacuolar-type H(+)-ATPase, inhibits acidification and protein degradation in lysosomes of cultured cells. *J Biol Chem, 266*(26), 17707-17712.

Youle, R. J., & Strasser, A. (2008). The BCL-2 protein family: opposing activities that mediate cell death. *Nat Rev Mol Cell Biol, 9*(1), 47-59. doi:10.1038/nrm2308

Zandarashvili, L., Langelier, M. F., Velagapudi, U. K., Hancock, M. A., Steffen, J. D., Billur, R., . . . Black, B. E. (2020). Structural basis for allosteric PARP-1 retention on DNA breaks. *Science, 368*(6486). doi:10.1126/science.aax6367

Zeh, H. J., Bahary, N., Boone, B. A., Singhi, A. D., Miller-Ocuin, J. L., Normolle, D. P., . . . Lotze, M. T. (2020). A Randomized Phase II Preoperative Study of Autophagy Inhibition with High-Dose Hydroxychloroquine and

Gemcitabine/Nab-Paclitaxel in Pancreatic Cancer Patients. *Clin Cancer Res, 26*(13), 3126-3134. doi:10.1158/1078-0432.Ccr-19-4042

Zhang, X., Gui, L., Zhang, X., Bulfer, S. L., Sanghez, V., Wong, D. E., . . . Chou, T. F. (2015). Altered cofactor regulation with disease-associated p97/VCP mutations. *Proc Natl Acad Sci U S A, 112*(14), E1705-1714. doi:10.1073/pnas.1418820112

Zhao, W., Steinfeld, J. B., Liang, F., Chen, X., Maranon, D. G., Jian Ma, C., . . . Sung, P. (2017). BRCA1-BARD1 promotes RAD51-mediated homologous DNA pairing. *Nature, 550*(7676), 360-365. doi:10.1038/nature24060

Zhao, Y. G., Codogno, P., & Zhang, H. (2021). Machinery, regulation and pathophysiological implications of autophagosome maturation. *Nat Rev Mol Cell Biol, 22*(11), 733-750. doi:10.1038/s41580-021-00392-4

Zhou, H. J., Wang, J., Yao, B., Wong, S., Djakovic, S., Kumar, B., . . . Wustrow, D. (2015). Discovery of a First-in-Class, Potent, Selective, and Orally Bioavailable Inhibitor of the p97 AAA ATPase (CB-5083). *J Med Chem, 58*(24), 9480-9497. doi:10.1021/acs.jmedchem.5b01346

Zhu, C., Rogers, A., Asleh, K., Won, J., Gao, D., Leung, S., . . . Shao, J. (2020). Phospho-Ser(784)-VCP Is Required for DNA Damage Response and Is Associated with Poor Prognosis of Chemotherapy-Treated Breast Cancer. *Cell Rep, 31*(10), 107745. doi:10.1016/j.celrep.2020.107745